

A next-generation color appearance model for self-luminous stimuli

Thanh Hang PHUNG

Jury:

Prof. dr. Peter Hanselaer, promotor (Light and Lighting Laboratory, KU Leuven)

Prof. dr. Philip Dutré, promotor (Department of Computer Science, KU Leuven)

Prof. dr. Frédéric Leloup, promotor (Light and Lighting Laboratory, KU Leuven)

Prof. dr. Jiabin Li, chair (Department of Civil Engineering, KU Leuven)

Prof. dr. Kevin Smet, assessor (Light and Lighting Laboratory, KU Leuven)

Dr. Marc Mahy, assessor (Agfa-Gevaert Group, Mortsel)

Prof. dr. Maarten Kamermans, assessor (Netherlands Institute for Neuroscience)

Prof. dr. Ingrid Heynderickx, examiner (Human-Technology Interaction Group, TU Eindhoven)

Prof. dr. Karl Farrow, examiner (nerf, Department of Biology, KU Leuven)

Dissertation presented in partial fulfillment of the requirements for the degree of Doctor in Engineering Technology

October 2022

© 2022 Katholieke Universiteit Leuven, Arenberg Doctoral School of Science, Engineering & Technology – Faculty of Engineering, ESAT/ELECTA, Kasteelpark Arenberg 10, B-3001 Leuven, Belgium.

Alle rechten voorbehouden. Niets uit deze uitgave mag worden vermenigvuldigd en/of openbaar gemaakt worden door middel van druk, fotokopie, microfilm, elektronisch of op welke andere wijze ook zonder voorafgaande schriftelijke toestemming van de uitgever.

All rights reserved. No part of the publication may be reproduced in any form by print, photoprint, microfilm, electronic or any other means without written permission from the publisher.

Acknowledgements

Coming to Belgium with the luggage full of passion and curiosity for human color vision, I started my colorful and adventurous journey as a PhD researcher at the Light&Lighting Laboratory, KU Leuven. The ambition of my research was to take the first step to establish an image-based color appearance model for self-luminous stimuli, which can predict the appearance of self-luminous colors with a set of perceptual attributes from their optical properties in complex scenarios. With the ubiquitous presence of self-luminous stimuli in our daily life such as smartphone displays, TVs, billboards and luminaires, the development of such a color appearance model is essential to ensure a visual experience with high level of comfort and satisfaction.

Looking back, that was more than four years of quite an adventure both with the academic challenges and a pandemic, which would have been tremendously difficult for me if I had been alone. Luckily, I have been constantly receiving an enormous amount of supports from a lot of people around me. I would like to dedicate this part of my dissertation to them.

First and foremost, I would like to express my deepest gratitude to my promotor - Prof. Dr. Peter Hanselaer. I believe our encounter, though originally did not go as intended, is an amazing story. Your patience and guidance have led me through the darkest days of my doctoral research, both literally and figuratively. Your innovative and critical thinking is the true inspiration that leads me forward in my research career.

I would also like to thank my co-promotors, Prof. Dr. Frédéric Leloup and Prof. Dr. Philip Dutré, for your help with reviewing my publications and valuable ideas for my research. I am also thankful for the support and guidance from my assessors: Prof. Dr. Kevin Smet, Prof. Dr. Maarten Kamermans and Dr. Marc Mahy. Thanks to your advice and valuable insights, I could bring great improvements to the performed work.

Additionally, I would like to take the opportunity to thank all the examination committee members for their time and effort to evaluate my doctoral research and give me feedback to enhance the quality of this dissertation.

To all my former and current colleagues at the Light&Lighting Laboratory, thank you very much for your cooperation and your support. I really enjoyed the nice times we shared, especially the lunchtime chats and the coffee breaks.

I would like to particularly thank the official members (Stijn H, Nick, Gareth, Jonas, Rik, Stijn B, Jeroen and Chingwei) and special members (Jan, Tommaso, Kong, Jojo, Saskia) of 2.5 for creating such a supportive and welcoming environment. And I am not just talking about all the useful academic and technical knowledge exchanges (to Jan: you saved my PhD!!!). You simply turned a professional office into a work family full of joy and care. My PhD journey would have been less colorful, had it not been for you guys!

To “133 family” (Phuong Anh, Bac, Nghia, Trang, Chien, Duc Anh, Minh, Duc), thank you all for the great moments we shared. You made me feel not so far from home! And to Charlotte, Nhi, Dat, Nguyet Anh and Ai My, the best buddies I could ever ask for: Thank you for always supporting me and lifting me up when I was at the lowest. I could not find the right words to express how lucky I feel to have you rooting for me during this long journey.

To my mom, thank you for being the greatest mother! Despite your doubts and worries about your little girl whenever I struggled, you have been supporting me unconditionally with every step of my career. You let me explore my full potential with great pieces of advice. You encourage me to try, to fail, to bounce back, to move forward and to be fearless. To my stepdad, even though you are not with us in this world anymore, I believe you are still watching over me as my guardian angel and I hope I have made you proud. You are the most amazing father that one can have, and I do not think any word can express how awesome you were. To my dad and my stepmom, thank you for always caring about me, even when we are miles apart and the time does not allow us to see each other a lot.

And finally, to my love – Alexander: Thank you for the love and support you have been giving me. I am so happy and lucky to have you next to me, patiently listen to my stories and share all the good and bad times together. You make me believe more in myself and make me feel safe, even when it was a stormy world out there and I was in the “battlefield” with all the rebuttals. I can possibly say: you make a warrior out of me!

This doctoral research was made possible thanks to the funding from the Research Council of KU Leuven (C24/17/051).

Thanh Hang Phung

Ghent, October 2022

Abstract

With the rapid growth of technology, the exposure to self-luminous stimuli, such as luminaires, smartphone displays, TVs and billboards, is increasing tremendously. The designs of such light emitting devices and systems are now required to be not only functional and energy efficient, but also to have a high level of comfort, safety and personalization. Despite the need for more human-centric tools to measure the quality of self-luminous stimuli, most current quality metrics for light sources are still largely based on technical parameters such as energy efficiency or illuminance distribution. This calls for a transition from an illuminance-based approach to a spectral radiance-based approach to creating a lighting quality metric that can accurately represent the visual experience of the users. The very first step to achieve such an ambitious goal is to understand and model how humans perceive the color appearance of self-luminous stimuli from their physical properties.

Modeling the appearance of colors from their physical properties has come a long way in its history of almost 50 years. Starting with several uniform color spaces (CIELAB and CIELUV), which can tackle a certain level of chromatic adaptation effects and provide visual appearance prediction with lightness, chroma and hue, more and more color appearance models have been proposed, such as CAM97u, CAM02u, CAMFu, CIECAM02 and CIECAM16. These models take into account more complex visual processing stages such as chromatic and luminance adaptations and provide a more extended set of perceptual attributes to describe color appearance. The applications of the abovementioned color appearance models, especially CIECAM02, a model recommended by the “Commission Internationale d’Eclairage” (CIE), can be found across different fields such as cross-media color reproduction, printing image quality and color management for displays. However, the applications of a standardized color appearance model such as CIECAM02 to self-luminous stimuli still encounter some restrictions: the underestimation of how saturation can influence the perceived brightness (i.e. Helmholtz-Kohlrausch (H-K) effect), the independency between the spectral radiance of the background and the stimulus or the difficulty in choosing the white

point of the scene. That inspired the development of two new color appearance models for self-luminous stimuli: CAM15u for unrelated stimuli and CAM18sl for related stimuli. These models require simpler input compared to the traditional models while being capable of considering various visual phenomena related to self-luminous stimuli.

Although multiple color appearance models have been developed for both surface/object colors and self-luminous colors, most existing models are still established based on visual data limited to fairly simple arrangements where a uniform stimulus is presented on a uniform background. This experimental condition does not necessarily represent realistic situations, where the complexity level of the viewing condition can be much higher. This motivates the development of a few complex color appearance models which consider the spatial information in simulating the color appearance of images such as S-CIELAB, iCAM and iCAM06. However, these models are strongly based on previously mentioned color appearance models for surface/object colors or for displays with well-defined white points. This suggests the need to have a new color appearance model that can include complex spatial information into modeling the visual appearance of both self-luminous and object stimuli, which we refer to as a Lighting Appearance Model.

The goal of this doctoral research is to set the first steps to move towards a Lighting Appearance Model by investigating the possibility to create an image-based brightness model for neutral self-luminous stimuli seen on a rather complex situation. Starting with investigating the possibility of applying an existing image color appearance model to simple self-luminous scenes, an evaluation of iCAM's performance for predicting brightness for neutral self-luminous stimuli was performed. The results showed that while iCAM could well predict the brightness perception of related neutral self-luminous stimuli, there were some limitations of iCAM in calculating the brightness of unrelated stimuli and the H-K effect, the background size effect and the stimulus size effect were not yet explicitly considered in the model. This suggests that a new image-based appearance model should be approached for self-luminous stimuli.

The next step was to explore the potential of extending CAM18sl to a more complex background for neutral self-luminous stimuli. This was

conducted by studying the impact of various isolated ring-shaped parts from a uniform neutral background shown at different luminance levels. By using the ring-shaped design, it ensures an equal impact from the background to the stimulus from all directions. The experimental results showed that the presence of a ring reduced the perceived brightness of a central stimulus. The effect increased when the distance decreased and decreased when the thickness and luminance level of the additional luminous ring decreased. Based on the experimental data, two brightness models with two different approaches were proposed: the first model followed the traditional stimulus-background approach as used in CAM18sl and the second model was developed using an image-based approach to model the observed phenomenon for more complex scenes. The proposed models showed substantially good performance, though improvements are still required.

Finally, a series of experiments were performed to study the possible extension of the proposed models to chromatic backgrounds. A similar experimental method was used with colored luminous rings (red, green, blue, cyan, magenta and yellow) in addition to the neutral luminous rings, and the additional rings were shown at a fixed distance to investigate how different photoreceptors responses could influence the brightness perception of the central neutral stimulus. The experimental results showed that blue and magenta rings had a significantly higher impact in inhibiting the brightness of the central stimulus than the rings presented in other colors. An early attempt to model the phenomenon was proposed, yet future works are needed to create a complete model.

Samenvatting

Als gevolg van de snelle evolutie van de lichttechnologie neemt de aanwezigheid van lichtgevende stimuli, zoals armaturen, smartphone displays, TV's en billboards, enorm toe. Het ontwerp van dergelijke toestellen en verlichtingssystemen moet niet alleen functioneel en energie-efficiënt zijn, maar moet ook een hoog niveau van comfort, veiligheid en personalisatie nastreven. Ondanks de behoefte aan een meer "human-centric" benadering van de kwaliteitsvereisten van een verlichtingssysteem, zijn de meeste huidige kwaliteitsmetrieken voor lichtbronnen en lichtontwerpen nog steeds grotendeels gebaseerd op eenzijdige technische parameters zoals energie-efficiëntie of verlichtingssterkteverdeling. Dit vereist een overgang van een op verlichtingssterkte gebaseerde benadering naar een op spectrale radiantie gebaseerde benadering inclusief de ontwikkeling van een metriek voor verlichtingskwaliteit die de visuele ervaring van de gebruikers accuraat kan weergeven. De allereerste stap om een dergelijk ambitieus doel te bereiken is te begrijpen en te modelleren hoe mensen lichtbronnen waarnemen op basis van de fysische/optische eigenschappen.

Het modelleren van de waarneming van een stimulus op basis van de fysische eigenschappen heeft in zijn geschiedenis van bijna 50 jaar een lange weg afgelegd. Startend met verschillende uniforme kleuruimten (CIELAB en CIELUV) die een bepaald niveau van chromatische adaptatie toepassen en een voorspelling van visuele karakteristieken zoals lichtheid, chroma en tint kunnen bieden, zijn er steeds meer "Colour Appearance Models" (CAM) voorgesteld, zoals CAM97u, CAM02u, CAMFu, CIECAM02 en CIECAM16. Deze modellen houden rekening met complexere visuele verwerkingsfasen zoals chromatische en luminantie-adaptatie en bieden een uitgebreidere reeks perceptuele attributen om de perceptie te beschrijven. De toepassingen van de bovengenoemde modellen, met name CIECAM02, een model dat wordt aanbevolen door de "Commission Internationale d'Eclairage" (CIE), zijn te vinden op verschillende gebieden zoals cross-media kleurweergave, afdrukbeeldkwaliteit en kleurbeheer voor beeldschermen. De toepassing van een gestandaardiseerde CAM zoals CIECAM02 op lichtbronnen als

dusdanig stuit echter nog steeds op enkele beperkingen: de onderschatting van de wijze waarop de verzadiging de waargenomen helderheid kan beïnvloeden (het Helmholtz-Kohlrausch (H-K) effect), de onafhankelijkheid tussen de spectrale uitstraling van de achtergrond en van de stimulus of de moeilijkheid om het witpunt van de scène te kiezen. Dit alles inspireerde tot de ontwikkeling van twee nieuwe CAMs voor lichtgevende stimuli of lichtbronnen: CAM15u voor “unrelated” stimuli en CAM18sl voor “related” stimuli. Deze modellen zijn eenvoudiger in vergelijking met de traditionele modellen, terwijl ze toch in staat zijn verschillende visuele fenomenen te voorspellen.

Hoewel er meerdere CAMs werden ontwikkeld voor zowel oppervlakte/object stimuli als lichtgevende stimuli, zijn de meeste bestaande modellen nog steeds opgesteld op basis van visuele gegevens die beperkt zijn tot vrij eenvoudige situaties waarbij een uniforme stimulus wordt gepresenteerd op een uniforme achtergrond. Dit is weinig realistisch en leidde tot de ontwikkeling van enkele complexere modellen die rekening houden met de ruimtelijke informatie, zoals S-CIELAB, iCAM en iCAM06. Deze modellen zijn echter sterk gebaseerd op eerder genoemde CAMs voor oppervlakte/object stimuli of voor beeldschermen met een goed gedefinieerd witpunt. Dit suggereert de nood aan een “Lighting Appearance Model” dat de complexe ruimtelijke informatie kan opnemen in de modellering van de visuele perceptie van complexe scènes.

Het doel van dit doctoraatsonderzoek is om de eerste stappen te zetten in de richting van een Lighting Appearance Model door de mogelijkheid te onderzoeken om een beeldgebaseerd helderheidsmodel te creëren voor neutrale lichtgevende stimuli binnen een eerder complexe omgeving. Op basis van het onderzoek van de mogelijkheid om een bestaand “imaging” CAM toe te passen op eenvoudige lichtgevende stimuli, werd een evaluatie uitgevoerd van de performantie van iCAM voor het voorspellen van de helderheid van neutrale lichtgevende stimuli. De resultaten toonden aan dat hoewel iCAM de helderheidsperceptie van “related” neutrale lichtgevende stimuli goed kon voorspellen, er enkele beperkingen waren bij het berekenen van de helderheid van “unrelated” stimuli en dat het H-K effect, het “background size” effect en het “stimulus size” effect nog niet expliciet werden meegenomen in het model.

De volgende stap bestond er in om de mogelijkheid om CAM18sl uit te breiden naar situaties met een meer complexe achtergrond te onderzoeken. Dit onderzoek werd uitgevoerd door het bestuderen van de impact van verschillende geïsoleerde ringvormige delen van een uniforme neutrale achtergrond op de waargenomen “brightness” of helderheid van een centrale stimulus. Door een ring te gebruiken kon er worden gezorgd voor een gelijke impact van de achtergrond op de centrale stimulus vanuit alle richtingen. De experimentele resultaten toonden aan dat de aanwezigheid van de ring de helderheid van de centrale stimulus deden afnemen en dat dit effect afhankelijk was van de afstand, de dikte en het luminantieniveau van de lichtgevende ring. Op basis van de experimentele gegevens werden twee helderheidsmodellen met twee verschillende benaderingen voorgesteld: het eerste model volgde de traditionele stimulus-achtergrond benadering zoals gebruikt in CAM18sl en het tweede model werd ontwikkeld met behulp van een beeld-gebaseerde benadering (zoals iCAM). De voorgestelde modellen bleken behoorlijk te presteren, alhoewel er nog ruimte tot verbetering blijft.

Tenslotte werden een reeks experimenten uitgevoerd om de uitbreiding van de voorgestelde modellen tot chromatische achtergronden te bestuderen. Een vergelijkbare experimentele methode werd gebruikt maar nu met gekleurde lichtgevende ringen (rood, groen, blauw, cyaan, magenta en geel) in aanvulling op de neutrale lichtgevende ringen, en de extra ringen werden getoond op een vaste afstand. Dit laat toe om te onderzoeken hoe verschillende fotoreceptoren (L,M en S) de helderheidsperceptie van de centrale neutrale stimulus beïnvloeden. De experimentele resultaten toonden aan dat blauwe en magenta ringen een significant grotere invloed hadden op de helderheid van de centrale stimulus dan de ringen die in andere kleuren werden gepresenteerd. Een eerste poging om het fenomeen te modelleren werd voorgesteld.

List of abbreviations

CAM	Color appearance model
CCD	Charge-coupled Device
CIE	International commission on illumination
DoG	Difference of Gaussian
EEW	Equal-energy white
FOV	Field of view
FWHM	Full width half maximum
GDPR	General data protection regulation
GUI	Graphic user interface
HDR	High dynamic range
H-K effect	Helmholtz-Kohlrausch effect
iCAM	Image color appearance model
IPL	Inner plexiform layer
ipRGC	Intrinsic photosensitive Retinal Ganglion Cell
LAM	Lighting appearance model
M-M equation	Michaelis-Menten equation
OLED	Organic light emitting diode
OPL	Outer plexiform layer
RAS	Relative adaptive shift
RFV	Receptive field value
RGB	Red, green, blue
RMSE	Root mean squared error
STRESS	Standardized residual sum of squares
TI	Threshold increment
UGR	Unified Glare Rating

Table of Contents

Acknowledgements	I
Abstract.....	IV
Samenvatting	VII
List of abbreviations	X
1. Introduction	2
1.1. Human vision	3
1.2. Retina Models	5
1.3. Color Appearance Terminology	7
1.3.1. Type of stimuli and viewing conditions	7
1.3.2. Perceptual attributes	10
1.4. Color Appearance Modelling	11
1.4.1. Introduction.....	11
1.4.2. Non-image Color Appearance Model for self-luminous stimuli	14
1.4.3. Image Color Appearance Models.....	22
1.5. A next-generation color appearance model for self-luminous stimuli.....	27
1.5.1. Introduction.....	27
1.5.2. Lighting Appearance Model	28
1.5.3. Main goal of this doctoral research.....	30
1.5.4. Applications	31
1.5.5. Overview.....	32
1.6. References for Chapter 1.....	33
2. Assessing the application of an Image Color Appearance Model to basic self-luminous scenes	42
2.1. Introduction	42
2.2. Main results and discussion.....	43
2.3. Publication 1	44

3. Brightness appearance of self-luminous stimuli with a non-uniform background.....	66
3.1. Introduction	66
3.2. Pilot experiment	66
3.2.1. Experiment	67
3.2.2. Preliminary results	69
3.3. Extended pilot experiment	71
3.3.1. Experiment	71
3.3.2. Results	72
3.4. Main results and discussion.....	73
3.5. Publication 2	75
4. Towards an image-based brightness model for neutral self-luminous stimuli	106
4.1. Introduction	106
4.2. Main results and discussion.....	106
4.3. Publication 3	109
5. Impact of colored background elements on brightness perception of neutral self-luminous stimuli	142
5.1. Introduction	142
5.2. Experiment	142
5.3. Results and Discussion	147
5.3.1. Observer variability.....	147
5.3.2. Experimental results.....	148
5.4. Conclusion	158
5.5. References for Chapter 5.....	159
6. Valorization Plan: A tool for assessing lighting design quality based on glare.....	163
6.1. Background and key problems.....	163
6.2. Freedom to operate	164
6.2.1. Scientific Literature.....	165

6.2.2.	Patents	166
6.3.	Products and services	167
6.3.1.	A tool for glare assessment	167
6.3.2.	Future product: A new tool for assessing glare based on an image color appearance model	172
6.4.	Exploitation trajectory	173
6.4.1.	Partner	173
6.4.2.	Timeline for market entry	173
6.4.3.	Financial plan	174
6.4.4.	Legal rights	175
6.4.5.	Data distribution	176
6.5.	Potential impact of the valorization plan	177
6.6.	References for Chapter 6	178
7.	Conclusions and Future Work	182
7.1.	Conclusions	182
7.1.1.	Performance of iCAM for simple self-luminous scenes	182
7.1.2.	Brightness perception of neutral self-luminous stimuli on a non-uniform neutral self-luminous background	183
7.1.3.	Towards an image-based brightness model for neutral self-luminous stimuli	184
7.1.4.	From a neutral ring to a colored ring	185
7.1.5.	Imaging CAM and glare: an exploitation track of the doctoral research	186
7.2.	Future work	186
7.2.1.	Possible improvements to the current research ..	187
7.2.2.	Future research	187
7.3.	References for Chapter 7	190
	Curriculum vitae	194

Chapter 1

Introduction

1. Introduction

Color has been one of the most fascinating topics in our daily life. From fine arts to poetry, from psychology to media content shown on our screens, color has played an important role in keeping our life lively and beautiful.

As a subjective sensation of light, color has triggered so many curious minds to try to explain how humans perceive colors and how to apply the discovered knowledge to improve the quality of life. Many attempts have been performed to explore how the human visual system works and how to describe colors in terms of perceptual attributes from the physical properties of the emitted or reflected light. As a result, various color theories and color appearance models have been introduced. Such knowledge has been widely applied across multiple applications, such as textile, printing, media content reproduction and lighting, to ensure a truthful color reproduction with a high level of comfort and safety for the end users.

Throughout the history of color appearance modeling, many color appearance models (CAMs) have been proposed, especially for object colors and displays. However, the number of CAMs that are designed for self-luminous stimuli which have completely independent spectral properties from the background is still rather limited. Another issue is that most current CAMs for self-luminous stimuli are developed based on simple situations where a uniform stimulus is displayed against a uniform background, which does not represent the majority of real-life scenarios. With the rapid development of lighting technology and growing demand for human-centric lighting, a new CAM for self-luminous stimuli, which is capable of accounting for complex spatial information, can be beneficial for creating high-quality lighting designs. Motivated by that idea, the aim of this doctoral research is to set the first steps to move toward a next-generation CAM for self-luminous stimuli, which we call a Lighting Appearance Model (LAM).

In this chapter, to provide a background for understanding the scope of the research in later sections, the basic mechanisms of human vision, together with the general introduction of color terminology, are presented. Next, a brief overview of color appearance models is given, and the rationale of this doctoral research is discussed, followed by the objectives of the research and the structure of this dissertation.

1.1. Human vision

Human visual perception is a complex multi-stage process that is highly influenced by the anatomy of the eye.

William Shakespeare once said: "The eyes are the windows to the soul." This statement holds true physiologically when the eye is a sophisticated organ that acts as the first door to the human visual pathway, as illustrated in Figure 1.1. When light reaches the eye, it is first refracted by a transparent outer surface on the front side of the eye -called the cornea- before passing through the pupil. The pupil, whose size is controlled by the iris, then acts as an aperture that controls the amount of light entering the retina with a special mechanism: the pupillary light reflex. In dimmed environments, the pupil dilates such that more light can enter the eye and hit the retina, while in highly lit settings, an iris contraction reduces the pupil diameter to limit the incident light and protect the retina [1].

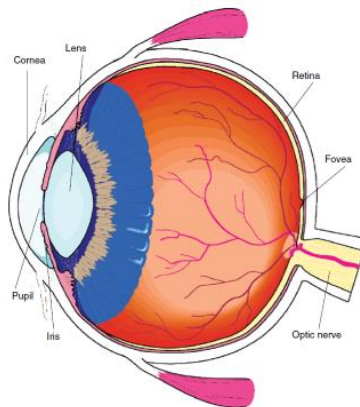


Figure 1.1: Schematic cross-section of the human eye [1]

The retina is positioned at the back of the eye, which composes of multiple layers of photoreceptors and neural cells (Figure 1.2).

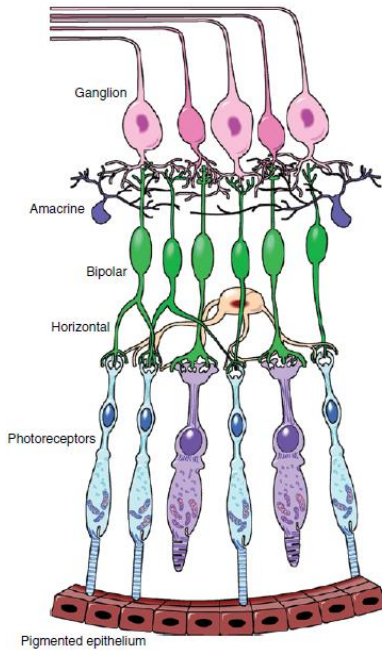


Figure 1.2: Schematic diagram of the retina in the human eye [1]

At the back of the retina are the photoreceptors: rods and cones, whose names were given after their respective shapes. The rods are responsible for scotopic (low light) vision, and as there is only one type of rod, they only detect differences in brightness and do not provide color vision. The cones are activated in photopic conditions, where the environment is better illuminated. In the mesopic condition, where the luminance level is between scotopic and photopic levels, both types of photoreceptors contribute to the visual experience. The cones are categorized into three types: long (ρ), middle (γ) and short (β) wavelength-sensitive cones, which correspond to their spectral sensitivity. The peak sensitivities of each cone type are approximately 569 nm, 541 nm and 448 nm, respectively [2]. Besides having a non-uniform spatial distribution in the retina, the relative density of each cone type is also largely different. Despite a broad variation among individuals, the average cone densities $\rho:\gamma:\beta$ are estimated to be 40:20:1 [3].

The photoreceptors are connected to the bipolar cells and to the horizontal cells, which also connect the photoreceptors to the bipolar cells. These connections form the Outer Plexiform Layer (OPL). The bipolar cells are connected to amacrine cells and ganglion cells, forming the Inner Plexiform Layer (IPL) [4]. On top of the retina are the ganglion cells, which form the optic nerve just outside of the fovea. Among these ganglion cells, there are Intrinsically Photosensitive Retinal Ganglion Cells (ipRGCs) which contain melanopsin, a type of photopigment that plays an essential role in managing the circadian rhythms [5,6].

When a light signal (characterized by its spectral radiance) hits the retina, it will first excite the photoreceptors, whose signals are then compressed and transmitted through the horizontal cells, bipolar cells and ganglion cells. The responses from the ganglion cells are then sent via the optical nerve to the visual cortex for visual information processing [1].

1.2. Retina Models

Understanding and modeling the human visual system has been an active research area in the past centuries. Various attempts have been reported to model how visual signals are processed in the retina. Retina modeling can be dated back to 1906, when Mach made a connection between retinal processing and spatial filtering [7]. Based on the same ideology, a few studies were proposed to simulate the spatial responses of retinal cells in cats [8], or to describe the horizontal cells' low-pass spatial behavior [9] using a Difference-of-Gaussian (DoG) filter.

Throughout the long history of retina modeling, various models have been developed and they can be classified into several different categories based on their focus. Some studies focused on precisely mimicking the detailed reproduction of retinal connectivity in successive layers [10], while others shifted their attention more to obtaining functionally efficient retinal output with a series of spatial filtering stages [11–13]. In general, these models provide a thorough simulation of retinal processing at certain stages, such as cone responses [12–14] or temporal filtering properties in primate ganglion cells [11]. More recent retina models [4,15–17] have made a few attempts to find the balance between modeling the functionality and the

biological accuracy of retinal processing. Thanks to the advancement in computational efficiency, it has been made possible for such models to implement complex retinal processing at different stages with higher biological preciseness.

Besides the biological-focused retina models, a number of retina-based models have also been established for more applied purposes such as predicting visual perception, signal processing and computer vision. Applying the spatial filtering properties of the retina, a few studies investigated the possibility of predicting spatial brightness illusions [18–21]. While early models [18,19] only simulate brightness perception in one single dimension, i.e., only for a certain row or column of an image, later models [20,21] have advanced to predict two-dimensional brightness perception from an input image. Some other models also try to mimic the entire retina signal processing and provide changes in visual information at each stage of retinal cell layers [22,23]. Retinal processing is also applied to explain various properties in image processing, such as sampling, color-coding and non-linearity, which can improve the related applications [24]. Additionally, the physiology of the retina also inspired the development of tone-mapping operators for High Dynamic Range (HDR) imaging [25].

Despite the vast diversity in retina modeling and its applications, the majority of retina models share the following general workflow: the model starts with one input image or a series of input images representing the scene projected on the retina. Then, the retina processing is simulated with spatial and (or) temporal filtering. The processing happening in the retina can be divided into sub-stages either at a more general level, such as Outer Plexiform and Inner Plexiform Layers [4,15,25] or at a more detailed level, such as each retinal cell layer [16,17]. Depending on the application of the proposed model, a typical output for a retina model can be the neural responses sent to the visual cortex in the unit of neural spikes [15–17], or the perceived luminance or the perceived brightness, or the color of the image [4,21,25]. Nevertheless, a retinal model that outputs a complete set of visual attributes as described in CAMs is still missing.

1.3. Color Appearance Terminology

As previously discussed, one of the main applications of human visual system modeling is to predict color appearance. Color appearance is the aspect of visual perception by which things are recognized by their color, as defined by the International Commission on Illumination (CIE) [26]. To describe color appearance, it is essential to understand the standardized vocabulary for color appearance. In this section, the basic color appearance terminology will be given.

1.3.1. Type of stimuli and viewing conditions

Depending on the type of stimulus and the viewing conditions, the perception of color appearance can be highly influenced. To describe different color appearance modes, a number of specific color appearance terms have been defined by the CIE with the entry numbers in the International Lighting Vocabulary as follows [26]:

- **Corresponding colors** (17-23-012):
"pairs of color stimuli that have the same color appearance when one is seen in one set of adaptation conditions and the other is seen in a different set."
- **(Self-)luminous color** (17-22-045):
"color perceived to belong to an area that appears to be emitting light as a primary light source, or that appears to be specularly reflecting such light" (Figure 1.3-a).
- **Non-luminous color** (17-22-046):
"color perceived to belong to an area that appears to be transmitting or diffusely reflecting light as a secondary light source" (Figure 1.3-b).
- **Object color** (17-22-042):
"color perceived as belonging to an object" (Figure 1.3-c).
- **Surface color** (17-22-043):
"color perceived as belonging to a surface from which the light appears to be diffusely reflected or radiated" (Figure 1.3-d).

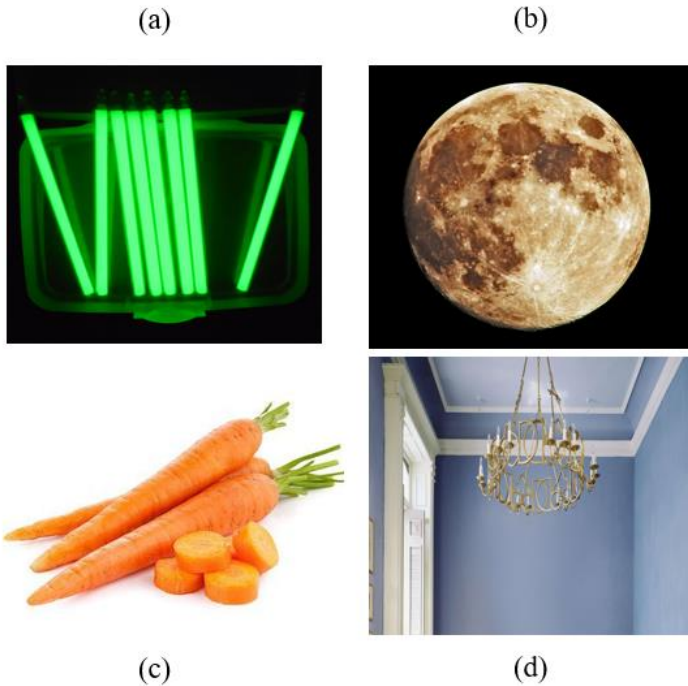


Figure 1.3: Examples of different types of stimuli: (a) self-luminous vials, (b) non-luminous moon which reflects the light from the sun, (c) Object color of the carrots, (d) Surface color of the wall.

- **Volume color** (17-22-054):
"color perceived as belonging to the bulk of the substance."
- **Aperture color** (17-22-044):
"perceived color seen through an aperture - an opening that defines the area over which average optical emission is measured - which prevents its association with a specific object or source."
- **Related colors** (17-22-047):
"color perceived to belong to an area seen in relation to other colors" (Figure 1.4-b).
- **Unrelated color** (17-22-048):
"color perceived to belong to an area seen in isolation from other colors" (Figure 1.4-a).

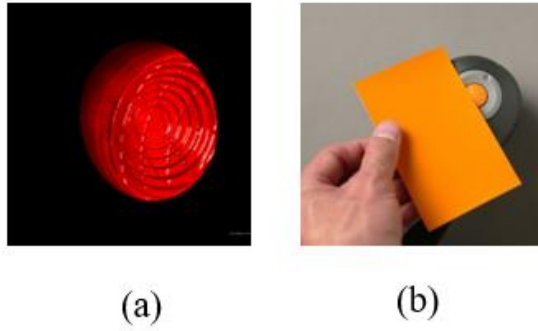


Figure 1.4: Examples of (a) unrelated color, (b) related color.

Another important aspect of describing a viewing condition is the viewing field configuration. Several elements in the viewing field are illustrated in Figure 1.5 and can be defined as follows [1]:

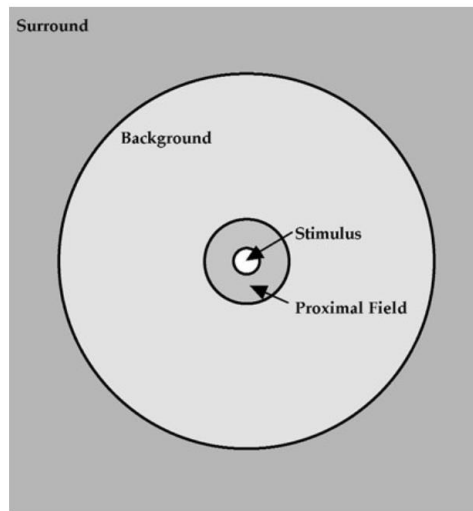


Figure 1.5: Components of the viewing field [1]

- **Stimulus:**
The color element for which a measure of color appearance is desired.
- **Proximal field:**
The adjacent environment extends about 2° from the edge of the stimulus in all or most directions.

- **Background:**

The immediate environment extending about 10° from the edge of the stimulus (or proximal field, if defined) in all, or most directions.

- **Surround:**

The field outside the background. This can be the extended viewing environment, such as the whole room in which the stimuli are being viewed.

1.3.2. Perceptual attributes

To describe color from the perceptual point of view, univariate perceptual attributes are used and classified into absolute and relative categories. The three absolute perceptual color attributes are defined as [1]:

- Brightness Q : "attribute of visual sensation according to which an area appears to emit/reflect more or less light" (described as bright and dim).
- Hue quadrature H : "attribute of a visual sensation according to which an area appears to be similar to one, or to proportions of a combination of adjacent pairs, of the perceived colors red, yellow, green and blue."
- Colorfulness M : "attribute of visual sensation according to which an area appears to display more or less of its hue (described as vivid and dull)."

From these three absolute attributes, three relative attributes can be deduced:

- Lightness J : "the brightness Q judged relative to the brightness of a similarly illuminated reference white diffusely reflecting surface (light and dark) (only for related colors)."
- Chroma C : "the colorfulness M judged in proportion to the brightness of a similarly illuminated reference white diffusely reflecting surface (strong and weak) (only for related colors)."
- Saturation S : "colorfulness M of an area judged in proportion to its brightness Q ."

1.4. Color Appearance Modelling

1.4.1. Introduction

A Color Appearance Model (CAM) is a model which describes the color appearance of a stimulus in terms of perceptual attributes, as previously mentioned, under various viewing conditions. Most existing CAMs apply trichromatic vision and the color opponency theory to describe human color perception [27]. This implies that the perception of color is controlled with three receptor complexes with two color opponent signals: red-green and blue-yellow and the achromatic signal.

The construction of a CAM typically starts with the physical property of the uniform stimulus and the uniform background, expressed either in terms of XYZ tristimulus values or spectral radiance. From this input, the cone excitations can be computed either by a linear transformation from XYZ or by using the cone fundamentals and spectral radiance [1,28–30].

The human visual system is capable of adjusting its operation properties to adapt to various illumination conditions. This process is referred to as visual adaptation [31]. The visual adaptation process can be classified into two sub-processes: chromatic adaptation and luminance adaptation [32]. In order to accurately predict the appearance of colors, one of the first steps in CAM is to account for these visual adaptation processes.

Chromatic adaptation is the process where the human visual system adjusts to the change in the chromaticity of illumination to preserve the color appearance of the stimulus. It provides the (almost) constancy of color appearance across a wide variation of scenery [1]. Most existing adaptation models are developed based on the von Kries chromatic adaptation method [33]. In this method, a gain is applied to each cone spectral sensitivity such that the adapted appearance of the "white" remains the same (in the case of complete adaptation). As this process is mainly described in the sensitivity control of the three different cones [34,35], a chromatic adaptation transformation (CAT) is

normally applied after the XYZ tristimulus is transformed into a cone-like sensor space [36].

Luminance adaptation can be divided into dark and light adaptation. Dark adaptation refers to the adaptation occurring in the visual system when an observer changes to a darker environment. The scene appears completely dark at first, yet, after a period of time, the shapes and objects gradually become distinguishable. This process is driven by the rods in the retina. The visual system becomes more and more sensitive to the low-light environment, and after approximately 10 to 30 minutes [37], the sensitivity stays rather stable. Once the dark adaptation is complete, the rod signal completely dominates the cone signals [30,32].

Light adaptation happens in the opposite direction of dark adaptation. When an observer changes from a darker to a better-lit environment, the cone signal becomes dominant while the rod signal is suppressed, and the visual system becomes less sensitive to light [30,32].

In our daily life, we come across a broad range of luminance levels, which covers at least 10 orders of magnitude from a dark night to a bright sunny afternoon. To enable our visual system to see under such a huge luminance variation, a special mechanism called cone compression occurs in the first stage of the visual system. It is believed that the human cone responses follow a sigmoidal curve, similar to how primate cones respond [38]. This compression process is commonly modeled with a sigmoidal function based on the Michaelis-Menten equation [39,40]:

$$\alpha_a = \frac{\alpha^n}{\alpha^n + \sigma^n} \quad (1.1)$$

Where α is the cone excitation, α_a is the compressed cone response, n determines the slope of the response curve, and σ represents the semi-saturation constant – the input at which half of the maximum response is reached. When σ is constant, no adaptation will happen, while when σ increases, the adapted cone signal will decrease (Figure 1.6). Using Eq. (1.1) with a variable σ allows for an analytical description of both compression and luminance adaptation.

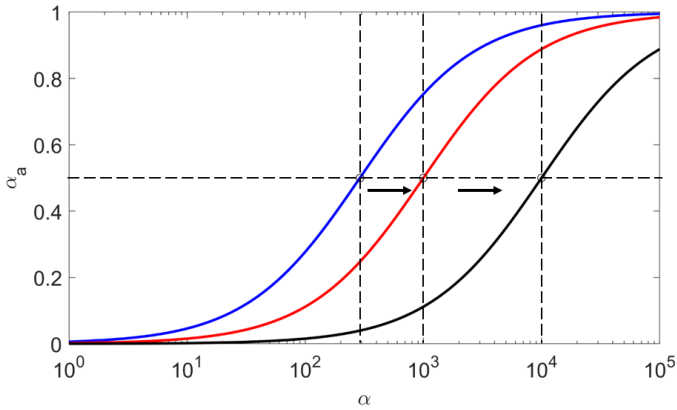


Figure 1.6: Three different sigmoidal functions with an increase in semi-saturation constant σ [41]

Once the adapted cone signals are computed, the three following neural signals can be deduced: The achromatic signal – a weighted sum of the three adapted cone responses, and two color opponent signals (red-green and blue-yellow). From these neural signals, a set of perceptual attributes are computed as the output for a CAM.

A brief overview of the described processing in human color vision, which a CAM is based on, is illustrated in Figure 1.7.

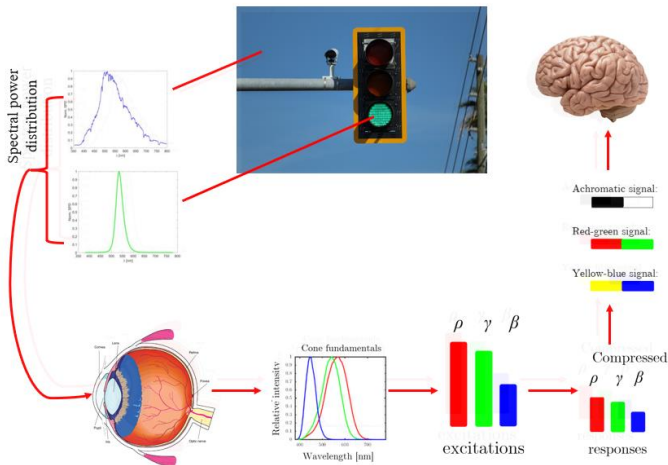


Figure 1.7: A brief overview of human color vision.

1.4.2. Non-image Color Appearance Model for self-luminous stimuli

Based on the discussed principle, multiple CAMs have been developed, such as Nayatani et al. model [42], the Hunt model [43], CIECAM97s [44], CAM20u [45] and especially CIECAM02 [36] and CIECAM16 [46], the color appearance models that are recommended by the CIE. The applications of a CAM vary from improving image quality in printing to color management for displays, image processing (medical and forensic imaging) and movie productions. CIECAM02 has been the most widely used CAM for such applications, yet, the model still faces some drawbacks, such as the underestimation of the Helmholtz-Kohlrausch effect [45,47,48] or no inclusion of the stimulus size effect in the appearance of the subject's colors [48,49]. The rapid growth of imaging science and lighting technologies calls for a comprehensive color appearance model which can assist the accurate color reproduction across different media. Moreover, applying a traditional CAM such as CIECAM02 to self-luminous stimuli, such as streetlights or LED billboards, can be challenging due to the independency between the spectral radiance of the stimulus and the background, and the ambiguity in defining the reference white point [50]. This inspires the development of new color appearance models for self-luminous stimuli, such as CAM15u [51] – a CAM for unrelated self-luminous stimuli- and CAM18sl [50] – a CAM for related self-luminous stimuli. A summary of non-image CAM is given in Figure 1.8. It is worth noting that these CAMs are still limited to applications comprising uniform stimuli seen against a uniform background.

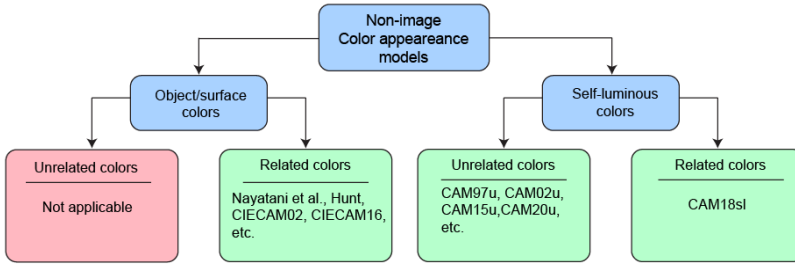


Figure 1.8: Non-image CAM classification

In this section, CAM15u [51] and CAM18sl [50] - the two color appearance models for self-luminous stimuli- will be discussed in more detail.

CAM15u

The development of a CAM for unrelated stimuli dates back to 1982, when Hunt developed one of the first model for color appearance model [52]. In 1997, a revised version of the previous model - CAM97u was introduced [30,53]. Several improvements were proposed later on in 2002, resulting in the CAM02u model [54]. Though CAM97u and CAM02u were shown to have generally good performance in predicting hue and colorfulness of unrelated colors, it was also found that such models underestimated the Helmholtz-Kohlrausch effect, which leads to inaccurate predictions of the perceived brightness of saturated stimuli [55]. This inspires the development of CAM15u [51], which takes into consideration the contribution of colorfulness to brightness. The general workflow of CAM15u is presented in Figure 1.9.

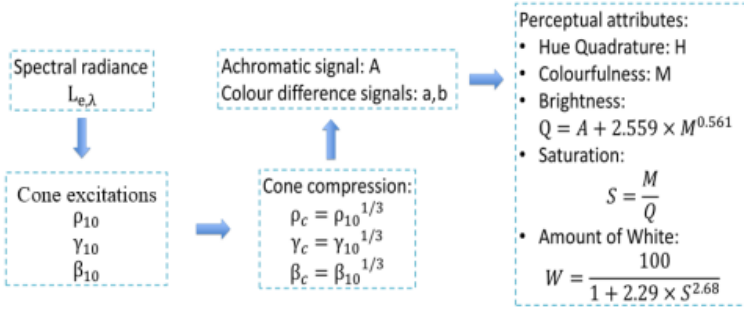


Figure 1.9: Schematic of CAM15u [41]

In CAM15u, the input is the spectral radiance of the 10° stimulus. From the spectral radiance, to simulate the response of the photoreceptors at the eye, the absolute normalized cone excitations (ρ , γ and β) are calculated using the CIE 2006 cone fundamentals $\bar{l}_{10}(\lambda)$, $\bar{m}_{10}(\lambda)$ and $\bar{s}_{10}(\lambda)$ as follows:

$$\begin{aligned}
 \rho &= k_\rho \int_{390}^{830} L_{e,\lambda}(\lambda) \bar{l}_{10}(\lambda) d\lambda \\
 \gamma &= k_\gamma \int_{390}^{830} L_{e,\lambda}(\lambda) \bar{m}_{10}(\lambda) d\lambda \\
 \beta &= k_\beta \int_{390}^{830} L_{e,\lambda}(\lambda) \bar{s}_{10}(\lambda) d\lambda
 \end{aligned} \tag{1.2}$$

in which $L_{e,\lambda}(\lambda)$ represents the spectral radiance of the stimulus. The coefficients k_ρ , k_γ and k_β are the normalization factors such that the cone excitations of the equal-energy white (EEW) stimulus are identical to the nominal value of the CIE 1964 10° luminance of that EEW stimulus.

For CAM15u, these coefficients are $k_\rho = 666.7$, $k_\gamma = 782.3$ and $k_\beta = 1444.6$.

Once the absolute cone excitations are computed, the compressed cone responses are obtained to model the visual adaptation process using the cubic root as follows:

$$\begin{aligned}\rho_c &= \rho_{10}^{1/3} \\ \gamma_c &= \gamma_{10}^{1/3} \\ \beta_c &= \beta_{10}^{1/3}\end{aligned}\tag{1.3}$$

After that, the achromatic signal is calculated as a weighted sum of the compressed cone responses. Though there are huge individual differences between observers, the ratio 40:20:1 is estimated to be the best average for the cone distributions in the retina [28,29].

$$A = 3.22 \left(2\rho_c + \gamma_c + \frac{1}{20}\beta_c \right)\tag{1.4}$$

The color-opponent signals a and b are computed following the proposal by Hunt [30]:

$$\begin{aligned}a &= \left(\rho_c - \frac{12}{11}\gamma_c + \frac{\beta_c}{11} \right) \\ b &= 0.117(\rho_c + \gamma_c - 2\beta_c)\end{aligned}\tag{1.5}$$

The perceptual attributes are then obtained from the achromatic signal and the color-opponent signals. The computation of perceptual attributes starts with calculating the hue angle h and the hue quadrature H . The hue angle, h , is taken as the inverse tangent of the color opponent signals:

$$h = \frac{180}{\pi} \tan^{-1}(b/a)\tag{1.6}$$

To transform the hue representation into a quadrature scale, a linear transformation is used to convert the hue angle h from a 0° - 360° range to a 0-400 range:

$$H = H_i + 100 \frac{h' - h_i}{h_{i+1} - h_i} \quad (1.7)$$

With h_i is the unique hue angle obtained from Table 1.1, H_i is the unique hue quadrature, $h' = h + 360$ if h is less than h_1 , otherwise $h' = h$, and a value of i is chosen so that $h_i \leq h' \leq h_{i+1}$.

Table 1.1: Overview of the unique hue data used for the calculation of the hue quadrature.

Unique hue	Red	Yellow	Green	Blue	Red
i	1	2	3	4	5
h_i	20.14°	90.00°	164.25°	237.53°	380.14°
H_i	0.0	100.0	200.0	300.0	400.0

The colorfulness, M , is determined by the strength of the color opponent signals a and b :

$$M = 135.52 \sqrt{(a^2 + b^2)} \quad (1.8)$$

As the brightness perception is influenced not only by the achromatic signal but also by the colorfulness of the stimulus (cf. Helmholtz-Kohlrausch (H-K) effect), the brightness in CAM15u is estimated as a function of the achromatic signal and the colorfulness:

$$Q = A + 2.559M^{0.561} \quad (1.9)$$

The parameters 2.559 and 0.561 are the factors that determine the strength of the H-K effect.

By definition, saturation is determined as the colorfulness judged in proportion to the brightness:

$$S = \frac{M}{Q} \quad (1.10)$$

While collecting the data for developing the model, it was noticed that for naïve observers, it was relatively easier to evaluate colorfulness by rating the "amount of white versus non-white" rather than using the

traditional definition of colorfulness by the CIE. This motivates the use of a new attribute, "amount of white" (the percentage of white seen within the stimulus), which can be easily assessed by naïve observers to increase the relevance of CAM's applications. This amount of white is found to follow a sigmoidal behavior as a function of the saturation:

$$W = \frac{100}{1 + 2.29s^{2.68}} \quad (1.11)$$

CAM18sl

Despite an extensive number of existing CAMs, there are still some challenges to applying such CAMs to related self-luminous stimuli: the underestimation of the H-K effect [51] and the ambiguity of the reference white point definition. To overcome the underestimation of the H-K effect, CAM15u [51] was specifically established for self-luminous stimuli. However, the application of the model is still limited to unrelated stimuli. This inspired the development of CAM18sl [50], a color appearance model for related self-luminous stimuli (as referred to in the overview of Figure 1.8).

Similar to CAM15u, CAM18sl also uses the spectral radiance of the stimulus and of the background as the input. Then, the absolute normalized cone excitations representing the responses of the photoreceptors for both stimulus and background are computed with the CIE 2006 cone fundamentals:

$$\begin{aligned} \rho &= 676.7 \int_{390}^{830} L_{e,\lambda}(\lambda) \bar{l}_{10}(\lambda) d\lambda \\ \gamma &= 794.0 \int_{390}^{830} L_{e,\lambda}(\lambda) \bar{m}_{10}(\lambda) d\lambda \\ \beta &= 1461.5 \int_{390}^{830} L_{e,\lambda}(\lambda) \bar{s}_{10}(\lambda) d\lambda \end{aligned} \quad (1.12)$$

The normalization coefficients are chosen such that the cone excitations of the EEW stimulus are identical to the nominal value of the CIE 2006 10° luminance of that EEW stimulus.

As the model is used for related self-luminous stimuli, the next step in the model is to account for chromatic adaptation. With the reference white point chosen as the EEW of the same luminance as the 4000 K test white background used in the experiments by Hermans et al. [50], the corresponding colors of the stimuli are calculated using the von Kries coefficient rule [33] in the CIE 2006 LMS cone space as follows:

$$\begin{bmatrix} \rho_c \\ \gamma_c \\ \beta_c \end{bmatrix} = \begin{bmatrix} \rho_{wr}/\rho_B & 0 & 0 \\ 0 & \gamma_{wr}/\gamma_B & 0 \\ 0 & 0 & \beta_{wr}/\beta_B \end{bmatrix} \begin{bmatrix} \rho \\ \gamma \\ \beta \end{bmatrix} \quad (1.13)$$

With $(\rho_{wr}, \gamma_{wr}$ and $\beta_{wr})$ are the mutual equal cone responses of the EEW reference white point at the same luminance as the test white, $(\rho_B, \gamma_B$ and $\beta_B)$ are the cone responses of the background which served as the test white and $(\rho_c, \gamma_c$ and $\beta_c)$ are the cone responses of the corresponding colors of the stimuli.

In the case of unrelated stimuli (dark background), $(\rho_B, \gamma_B$ and $\beta_B)$ are chosen the same as the cone responses of EEW as the EEW is still a valid reference white for near dark backgrounds [35]. As a result, the adaptation matrix turns into an identity matrix with the diagonal elements equal to 1.

After chromatic adaptation, the compressed cone responses and adaptive shifts are determined to illustrate the result of the visual adaptation process. As primates' cone responses follow a sigmoidal curve [38], the Michaelis-Menten equation [40] is used to compute the compressed cone response and it represents the shift caused by the level of adaptation of the cones in the retina.

$$\begin{aligned}
\rho_{c,a} &= \frac{\rho_c^{0.58}}{\rho_c^{0.58} + (291.20 + 71.8\alpha_{wr}^{0.78})^{0.58}} \\
\gamma_{c,a} &= \frac{\gamma_c^{0.58}}{\gamma_c^{0.58} + (291.20 + 71.8\alpha_{wr}^{0.78})^{0.58}} \\
\beta_{c,a} &= \frac{\beta_c^{0.58}}{\beta_c^{0.58} + (291.20 + 71.8\alpha_{wr}^{0.78})^{0.58}}
\end{aligned} \tag{1.14}$$

with $\rho_{c,a}$, $\gamma_{c,a}$ and $\beta_{c,a}$ are the adapted cone responses of the corresponding color of the stimulus. The adaptive shift is represented by α_{wr} , which is equal to $\rho_{wr} = \gamma_{wr} = \beta_{wr}$, and it represents the strength of the impact of the background.

Once the compressed and adapted cone signals are obtained, the color opponent signals can be calculated. Similar to other CAMs, the color opponent signals a and b are defined as follows:

$$\begin{aligned}
a &= 0.63 \left(\rho_{c,a} - \frac{12}{11} \gamma_{c,a} + \frac{\beta_{c,a}}{11} \right) \\
b &= 0.12 (\rho_{c,a} + \gamma_{c,a} - 2\beta_{c,a})
\end{aligned} \tag{1.15}$$

From the color opponent signals, the hue angle, h , can be deduced [30,56].:

$$h = \frac{180}{\pi} \tan^{-1}(b / a) \tag{1.16}$$

The hue quadrature is then calculated as the linear transformation from the hue angle as:

$$H = H_i + 100 \frac{h' - h_i}{h_{i+1} - h_i} \tag{1.17}$$

With h_i is the unique hue angle and H_i is the unique hue quadrature, the values of which are mentioned in Table 1. From the color opponent signals, the colorfulness M can be obtained:

$$M = 3260 \sqrt{a^2 + b^2} \tag{1.18}$$

To compute brightness Q , the achromatic signal needs to be determined as:

$$A = \left(2\rho_{c,a} + \gamma_{c,a} + \frac{1}{20}\beta_{c,a} \right) \quad (1.19)$$

Then, the brightness, including the H-K effect, can be calculated as:

$$Q = 0.937 \left(A + 0.0024M^{1.09} \right) \quad (1.20)$$

Saturation is computed as the ratio between colorfulness and brightness:

$$S = \frac{M}{Q} \quad (1.21)$$

In CAM97u and CAM15u, brightness was not expressed with any particular unit, and in CIECAM02, the concept of absolute brightness is also not yet used. In CAM18sl, an absolute brightness unit, *bright*, is introduced. 1 *bright* is defined as the brightness of an EEW 10° stimulus of 100 cd/m² on a dark background of 0 cd/m².

1.4.3. Image Color Appearance Models

The color appearance models discussed above investigate the appearance of a single uniform stimulus under a specific viewing condition and a uniform background. However, in a real situation, color is usually perceived in a much more complex scene than just a uniform stimulus on a uniform background and a surrounding environment. It results in the need to have a color appearance model which also considers spatial information. Johnson and Fairchild [57] proposed S-CIELAB, which predicts the color appearance for image reproduction. In 2002, Fairchild and Johnson [58] introduced an image color appearance model (iCAM) to predict different perception phenomena in a complex scene. Not long after, in 2006, Kuang et al. [59] proposed an image appearance model based on the iCAM framework, the so-called iCAM06, which is used for High Dynamic Range (HDR) image rendering. Also targeting HDR image rendering, Reinhard et al. introduced a calibrated image appearance model in 2012 [60]. A

summary of existing image CAMs is given in Figure 1.10. As can be observed, in contrast to Figure 1.8, it seems that today no image Color Appearance Models for self-luminous colors do exist.

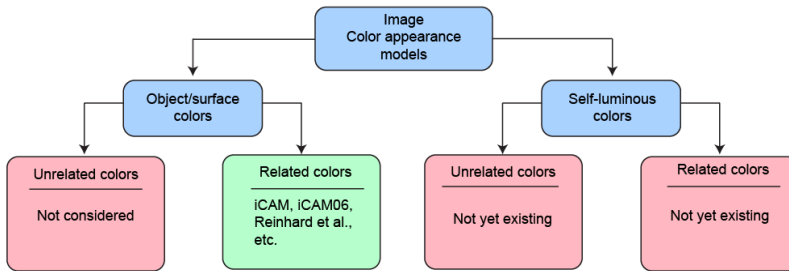


Figure 1.10: Image CAM classification

iCAM

Among the discussed image CAMs, iCAM is one of the earliest proposed models, which established the foundation for the development of later image CAMs such as iCAM06 [59]. By considering a spatially dependent transformation, iCAM can output visual attributes for each pixel from an input (X, Y, Z) image. In this section, the details of the iCAM framework [58] with the general workflow, as illustrated in Figure 1.11 are presented.

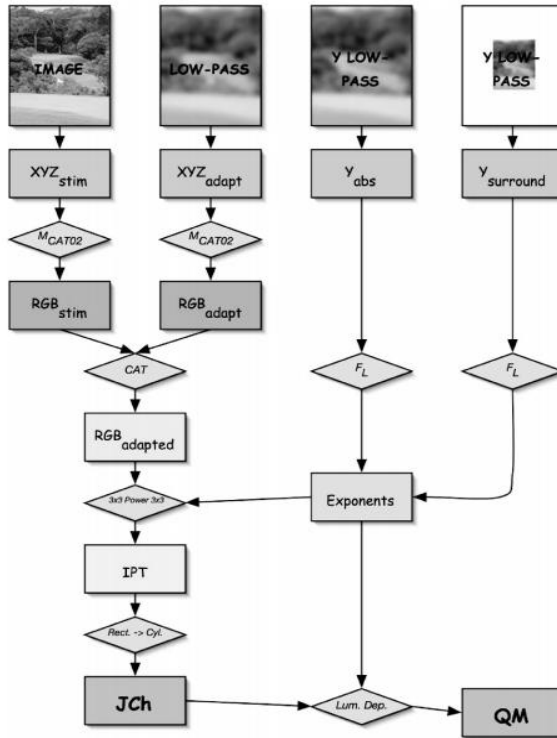


Figure 1.11: iCAM framework [58]

The model starts with taking an image in relative XYZ tristimulus values provided with absolute luminance units as the input (XYZ_{stim}); a Gaussian low-pass filter is applied to the XYZ image to account for the spatial dependencies and serve as the adapting stimulus in the chromatic adaptation transformation (XYZ_{adapt}). The low-pass absolute luminance image (Y_{abs}) is also used to compute the degree of adaptation (D) and to control multiple luminance-dependent effects such as Hunt and Stevens effect. For more complex situations, the surround luminance ($Y_{surround}$) can be computed from another low-pass image from a larger spatial scale.

The input image and low-pass blurred image are then transformed into spectrally sharpened RGB responses with a linear transformation as:

$$\begin{bmatrix} R \\ G \\ B \end{bmatrix} = M_{CAT02} \begin{bmatrix} X \\ Y \\ Z \end{bmatrix}, \text{ where } M_{CAT02} = \begin{bmatrix} 0.7328 & 0.4296 & -0.1624 \\ -0.7036 & 1.6975 & 0.0061 \\ 0.0030 & 0.0136 & 0.9834 \end{bmatrix} \quad (1.22)$$

After this conversion, the chromatic adaptation transformation (CAT) is performed using a linear von Kries transformation used in CIECAM02.

The degree of adaptation (D) is computed as a function of the adapting luminance L_A and the surround factor F :

$$D = F \left[1 - \left(\frac{1}{3.6} \right) e^{\left(\frac{-(L_A - 42)}{92} \right)} \right] \quad (1.23)$$

A map of L_A for each pixel is computed as 20% of the low-pass absolute luminance image and F is taken equal to 1 (average surround). The pixel-by-pixel corresponding colors of each pixel for a D65 reference white are computed as shown in equation (1.24):

$$\begin{pmatrix} R_{adapted} \\ G_{adapted} \\ B_{adapted} \end{pmatrix} = D \begin{pmatrix} R_{D65}/R_{adapt} & 0 & 0 \\ 0 & G_{D65}/G_{adapt} & 0 \\ 0 & 0 & B_{D65}/B_{adapt} \end{pmatrix} + (1 - D) \begin{pmatrix} R_{stim} \\ G_{stim} \\ B_{stim} \end{pmatrix} \quad (1.24)$$

with $R_{adapt} G_{adapt} B_{adapt}$ taken from the low-pass filtered image (XYZ_{adapt}) and with $R_{D65} G_{D65} B_{D65}$ being the relative normalized RGB tristimulus values of the D65 reference illuminant for the supplementary 2° observer.

The factor F_L for considering the luminance-dependent effects in the later stage of the model is computed with the low-pass filtered absolute luminance image as:

$$F_L = 0.2 \left[\frac{1}{5L_A + 1} \right]^4 (5L_A) + 0.1 \left\{ 1 - \left[\frac{1}{5L_A + 1} \right]^4 \right\}^2 (5L_A)^{\frac{1}{3}} \quad (1.25)$$

The corresponding colors of each pixel of the image after chromatic adaptation transformation is then converted back to $X_{adapted} Y_{adapted} Z_{adapted}$ and then into LMS cone space before it is transformed into the *IPT* opponent color space:

$$\begin{bmatrix} L \\ M \\ S \end{bmatrix} = \begin{bmatrix} 0.4002 & 0.7075 & -0.0807 \\ -0.2280 & 1.1500 & 0.0612 \\ 0 & 0 & 0.9184 \end{bmatrix} \begin{bmatrix} X_{adapted} \\ Y_{adapted} \\ Z_{adapted} \end{bmatrix} \quad (1.26)$$

$$\begin{bmatrix} L' \\ M' \\ S' \end{bmatrix} = \begin{bmatrix} L \\ M \\ S \end{bmatrix}^{0.43} \quad (1.27)$$

$$\begin{bmatrix} I \\ P \\ T \end{bmatrix} = \begin{bmatrix} 0.4000 & 0.4000 & 0.2000 \\ 4.4550 & -4.8510 & 0.3960 \\ 0.8056 & 0.3572 & -1.1628 \end{bmatrix} \begin{bmatrix} L' \\ M' \\ S' \end{bmatrix} \quad (1.28)$$

The color appearance parameters (Lightness (J), Chroma (C) hue angle (h), Brightness (Q) and Colorfulness (M)) can be obtained by converting the rectangular *IPT* coordinates into cylindrical coordinates as in Eqs. (1.29-1.33):

$$J = I \quad (1.29)$$

$$C = \sqrt{P^2 + T^2} \quad (1.30)$$

$$h = \tan^{-1}\left(\frac{P}{T}\right) \quad (1.31)$$

$$Q = \sqrt[4]{F_L J} \quad (1.32)$$

$$M = \sqrt[4]{F_L C} \quad (1.33)$$

1.5. A next-generation color appearance model for self-luminous stimuli

1.5.1. Introduction

Thanks to the advancement of technology, the lighting industry has rapidly grown with new possibilities to manipulate the spectrum (with new phosphors and quantum dots) and the spatial light distribution (with free-form optics and OLEDs). According to the European Photonics roadmap, this evolution has offered "as yet unexplored new opportunities for new, value-added lighting applications, offering energy savings, superior lighting control for context-dependent lighting, improved quality of light, and increased functionalities such as adaptive lighting" [61]. As a result, while energy efficiency remains an important domain in lighting research, there has been a major shift in the research interest towards lighting quality, safety, comfort and personalized/smart lighting. More and more studies have been performed to investigate the topics of glare for non-uniform luminaires [62,63], functional contrasts [64–66], preference [67,68], saturation and age-dependent lighting requirements [69,70]. For applications such as museum, retail and office lightings, attentions have been given towards tunable light spectra and optimized design solutions [71–74].

Despite a well-defined range of opportunities and applications, the knowledge, tools and models required to determine the photometric and colorimetric specifications which can comply to the expected

lighting quality and the visual experience of the total lit environment from the end-user having a particular age are still missing. This calls for a shift from an illuminance-based design to a spectral radiance-based design [75–78]. The first small yet essential step to achieve this ambitious goal is to develop a color appearance model which can predict the visual perception and appearance of self-luminous elements within a scene.

As previously discussed, even though many CAMs have been proposed for simple stimulus-background situations of surface colors [36,42–44,46] and self-luminous stimuli [50,51], image-based CAMs for complex scenes are still restricted mainly to surface colors [57–60] (Figure 1.10). This leads to the need for a new, comprehensive color appearance model which properly considers the spatial complexity of the self-luminous scenes.

1.5.2. Lighting Appearance Model

The evolution of retina models and imaging techniques has motivated the development of more physiologically-based models for different applications such as image processing [24], HDR image rendering [79] and glare prediction for non-uniform light sources [62]. The available knowledge, together with the demand of having a more comprehensive model for color appearance prediction for light sources, have inspired our research group's long-term goal of developing a Lighting Appearance Model (LAM), a next-generation appearance model inspired by the physiologically-based retinal networks which can predict the appearance of surface colors and light sources in complex scenes. The main framework of such a LAM is illustrated in Figure 1.12.

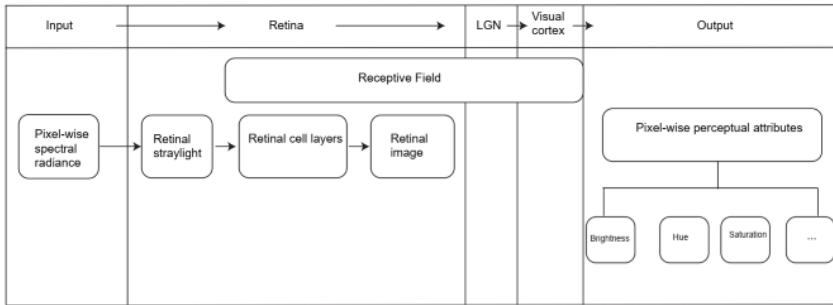


Figure 1.12: A Lighting Appearance Model structure

The LAM should start with an input image that contains the complete optical specification of each pixel of the scene. With the development of hyperspectral imaging, it is now possible to have a pixel-wise spectral radiance map. A hyperspectral image is typically represented as a data cube with spatial information saved in two dimensions, while the third dimension stores the spectral information at each pixel location (Figure 1.13) [80]. By having access to the spectral information of each pixel, it is possible to perform various manipulations to achieve perceptually related pixel-by-pixel data such as cone excitations and intrinsic photosensitive Retinal Ganglion Cells (ipRGCs) response.

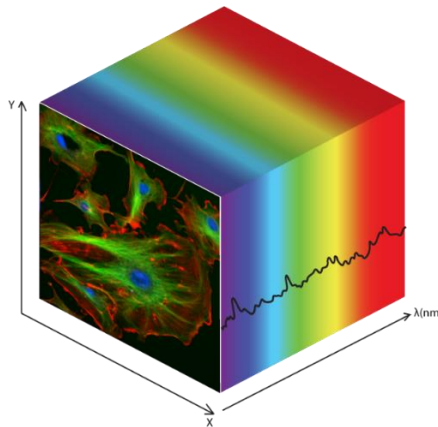


Figure 1.13: Hyperspectral Data Cube [81]

From the input image, several visual processing steps based on the physiology of the human visual system from the retina to the brain

should be taken. First, the image formation of the scene in the object space onto the retina has to be considered, including pupil diameter, absorption in the ocular media and the correction for intraocular straylight. As at each retinal location, there is only one cone and as the cone density can change over the eccentricity, the next step is to resample the retinal image as three cone mosaic images [82]. After that, light absorption by the cones, followed by cone compression should be taken into account. Then, several stages of processing at different retinal cell layers, from cones to horizontal cells to ganglion cells, will be simulated with the receptive field models. The processed signals from the retina, which are sent through the Lateral Geniculate Nucleus (LGN) to the visual cortex (V1-V5) in the brain [1], will then be modeled with the neural networks. The output of a LAM will be a set of pixel-by-pixel perceptual attributes such as brightness, lightness, chroma, hue, colorfulness, saturation and amount of white.

To achieve such an ambitious goal, a wide range of topics will need to be studied. First and foremost, it is crucial to understand the structure and the mechanisms of human visual systems by investigating the topics such as retinal straylight, cone mosaic, retina modeling, visual adaptation and visual receptive fields. Additionally, the principles and current technologies of capturing and processing hyperspectral images should also be investigated. The available resources in retinal straylight modeling [83–85], retina receptive field [86–88], retina simulation [15,89] and hyperspectral imaging [90] can provide valuable insights to develop such a physiologically-based framework.

1.5.3. Main goal of this doctoral research

As the first step to move toward a LAM, the main goal of this doctoral research is to consider a non-image and an image CAM for related self-luminous stimuli but restricted to achromatic stimuli (which are also interchangeably referred to as "neutral stimuli" in later chapters) and to the brightness attribute only.

The first step is to evaluate the possibility of applying an existing image CAM for object colors to self-luminous scenes. The performance of iCAM on simple self-luminous scenes for different scenarios, such as brightness perception in achromatic self-luminous scenes, the H-K effect, the stimulus size effect and background size effect, is assessed. Next, the possible extension of CAM18sl (non-imaging CAM for self-

luminous stimuli) to a more complex background is investigated. To do so, the impact of various parts from a uniform background at different luminance levels is studied by isolating a ring-shaped section in the background. This allows an equal impact of the distance of the background element from all directions on the brightness of the central stimulus to be observed. Based on the experimental result, a brightness model for achromatic self-luminous stimuli seen on a non-uniform background is developed using the traditional stimulus-background approach. Afterward, to extend the applications of the model to scenes with higher complexity, an image-based approach to tackle the same problem is proposed. Finally, preliminary studies are conducted to extend the applications of the proposed model to chromatic background situations.

The modeling is performed based on visual data collected with psychophysical experiments and physical data collected with spectral radiometric measurements. The details of the experimental procedures are provided in the respective chapters of this dissertation.

1.5.4. Applications

An image color appearance model for self-luminous stimuli or LAM would be useful for a wide range of applications.

Such a model will facilitate lighting design to move forward from the traditional illuminance-based design to a better evaluation of the quality of lighting in terms of glare (closely related to brightness) and contrast and will provide an interesting and valuable instrument to describe the visual experience of the total lit environment, indoor as well as outdoor. For outdoor applications such as road lighting and signalization, such a model will become the tool to explore the limits of energy consumption while maintaining safety standards (e.g., contrast thresholds).

Finally, the availability of a reliable and robust LAM can be used to enhance the experience of Virtual Reality devices, which will soon become an essential tool for lighting design, diagnostic testing and retail applications.

1.5.5. Overview

In Chapter 2, the performance of iCAM when applied to simple self-luminous scenes is evaluated on various aspects such as brightness perception in achromatic self-luminous scenes, the H-K effect, the stimulus size effect and the background size effect.

Chapter 3 presents a model predicting the influence of different parts from a uniform background, exemplified as an achromatic self-luminous ring, on the perceived brightness of an achromatic self-luminous stimulus.

In Chapter 4, an image-based brightness model, which includes straylight correction, is proposed to predict the observed phenomenon in Chapter 3.

Chapter 5 discusses the preliminary experimental results investigating the impact of a colored self-luminous ring on the perceived brightness of an achromatic self-luminous stimulus.

In Chapter 6, the valorization of this PhD research is presented as an exploitation plan describing the collaboration between KU Leuven and Schréder to develop a new tool for assessing the quality of street lighting design with a focus on an image-based glare prediction.

Chapter 7 provides an overview of the major achievements and contributions of this doctoral research, and suggestions for future works are presented.

1.6. References for Chapter 1

1. M. D. Fairchild, *Color Appearance Models*, 2nd ed. (John Wiley & Sons, Ltd, 2013).
2. A. Stockman and L. T. Sharpe, "The spectral sensitivities of the middle- and long-wavelength-sensitive cones derived from measurements in observers of known genotype," *Vision Res.* **40**, 1711–1737 (2000).
3. J. Carroll, J. Neitz, and M. Neitz, "Estimates of L:M cone ratio from ERG flicker photometry and genetics," *J. Vis.* **2**, 531–542 (2002).
4. J. Héroult and B. Durette, "Modeling Visual Perception for Image Processing," in *Computational and Ambient Intelligence* (Springer Berlin Heidelberg, 2007), pp. 662–675.
5. D. M. Berson, "Phototransduction by Retinal Ganglion Cells That Set the Circadian Clock," *Science* (80-.). **295**, 1070–1073 (2002).
6. S. Hattar, H. W. Liao, M. Takao, D. M. Berson, and K. W. Yau, "Melanopsin-containing retinal ganglion cells: architecture, projections, and intrinsic photosensitivity,," *Science* **295**, 1065–70 (2002).
7. E. Mach, "Über den Einfluss raumlich und zeitlich variierender Lichtreize auf die Gesichtswahrnehmung," *Sitzungsberichte der Math. Klasse der Kais. Akad. der Wissenschaften* (Ratlioff, 1965, Transl. **115**, 633–648 (1906).
8. C. Enroth-Cugell and J. G. Robson, "The contrast sensitivity of retinal ganglion cells of the cat," *J. Physiol.* 517–552 (1966).
9. K. I. Naka and W. A. Rushton, "The generation and spread of s-potentials in fish (cyprinidae)," *J. Physiol.* **192**, 437–461 (1967).
10. M. H. Hennig, K. Funke, and F. Wörgötter, "The influence of different retinal subcircuits on the nonlinearity of ganglion cell behavior.," *J. Neurosci.* **22**, 8726–38 (2002).
11. J. H. van Hateren, L. Rüttiger, H. Sun, and B. B. Lee, "Processing of natural temporal stimuli by macaque retinal ganglion cells," *J. Neurosci.* **22**, 9945–9960 (2002).

12. J. H. van Hateren, "A cellular and molecular model of response kinetics and adaptation in primate cones and horizontal cells," *J. Vis.* **5**, 331–347 (2005).
13. J. H. van Hateren and H. P. Snippe, "Simulating human cones from mid-mesopic up to high-photopic luminances," *J. Vis.* **7**, 1–1 (2007).
14. M. Kamermans, D. A. Kraaij, and H. Spekreijse, "The cone/horizontal cell network: a possible site for color constancy," *Vis. Neurosci.* **15**, 787–797 (1998).
15. A. Wohrer and P. Kornprobst, "Virtual Retina: A biological retina model and simulator, with contrast gain control," *J. Comput. Neurosci.* **25**, 219–249 (2009).
16. J. Decuyper, J.-L. Capron, T. Dutoit, and M. Renglet, "Implementation of a Retina Model Extended to Mesopic Vision," in *Proceedings of the 27th Session of the CIE : Sun City, South Africa, 10 July - 15 July 2011 Vol. 1* (CIE Central Bureau, 2011).
17. P. Martínez-Cañada, C. Morillas, and F. Pelayo, "A Conductance-Based Neuronal Network Model for Color Coding in the Primate Foveal Retina," *Lect. Notes Comput. Sci.* **2**, 63–74 (2017).
18. R. J. Watt and M. J. Morgan, "A theory of the primitive spatial code in human vision," *Vision Res.* **25**, 1661–1674 (1985).
19. F. Kingdom and B. Moulden, "A multi-channel approach to brightness coding," *Vision Res.* **32**, 1565–1582 (1992).
20. G. Schouten, "Luminance-Brightness Mapping: the Missing Decades," Eindhoven: Technische Universiteit Eindhoven (1993).
21. J. A. McArthur and B. Moulden, "A two-dimensional model of brightness perception based on spatial filtering consistent with retinal processing," *Vision Res.* **39**, 1199–1219 (1999).
22. J. Héroult, "A model of colour processing in the retina of vertebrates: From photoreceptors to colour opposition and colour constancy phenomena," *Neurocomputing* **12**, 113–129 (1996).

23. R. L. De Valois and K. K. De Valois, "A multi-stage color model," *Vision Res.* **33**, 1053–1065 (1993).
24. J. Héroult and B. Durette, "Modeling visual perception for image processing," in *Lecture Notes in Computer Science (Including Subseries Lecture Notes in Artificial Intelligence and Lecture Notes in Bioinformatics)* (Springer Berlin Heidelberg, 2007), Vol. 4507 LNCS, pp. 662–675.
25. L. Meylan, D. Alleysson, and S. Süsstrunk, "Model of retinal local adaptation for the tone mapping of color filter array images," *J. Opt. Soc. Am. A* **24**, 2807 (2007).
26. CIE Central Bureau: Vienna Austria, "CIE S 017/E:2020: ILV: CIE International Lighting Vocabulary," **CIE S 017/**, (2020).
27. L. M. Hurvich and D. Jameson, "An opponent-process theory of color vision," *Psychol. Rev.* **64**, 384–404 (1957).
28. J. Carroll, J. Neitz, and M. Neitz, "Estimates of L:M cone ratio from ERG flicker photometry and genetics," *J. Vis.* **2**, 531–542 (2002).
29. J. J. Vos and P. L. Walraven, "On the derivation of the foveal receptor primaries," *Vision Res.* **11**, 799–818 (1971).
30. R. W. G. Hunt and M. Pointer, *Measuring Colour*, 4th ed. (Wiley, 2011).
31. C. W. G. Clifford, M. A. Webster, G. B. Stanley, A. A. Stocker, A. Kohn, T. O. Sharpee, and O. Schwartz, "Visual adaptation: Neural, psychological and computational aspects," *Vision Res.* **47**, 3125–3131 (2007).
32. M. D. Fairchild, *Color Appearance Models* (2005).
33. J. von Kries, "Theoretische Studien über die Umstimmung des Sehorgans.," *Festschrift der Albrecht-Ludwigs-Universität Freibg.* 143–158 (1902).
34. K. Smet, Q. Zhai, R. M. Luo, and P. Hanselaer, "Investigating chromatic adaptation using memory colours," in *Proc. of the 4th Symposium on Colour and Visual Appearance* (CIE; Vienna, 2016).
35. K. A. G. Smet, Q. Zhai, M. R. Luo, and P. Hanselaer, "Study

- of chromatic adaptation using memory color matches, Part I: neutral illuminants," *Opt. Express* **25**, 7732–7748 (2017).
36. N. Moroney, M. D. Fairchild, R. W. Hunt, C. Li, M. Ronnier Luo, and T. Newman, "The CIECAM02 color appearance model," in *10th Color and Imaging Conference Final Program and Proceedings* (2002), pp. 23–27.
 37. E. Brittanica, "Sensory Reception: Human Vision: Structure and function of the Human Eye," *Encycl. Brittanica* **27**, 179 (1987).
 38. J. M. Valeton and D. van Norren, "Light adaptation of primate cones: an analysis based on extracellular data," *Vision Res.* **23**, 1539–1547 (1983).
 39. J. M. Valeton, "Photoreceptor light adaptation models: An evaluation," *Vision Res.* **23**, 1549–1554 (1983).
 40. V. L. Michaelis, M. L. Maud Menten, R. S. Goody, and K. A. Johnson, "Die Kinetik der Invertinwirkung The Kinetics of Invertase Action," *Biochem. Z.* **49**, 333–369 (1913).
 41. S. Hermans, "Modelling the perception of light sources," KU Leuven (2019).
 42. Y. Nayatani, K. Takahama, and H. Sobagaki, "Prediction of color appearance under various adapting conditions," *Color Res. Appl.* (1986).
 43. R. W. G. Hunt, *The Reproduction of Colour* (John Wiley & Sons, Ltd, 2005).
 44. M. R. Luo and R. W. G. Hunt, "The structure of the CIE 1997 colour appearance model (CIECAM97s)," *Color Res. Appl.* **23**, 138–146 (1998).
 45. C. Gao, C. Li, K. Shi, M. R. Luo, and M. R. Pointer, "CAM20u: An extension of CAM16 for predicting the color appearance of unrelated colors," *Color Res. Appl.* **46**, 749–758 (2021).
 46. C. Li, Z. Li, Z. Wang, Y. Xu, M. R. Luo, G. Cui, M. Melgosa, M. H. Brill, and M. Pointer, "Comprehensive color solutions: CAM16, CAT16, and CAM16-UCS," *Color Res. Appl.* **42**, 703–718 (2017).

47. M. Kim, J.-H. Jo, Y. Park, and S.-W. Lee, "Amendment of CIECAM02 with a technical extension to compensate Helmholtz-Kohlrausch effect for chromatic characterization of display devices," *Displays* (2018).
48. K. Xiao, M. R. Luo, and C. Li, "Colour size effect modelling," *Color Res. Appl.* **37**, 4–12 (2012).
49. K. Xiao, M. R. Luo, C. Li, G. Cui, and D. Park, "Investigation of colour size effect for colour appearance assessment," *Color Res. Appl.* **36**, 201–209 (2011).
50. S. Hermans, K. A. G. Smet, and P. Hanselaer, "Color appearance model for self-luminous stimuli," *J. Opt. Soc. Am. A* **35**, 2000–2009 (2018).
51. M. Withouck, K. A. G. Smet, W. R. Ryckaert, and P. Hanselaer, "Experimental driven modelling of the color appearance of unrelated self-luminous stimuli: CAM15u," *Opt. Express* **23**, 12045 (2015).
52. R. W. G. Hunt, "A model of colour vision for predicting colour appearance," *Color Res. Appl.* **7**, 95–112 (1982).
53. R. W. G. Hunt, "Revised colour-appearance model for related and unrelated colours," *Color Res. Appl.* **16**, 146–165 (1991).
54. C. Fu, C. Li, G. Cui, M. R. Luo, R. W. G. Hunt, and M. R. Pointer, "An investigation of colour appearance for unrelated colours under photopic and mesopic vision," *Color Res. Appl.* **37**, 238–254 (2012).
55. M. Withouck, K. A. G. Smet, W. R. Ryckaert, M. R. Pointer, G. Deconinck, J. Koenderink, and P. Hanselaer, "Brightness perception of unrelated self-luminous colors," *J. Opt. Soc. Am. A* **30**, 1248 (2013).
56. M. H. Kim, T. Weyrich, and J. Kautz, "Modeling human color perception under extended luminance levels," in *ACM Transactions on Graphics* (2009), Vol. 28, p. 1.
57. G. M. Johnson and M. D. Fairchild, "A Top Down Description of S-CIELAB and CIEDE2000," *Col Res Appl* **28**, 425–435 (2003).
58. M. D. Fairchild and G. M. Johnson, "Meet iCAM: A next-

- generation color appearance model," in *10th Color and Imaging Conference Final Program and Proceedings* (2002), pp. 33–38.
59. J. Kuang, G. M. Johnson, and M. D. Fairchild, "iCAM06: A refined image appearance model for HDR image rendering," *J. Vis. Commun. Image Represent.* **18**, 406–414 (2007).
 60. E. Reinhard, T. Pouli, T. Kunkel, B. Long, A. Ballestad, and G. Damberg, "Calibrated image appearance reproduction," *ACM Trans. Graph.* **31**, 1–11 (2012).
 61. European Technology Platform Photonics21, "Towards 2020 – Photonics driving economic growth in Europe," 108 (2013).
 62. G. H. Scheir, P. Hanselaer, and W. R. Ryckaert, "Pupillary light reflex, receptive field mechanism and correction for retinal position for the assessment of visual discomfort," *Lighting Research and Technology* (2017).
 63. M. Safdar, M. R. Luo, M. F. Mughal, S. Kuai, Y. Yang, L. Fu, and X. Zhu, "A neural response-based model to predict discomfort glare from luminance image," *Light. Res. Technol.* **50**, 416–428 (2018).
 64. J. Ménard and J. Cariou, "Road lighting: Assessment of an installation based on the contrast of a standard target," *Light. Res. Technol.* **26**, 19–22 (1994).
 65. A. Ekrias, M. Eloholma, and L. Halonen, "Effects of Vehicle Headlights on Target Contrast in Road Lighting Environments," *J. Light Vis. Environ.* **32**, 302–314 (2008).
 66. A. Bacelar, J. Cariou, and M. Hamard, "Calculational visibility model for road lighting installations," *Light. Res. Technol.* **31**, 177–180 (1999).
 67. Y. Lin, M. Wei, K. A. G. Smet, A. Tsukitani, P. Bodrogi, and T. Q. Khanh, "Colour preference varies with lighting application," *Light. Res. Technol.* **49**, (2017).
 68. M. Davidovic, L. Djokic, A. Cabarkapa, A. Djuretic, V. Skerovic, and M. Kostic, "Drivers' Preference for the Color of LED Street Lighting," *IEEE Access* **7**, 72850–72861 (2019).
 69. P. C. Hughes and R. M. Neer, "LIGHTING FOR THE ELDERLY - A PSYCHOBIOLOGICAL APPROACH TO

- LIGHTING.," *Hum. Factors* **23**, 65–85 (1981).
70. W. Van Bommel, "Dynamic Lighting at work-both in level and colour," in *CIE* (2006).
 71. A. Hurlbert and C. Cuttle, "New Museum Lighting for People and Paintings," *LEUKOS - J. Illum. Eng. Soc. North Am.* **16**, 1–5 (2020).
 72. G. Clare and N. Hancer, "The Influence of Tunable LED Lighting Systems on Consumer Food Label Perceptions," *Food Nutr. Sci.* **07**, 566–576 (2016).
 73. X. F. Feng, W. Xu, Q. Y. Han, and S. D. Zhang, "Colour-enhanced light emitting diode light with high gamut area for retail lighting:," *Light. Res. Technol.* **49**, 329–342 (2015).
 74. F. J. Burgos-Fernández, M. Vilaseca, E. Perales, J. A. Herrera-Ramírez, F. M. Martínez-Verdú, and J. Pujol, "Spectrally tunable light source based on light-emitting diodes for custom lighting solutions," *Opt. Appl.* **46**, 117–129 (2016).
 75. Y. NAKAMURA, "Toward Effective Use of Luminance in Lighting Design," *Proc. 23rd Sess. CIE* (1995).
 76. M. N. Inanici and M. Navvab, "The Virtual Lighting Laboratory: Per-pixel Luminance Data Analysis," *Leukos* **3**, 89–104 (2006).
 77. L. C. Ou, M. R. Luo, A. Woodcock, and A. Wright, "A study of colour emotion and colour preference. Part III: Colour preference modeling," *Color Res. Appl.* **29**, 381–389 (2004).
 78. O. Masuda and S. M. C. Nascimento, "Best lighting for naturalness and preference.," *J. Vis.* **13**, 4 (2013).
 79. L. Meylan, D. Alleysson, and S. Süsstrunk, "Model of retinal local adaptation for the tone mapping of color filter array images," *J. Opt. Soc. Am. A* **24**, 2807 (2007).
 80. E. G and S. D, *Principles of Hyperspectral Imaging Technology* (Academic Press, 2010).
 81. "Hypespectral Imaging," <http://www.photonetc.com/hyperspectral-imaging>.
 82. D. H. Brainard, "Color and the Cone Mosaic," *Annu. Rev. Vis.*

Sci **1**, 519–565 (2015).

83. T. J. van den Berg, "Visual efficiency of scattering and fluorescence in the human eye lens," *J. Biomed. Opt.* **1**, 262 (1996).
84. T. J. T. P. van den Berg, L. Franssen, and J. E. Coppens, "Ocular Media Clarity and Straylight," in *Encyclopedia of the Eye* (Elsevier, 2010), pp. 173–183.
85. J. E. Coppens, L. Franssen, and T. J. T. P. van den Berg, "Wavelength dependence of intraocular straylight," *Exp. Eye Res.* **82**, 688–692 (2006).
86. L. Peichl and H. Wässle, "Size, scatter and coverage of ganglion cell receptive field centres in the cat retina.," *J. Physiol.* **291**, 117–141 (1979).
87. C. D. Gilbert and T. N. Wiesel, "Receptive field dynamics in adult primary visual cortex," *Nature* **356**, 150–152 (1992).
88. K. Amano, B. A. Wandell, and S. O. Dumoulin, "Visual field maps, population receptive field sizes, and visual field coverage in the human MT+ complex," *J. Neurophysiol.* **102**, 2704–2718 (2009).
89. B. Wandell, "Image systems engineering tools for biology: ISETBIO," *J. Vis.* **17**, 10–11 (2017).
90. D. H. Foster and K. Amano, "Hyperspectral imaging in color vision research: tutorial," *J. Opt. Soc. Am. A* **36**, 606 (2019).

Chapter 2

Assessing the application of an Image Color Appearance Model to basic self-luminous scenes

2. Assessing the application of an Image Color Appearance Model to basic self-luminous scenes

2.1. Introduction

Throughout the development of color science and its applications, multiple non-imaging color appearance models (CAMs) for object colors have been proposed, namely, the Nayatani et al. model [1], the Hunt model [2], CIECAM97s [3], CIECAM16 [4] and especially CIECAM02 [5], which is recommended by the CIE.

The availability of non-imaging color appearance models to predict the color perception of self-luminous stimuli such as luminaires, billboards, traffic signs, and displays is much more limited. The application of CIECAM02 to these types of stimuli encounters some challenges such as the ambiguity of the reference white [6] and the fact that the spectral radiance of the stimulus and the background are totally independent. To overcome these challenges, CAM15u [7] for unrelated self-luminous stimuli and the more general CAM18sl [6] for related self-luminous stimuli have been proposed.

These aforementioned CAMs were mainly developed based on the experimental data collected from a fairly simple viewing condition where a uniform stimulus is shown on a uniform background. Considering spatial complexity, a limited number of imaging CAMs which consider spatial information such as iCAM [8], S-CIELAB [9], iCAM06 [10], Reinhard et al. [11] have been proposed. Among these models, by outputting the perceptual attributes for each pixel from an input image, iCAM [8] is the most comparable to a traditional CAM, while being able to render HDR image and control image quality.

In this chapter, the performance of iCAM [8], in particular its brightness correlate, applied to simple self-luminous scenes is evaluated. After a summary of the iCAM framework, the results regarding the evaluation of brightness obtained with the model are compared to the outcome of non-imaging models applicable and dedicated to this kind of simple scenes. Attention is given to the predictive power of iCAM regarding the impact of the luminance of the background, the Helmholtz-Kohlrausch effect, the background size effect and stimulus size effect on the brightness of the stimulus. Two

filter kernel sizes are also implemented to examine the impact of changing the filter size in iCAM processing.

2.2. Main results and discussion

The results show that iCAM adopting a large kernel can well predict the effect of background and stimulus luminance on the perceived brightness. The model is also capable of estimating the background size effect in case of a combination of dark surround and bright background. However, there are limitations in predicting such effects when the stimuli are shown on a completely dark background due to the local adaptation determined by the low pass filtered image. Furthermore, iCAM also does not include the H-K effect and the stimulus size effect in its brightness prediction. These observations call for a new, more comprehensive imaging color appearance model dedicated to self-luminous scenes.

In hindsight, the current evaluation was performed on rather simple scenarios, which was not what iCAM was intended for. This can imply some limitations between the compatibility of the model and the provided data. Furthermore, it could have been greatly beneficial if evaluations of various spatial/image CAMs could have been performed. However, as most of existing spatial/image CAMs do not output a full set of perceptual attributes like traditional CAMs, this idea might encounter a few restrictions for correctly converting the current outputs to perceptual attributes.

The detailed description of the iCAM model and the evaluation of its performance for self-luminous scenes is presented in the following paper:

Phung, TH, Leloup, FB, Smet, KAG, Hanselaer, P. “**Assessing the application of an image color appearance model to basic self-luminous scenes**”. *Color Res Appl.* 2019; 44: 848– 858. <https://doi.org/10.1002/col.22414>.

The complete and unedited content of this paper is included in the following section.

2.3. Publication 1

Assessing the application of an Image Color Appearance Model to basic self-luminous scenes

Thanh Hang Phung (Msc.)¹: Thanhhang.Phung@kuleuven.be

Frédéric B. Leloup (Assoc. Prof.)¹: Frederic.Leloup@kuleuven.be

Kevin A.G. Smet (Assoc. Prof.)¹: Kevin.Smet@kuleuven.be

Peter Hanselaer (Prof.)¹: Peter.Hanselaer@kuleuven.be

¹ESAT/Light&Lighting Laboratory, KU Leuven

Correspondence: Thanh Hang Phung
Email: Thanhhang.Phung@kuleuven.be

Abstract: Image Color Appearance Models (Image CAMs) have been developed to predict the perception of complex scenes and are mainly used for image rendering and video reproduction applications. Among these Image CAMs, iCAM is an image color appearance model that takes an image as the input and provides the perceptual attributes for each pixel. On the other hand, non-imaging CAMs are widely used and validated but they always assume a simple test scene of a uniform flat stimulus, a quasi-neutral background and a surround. This study presents an evaluation of the performance of iCAM when applied to these simple self-luminous scenes in predicting the influence of background luminance, background size, saturation and stimulus size on stimulus brightness. The results show that iCAM is capable of predicting the effect of background luminance and some background size scenarios. However, for unrelated self-luminous stimuli (dark background), the model predictions do not match the reference data. An evaluation of the effect of the filter kernel size and its relation to the physiological mechanism of image processing inside the visual system has been investigated. Furthermore, the impact of saturation and stimulus size on brightness seems to be underestimated by the model because the Helmholtz-Kohlrausch and stimulus size effects are not included. Hence, these findings call for an enhanced image color appearance model.

Keywords: Image Color Appearance Model, self-luminous, perception.

I. Introduction

Quantifying human color perception has always been a key question in vision research. To address this question, many color appearance models (CAMs) have been developed. With respect to the prediction of the color perception of object colors under different viewing conditions, the Nayatani et al. model [1], the Hunt model [2], CIECAM97s [3], CAM16 [4] and especially CIECAM02 [5], which is recommended by the Commission Internationale de l'Éclairage (CIE), can be mentioned. Since its introduction, CIECAM02 has been used in a wide range of industrial applications. Various improvements have been proposed to overcome some limitations of CIECAM02 such as considering the Helmholtz-Kohlrausch effect [12,13], taking into account the stimulus size effect in the appearance of subject's colors [13,14], and solving some computational difficulties of CIECAM02 with a simpler model [4].

The availability of non-imaging color appearance models to predict the color perception of self-luminous stimuli such as luminaires, billboards, traffic signs, and displays is much more limited. The application of CIECAM02 to these types of stimuli encounters some challenges such as the ambiguity of the reference white [6] due to the fact that the spectral radiance of the stimulus and the background are totally independent. To overcome these challenges, CAM15u [7] for unrelated self-luminous stimuli and the more general CAM18sl [6] for related self-luminous stimuli have been proposed, although the effects of background size and stimulus size are not included in the latter model.

All the aforementioned CAMs, whether developed for object or self-luminous stimuli, assume a simple basic test scene: a uniform stimulus surrounded by a uniform background. The optical characteristics of the stimulus (the spectral radiance or CIE XYZ values) and the background (and eventually some categorical characteristics of the surround) are required to compute the perceptual attributes such as brightness, hue, colorfulness, lightness, chroma and saturation of the stimulus.

However, in real life situations, stimuli are perceived in much more complex scenes than just a uniform stimulus on a uniform background and a uniform surround environment, resulting in the need of having a color appearance model which also considers complex spatial

information. Despite such a great potential application field, only a limited number of models have been developed for spatial color vision modeling. In 2002, Fairchild et al. introduced iCAM [8] - an image color appearance model- to predict different perception phenomena in a complex scene. S-CIELAB [9] was proposed as a spatial color space to compute color differences in images. Not long after, Kuang et al. developed an image appearance model based on the iCAM framework, so-called iCAM06 [10], which performs High Dynamic Range (HDR) image rendering. In 2012, Reinhard et al. proposed a calibrated image appearance model [11] used for scene and video reproduction. Some elements from the image-based approach have also been used in other disciplines of vision research such as for predicting discomfort glare of non-uniform and complex luminaires by introducing the receptive field concept as a kernel [15,16].

Among the existing image appearance models, iCAM [8] can be referenced as the standard. This model uses the pixel by pixel tristimulus values of an image as the input and outputs the perceptual attributes (brightness, hue, colorfulness, lightness, chroma and saturation) for each pixel of the image. In addition to the main application of HDR image rendering, it has also been used in fairly simple scenes to predict different color phenomena such as crispening, spreading and simultaneous contrast [8].

In this study, the performance of iCAM [8], in particular its brightness correlate, applied to simple self-luminous scenes is evaluated. After a summary of the iCAM framework, the results regarding the evaluation of brightness obtained with the model are compared to the outcome of non-imaging models applicable and dedicated to this kind of simple scenes. Attention is given to the predictive power of iCAM regarding the impact of the luminance of the background, the Helmholtz-Kohlrausch effect, the background size effect and stimulus size effect on the brightness of the stimulus.

II. Implementation of iCAM Framework

In the original framework developed by Fairchild et al. [8], iCAM takes an image specified in relative CIE XYZ 2° tristimulus values for each pixel together with the absolute luminance information as the input. However, for the simple self-luminous scenes including a 10° stimulus considered in this study, the basic input is the spectral radiance of both the uniform stimulus and uniform background, giving rise to absolute CIE 1964 10° tristimulus values $(X, Y, Z)_{10^\circ, abs}$. A virtual image with

$(X, Y, Z)_{10^\circ, abs}$ as pixel values is created to represent a scene composed of a stimulus and a background, whereby 1 pixel corresponds to 1 cm \times 1 cm in a real scene. This virtual image is then used as input to iCAM.

To adapt the implementation of iCAM to $(X, Y, Z)_{10^\circ, abs}$ input, the relative XYZ values are computed from the $(X, Y, Z)_{10^\circ, abs}$ values by normalizing them using the maximum luminance ($Y_{10^\circ, abs, max}$) occurring in the scene [17]. This normalization procedure is in line with the one adopted in iCAM06 [10] (although in the inverse direction):

$$XYZ = \frac{(X, Y, Z)_{10^\circ, abs}}{Y_{10^\circ, abs, max}} \quad (2.1)$$

A Gaussian low-pass filtered version of the XYZ image is computed to serve as the adapting stimulus in the chromatic adaptation transformation. The absolute luminance data ($Y_{10^\circ, abs}$) is also filtered with a Gaussian low-pass filter and used to predict the local adapting luminance, which is in turn used to calculate the degree of adaptation (D) and to control various luminance-dependent effects such as the Hunt and Stevens' effects.

Next, a chromatic adaptation transformation is performed using the CAT02 chromatic adaptation transform [17]. In this process, both the relative XYZ input image and low-pass filtered image (also referred to as the “blurred image”) are converted into sharpened RGB signals using a linear transformation defined in Equation (2.2) [5]:

$$\begin{bmatrix} R \\ G \\ B \end{bmatrix} = M_{CAT02} \begin{bmatrix} X \\ Y \\ Z \end{bmatrix}, \text{ where } M_{CAT02} = \begin{bmatrix} 0.7328 & 0.4296 & -0.1624 \\ -0.7036 & 1.6975 & 0.0061 \\ 0.0030 & 0.0136 & 0.9834 \end{bmatrix} \quad (2.2)$$

The degree of adaptation (D) is computed as a function of the adapting luminance L_A and the surround factor F :

$$D = F \left[1 - \left(\frac{1}{3.6} \right) e^{\left(\frac{-(L_A - 42)}{92} \right)} \right] \quad (2.3)$$

L_A is taken equal to 20% of the low-pass $Y_{10^\circ,abs}$ channel of the image and F is taken equal to 1 (average surround). The pixel by pixel corresponding colors of each pixel for a D65 reference white are computed as shown in equation (2.4):

$$\begin{pmatrix} R_C \\ G_C \\ B_C \end{pmatrix} = \left[D \begin{pmatrix} R_{D65}/R_W & 0 & 0 \\ 0 & G_{D65}/G_W & 0 \\ 0 & 0 & B_{D65}/B_W \end{pmatrix} + (1-D) \begin{pmatrix} R \\ G \\ B \end{pmatrix} \right] \quad (2.4)$$

with $R_W G_W B_W$ taken from the low-pass filtered image and with $R_{D65} G_{D65} B_{D65}$ being the relative normalized RGB tristimulus values of the D65 reference illuminant for the supplementary 10° observer.

Besides being used to compute the degree of adaptation (D), the low-pass filtered $Y_{10^\circ,abs}$ image is also used to compute the factor F_L for controlling the luminance-dependent effects in the later processes of the model:

$$F_L = 0.2 \left[\frac{1}{5L_A + 1} \right]^4 (5L_A) + 0.1 \left\{ 1 - \left[\frac{1}{5L_A + 1} \right]^4 \right\}^2 (5L_A)^{\frac{1}{3}} \quad (2.5)$$

The next process of the model is to convert the corresponding colors back to $X_C Y_C Z_C$, and then convert those to LMS cone signals. Finally, the LMS cone signals are used to calculate opponent-color signals (light-dark, red-green, yellow-blue) in IPT color space [18]. The matrix used for converting XYZ to LMS cone signals is adjusted for a 10° stimulus as follows [19]:

$$\begin{bmatrix} L \\ M \\ S \end{bmatrix} = \begin{bmatrix} 0.400101 & 0.707351 & -0.0807779 \\ -0.226342 & 1.165540 & 0.0457096 \\ 0 & 0 & 0.931776 \end{bmatrix} \begin{bmatrix} X_C \\ Y_C \\ Z_C \end{bmatrix} \quad (2.6)$$

$$\begin{bmatrix} L' \\ M' \\ S' \end{bmatrix} = \begin{bmatrix} L \\ M \\ S \end{bmatrix}^{0.43} \quad (2.7)$$

$$\begin{bmatrix} I \\ P \\ T \end{bmatrix} = \begin{bmatrix} 0.4000 & 0.4000 & 0.2000 \\ 4.4550 & -4.8510 & 0.3960 \\ 0.8056 & 0.3572 & -1.1628 \end{bmatrix} \begin{bmatrix} L' \\ M' \\ S' \end{bmatrix} \quad (2.8)$$

From IPT, various perceptual attributes can be computed including Lightness (J), Chroma (C) hue angle (h), Brightness (Q) and Colorfulness (M), by converting from rectangular to cylindrical coordinates as in equations (2.9)-(2.13):

$$J = I \quad (2.9)$$

$$C = \sqrt{P^2 + T^2} \quad (2.10)$$

$$h = \tan^{-1}\left(\frac{P}{T}\right) \quad (2.11)$$

$$Q = \sqrt[4]{F_L J} \quad (2.12)$$

$$M = \sqrt[4]{F_L C} \quad (2.13)$$

III. Evaluation of iCAM performance

1. Brightness prediction of neutral stimuli and neutral backgrounds

In this section, the performance of iCAM in predicting the brightness of neutral self-luminous stimuli on neutral backgrounds is investigated. In previous studies, it has been shown that the brightness of a stimulus depends not only on the luminance of the stimulus itself but also on the luminance of the background [20,21]. The same conclusion is drawn in the study by Hermans et al. [22], where a model to predict the brightness of self-luminous stimuli and neutral backgrounds was developed, and later on integrated into CAM18sl [6]. Their experimental scenes will be used as reference data and the results predicted by iCAM will be compared with the outcome of CAM18sl.

The dataset includes 6 neutral stimuli ($u' = 0.232$ and $v' = 0.491$) with luminance levels ranging from 50 cd/m² to 900 cd/m², combined with one of the 15 neutral self-luminous backgrounds ($u' = 0.231$ and $v' = 0.492$), with luminance levels ranging from 0 to 960 cd/m², resulting in a total of 90 test scenes [22]. Each test scene consists of a

background panel of $5\text{ m} \times 3\text{ m}$ viewed at a distance of 2 m (corresponding to a Field of View (FOV) of $102^\circ \times 70^\circ$) and a circular stimulus with a diameter of 0.35 m (or a FOV of 10°). The corresponding virtual input image size equals $500\text{ pixels} \times 300\text{ pixels}$ with the central stimulus having a diameter of 35 pixels .

When applying iCAM, the effect of changing the kernel size of the low-pass filter has been investigated. Two kernel sizes are chosen for this test: the first kernel has a half-width of 4 pixels or a FOV of 1° (which corresponds to the visual angle coverage of the receptive field in the visual cortex V1 [23]) and that of the second one is half the size of the smaller dimension of the image. The latter half-width definition is the one used in the implementation of iCAM06 [10]. In this experiment, this corresponds to a FOV of 41° , which covers almost the orientation half-width of the neurons in the primary visual cortex [24].

In Figure 2.1, the pixel by pixel iCAM brightness values taken from a horizontal line crossing the center of the scene is shown for the two kernel sizes. The luminance of the stimulus and background are equal to 900 cd/m^2 and 750 cd/m^2 , respectively.

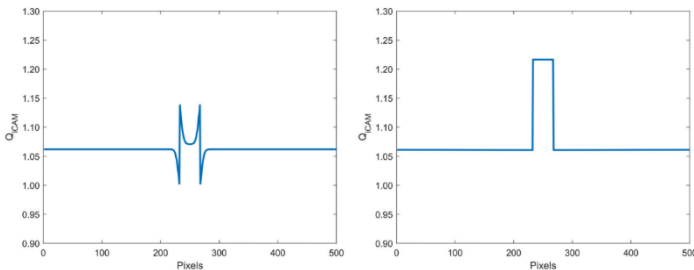


Figure 2.1: Impact of the filter kernel size in the prediction of the central stimulus brightness: Left: Small kernel, Right: Large kernel.

As illustrated in Figure 2.1, the filter kernel size affects the uniformity of the predicted brightness of the central stimulus. When the filter kernel is small, the impact of the neighboring pixels around the edge of the stimulus is mainly considered, predicting a higher contrast near the edge of the stimulus (Figure 2.1- left); the average standard deviation within the stimulus in all 90 scenes was 0.048 . On the other hand, for the larger filter kernel, the influence of a much broader area is taken into consideration, resulting in a more uniform brightness for the stimulus (Figure 2.1- right) (the average standard deviation within the stimulus equals 0.002). This perceived uniform brightness corresponds

more to the visual perception of the scene. The use of a wide kernel size is therefore favored.

In Figure 2.2, the predicted brightness of the stimulus is plotted as a function of the background luminance for both kernel sizes. The arithmetic mean value of the brightness of the stimulus pixels is taken to represent the overall brightness of the stimulus.

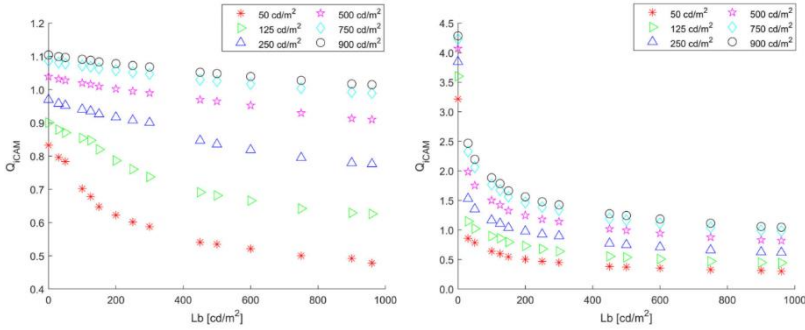


Figure 2.2: Predicted stimuli's brightness as a function of background luminance with small (left) and large (right) filter kernel. Each marker represents one stimulus luminance level.

The results of Figure 2.2 suggest that iCAM can predict the increase in brightness with rising stimulus luminance and the decrease in stimulus brightness on increasing background luminance, which was observed in the psychophysics experiment done on the real test scenes [22]. However, the behavior of the changes seems to be strongly dependent on the kernel size. For the narrow kernel size (4 pixels – FOV = 1°), the brightness variation changes slowly from a completely dark background to a background with high luminance; the higher the stimulus luminance, the less the impact of a variation in background luminance becomes. For the wider kernel, the brightness variation is predicted to change more with background luminance, independent of the luminance of the stimulus. At zero background luminance, a steep rise in brightness prediction is noticed. This steep rise is the result of the division by the low-pass filtered version of the image in the chromatic adaptation transformation (Eq.(2.4)). Indeed, as the filter kernel is relatively large, the relative importance of the background pixel XYZ values becomes higher and the XYZ values in the low-pass filtered image approach 0 when the background luminance becomes very low. This makes the stimulus' pixel XYZ values rise significantly when dividing by the low-pass filtered image. On the other hand, when

the filter kernel is small, the pixel XYZ values in the low-pass filtered image corresponding with the stimulus location are closer to the stimulus pixel values rather than to the background pixel values. Due to this, the predicted brightness of the stimuli will mainly fluctuate around 1. It should be mentioned that for backgrounds close to 0 cd/m^2 , the application of the chromatic adaptation transform becomes less relevant since the stimulus becomes an unrelated color.

It is worth noting that the computational model of CAM18sl brightness was developed based on the visual assessment of the experimental scenes, which are used as the reference in this evaluation. Considering its high correlation with the observer data [22], the outcome of CAM18sl is used as the ground-truth to evaluate the performance of iCAM in this evaluation. In Figure 2.3, the iCAM brightness Q_{iCAM} is plotted against the CAM18sl brightness $Q_{CAM18sl}$ for both kernel sizes. The scenes corresponding to a background luminance of 0 cd/m^2 are indicated with red open circles.

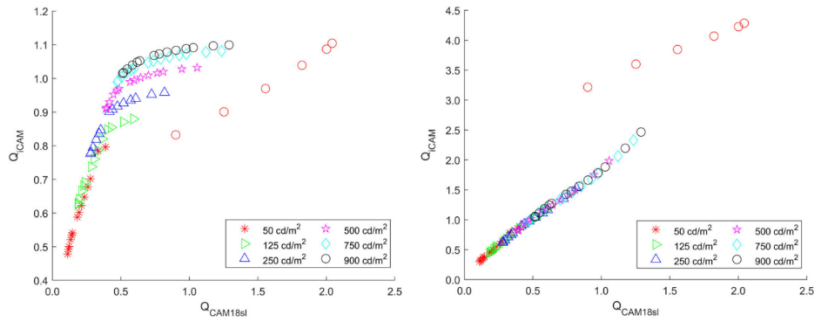


Figure 2.3: Comparison between the brightness predicted by CAM18sl and the brightness predicted by iCAM using small filter kernel (Left) and large filter kernel (Right). Red circles are the data points where the background is 0 cd/m^2

From Figure 2.3, it can be observed that, except for the data corresponding to a dark background, iCAM can predict the relative changes in perceived brightness of the central stimulus although the filter kernel size strongly affects the performance of iCAM. In the case of small filter kernel, the general trend of the brightness change (increasing brightness with increasing stimulus luminance and decreasing brightness with increasing background luminance) is correctly predicted on the graph, which results in a relatively high Spearman ranking correlation of 0.9534 and a Pearson's linear

correlation coefficient of 0.8587 for the scenes with a luminous background. However, it also appears that no unique correlation between the iCAM and CAM18sl for different combinations of stimulus and background exists, which leads to a systematic pattern as seen on the left figure. With the large filter kernel, iCAM and CAM18sl appear to predict the stimulus brightness change at the same rate, which results in a better correlation and a very good Spearman ranking correlation of 0.9988 and a Pearson's linear correlation coefficient of 0.9983 (for scenes with a luminous background).

Considering the data points corresponding to a dark background ($L_b = 0 \text{ cd/m}^2$), the computed brightness of the central stimulus seems to be severely underestimated by iCAM when using the small half-width kernel, while overestimated when using the wide half-width kernel.

In conclusion, it seems that the iCAM brightness for neutral stimuli and neutral backgrounds is linearly correlated to the CAM18sl brightness when using the wide kernel and when excluding background luminance values near zero.

2. Prediction of the Helmholtz-Kohlrausch effect

The Helmholtz-Kohlrausch (H-K) effect [17] is a well-known color phenomenon, stating that for two stimuli with the same luminance, the more saturated one will be perceived as brighter. Different attempts have been made to include this phenomenon into color appearance models [12,25]. To evaluate the prediction of the H-K effect by iCAM, a test has been performed using the same image configuration and experimental set-up as described in previous section. A set of 30 colored stimuli (6 different hues, 5 stimuli/hue) having a fixed luminance of 50 cd/m^2 is presented on a neutral background with $(X, Y, Z)_{10^\circ, abs} = [35.59, 33.65, 29.62]$, where $Y_{10^\circ, abs}$ represents the absolute 10° luminance in cd/m^2 . The chromaticity of the stimuli is shown in the CIE 1976 $u'v'$ chromaticity diagram in Figure 2.4.

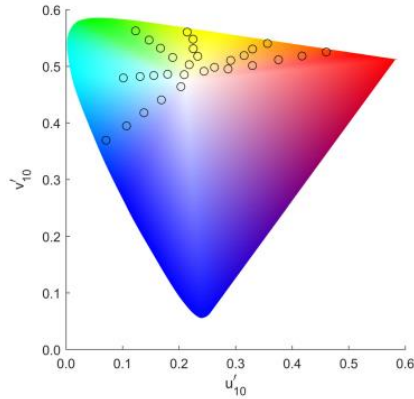


Figure 2.4: Selected stimuli plotted in the CIE 1976 $u'v'$ chromaticity diagram

Similar to the input images in the previous evaluation, the virtual input image is constructed and set to the size of 500×300 pixels with a circular central stimulus with a diameter of 35 pixels. Q_{iCAM} is plotted as a function of saturation of the stimulus in Figure 2.5, where the saturation is computed as the ratio of the iCAM Colorfulness to the iCAM Brightness [26] (which also corresponds to the ratio of Chroma to Lightness). Based on the analysis in the previous section, the wide kernel size has been used and will be used throughout the paper from now on.

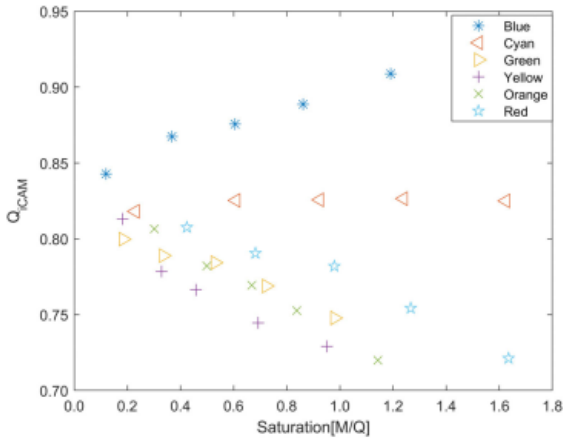


Figure 2.5: Brightness predicted by iCAM as a function of stimulus saturation

From Figure 2.5, it can be seen that iCAM fails to predict the H-K effect: brightness drops as the saturation increases for all hues, except for blue and cyan stimuli. To explain the outcome of iCAM, numerical values of the LMS cone responses as a function of saturation level have been plotted in Figure 2.6.

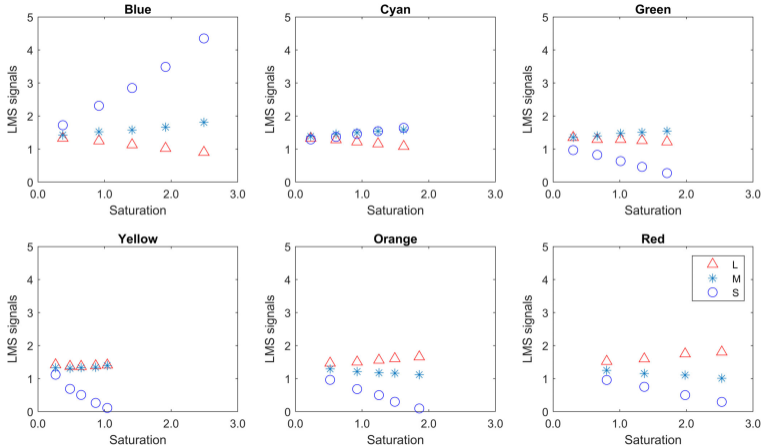


Figure 2.6: LMS signals as a function of stimulus saturation

As can be seen from Figure 2.6, as saturation increases, the L and M cone responses remain quite stable, while the S cone signals shows large changes for all hues, except cyan. The S cones response is therefore effectively the only signal contributing to the change in lightness (see equations (2.6-2.9)) as the saturation increases. The increases in S cone response for the blue stimuli, as can be observed in Figure 2.6, result in an increase in lightness, in agreement with the H-K effect, while decreases in S cone signal result in a decrease in lightness. Note that the model does not explicitly incorporate an additional H-K term in the brightness expression as opposed to CAM97u, CAM15u and CAM18sl.

3. Prediction of the effect of background size on brightness

Studies have shown that the background size also influences the perception of a stimulus on different aspects such as adaptation mechanism [27,28], color induction [29–31] and color constancy [32]. In a recent study by Sun et al. [33], it has been demonstrated that the background size also affects the perceived brightness of neutral stimuli: in case of a dark surround and bright background, an increasing background size causes the brightness of a central stimulus to fall, while for the inverse case (bright surround, dark background), the

stimulus brightness gradually increases with increasing background size. In that study, the background is defined as the part outside and in direct contact with the stimulus, and the surround is the region adjacent to the background.

In this study, iCAM's prediction of the background size effect on stimulus brightness is evaluated using a scene with a total FOV of $102^\circ \times 70^\circ$, a 10° central stimulus ($d = 35\text{cm}$ or 35 pixels), and a varying background with relative sizes equal to 0%, 12.5%, 25%, 50%, 75% and 100% the total scene size. The six different scene configurations are illustrated in Figure 2.7. The chromaticity of the stimulus, background and surround are equal to that of equal-energy white. Stimulus luminance is set fixed at 100 cd/m^2 . Two situations are considered: (1) a background luminance L_b of 450 cd/m^2 and a surround luminance L_s of 0 cd/m^2 and (2) a background luminance L_b of 0 cd/m^2 and a surround luminance L_s of 450 cd/m^2 .

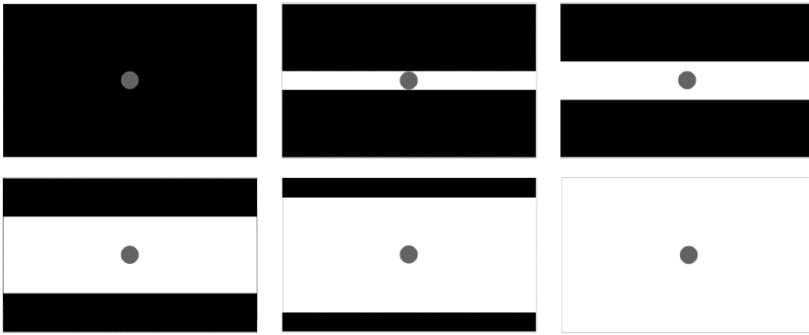


Figure 2.7: Different background-to-surround ratio for bright background and dark surrounds (left to right, top to bottom: 0%, 12.5%, 25%, 50%, 75%, and 100%).*

**The figure in the published version of this paper has a duplication between the conditions of 50% and 75% background sizes. Therefore, it is corrected in the version included in this dissertation.*

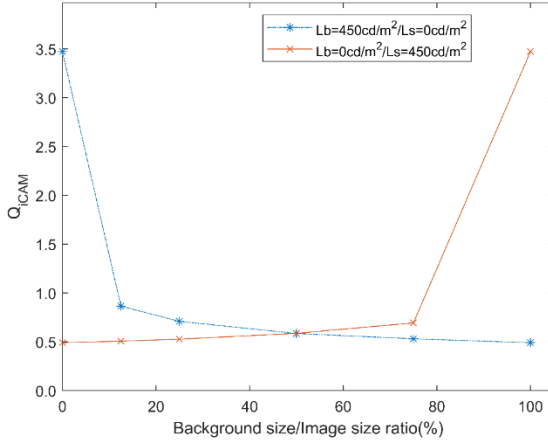


Figure 2.8: Predicted brightness as a function of relative background size

The iCAM brightness prediction for several background/surround ratios is shown in Figure 2.8. It is clear that iCAM brightness of the stimulus decreases as soon as a luminous background is introduced to the scene with a dark surround, and the brightness continues to drop as the background size gets larger and larger (and the surround gets smaller). The most significant fall in predicted brightness is observed when the background size rises from 0% to 12.5%: the brightness drops from 3.47 to 0.87, which is equivalent to 74.9% of the total brightness drop. Subsequently, the brightness gradually decreases. When the background size reaches the size of the dark surround (50%), 82.9% of the total brightness drop has occurred and further increase of background size does not change the brightness substantially anymore. These predictions are consistent with the results of previous studies done on the influence of background size on brightness [33]. In the second case (a bright surround and a dark background), an increase in perceived brightness of the stimulus is predicted when the dark background increases in size. As observed in Figure 2.8, Q_{iCAM} increases slowly from 0.49 to 0.69 when the background coverage increases from 0% to 75% of the size of the scene. When the dark background increases from 75% to 100% of the total scene coverage, Q_{iCAM} rises steeply by a factor of 5.02. The scene is now identical to the case when there is no luminous background and the stimulus is seen against a dark surround. The reported steep rise is again the result of the impact of the low-pass filtered image with a large kernel size when

the background luminance is at 0 cd/m², which has been explained in section III.1 of this study. This quick rise in brightness is, however, not reported in previous studies.

4. Evaluation of the effect of stimulus size on brightness

In addition to background size, background luminance and the H-K effect, stimulus size is another factor influencing the perceived brightness of a stimulus. The effect of stimulus size on brightness perception has been studied extensively and many adjustments have been proposed to include the effect of stimulus size into color appearance prediction [13,14,34–36]. In this section, the iCAM’s ability to correctly predict the stimulus size effect on brightness is investigated.

As observed previously in the brightness prediction for achromatic stimuli (section III.1), iCAM seems to generate inconsistent brightness data when the stimulus is seen against a completely dark background. Hence, for the evaluation of the stimulus size effect, the scene was chosen such that the stimulus is surrounded by a neutral background with absolute $(X, Y, Z)_{10^\circ, abs} = [30, 30, 30]$. The scene set-up is kept the same as in previous sections (an image size of 500×300 pixels and a circular central stimulus). A set of 40 stimuli (8 red, 8 green, 8 blue, 8 yellow and 8 achromatic stimuli) with various sizes (1°, 2°, 5°, 10°, 15°, 20°, 25° and 30°) was chosen. The test stimuli have chromaticity coordinates and luminance as given in Table 2.1.

	$L_{10}(\text{cd/m}^2)$	u'_{10}	v'_{10}
Red	20.00	0.4571	0.5239
Blue	22.33	0.1446	0.2686
Yellow	19.86	0.2165	0.5513
Green	20.35	0.0967	0.5654
Achromatic	102.23	0.1958	0.4690

Table 2.1: Luminance (10°) and CIE 1976 $u'v'$ chromaticity coordinates of the test stimuli [35]

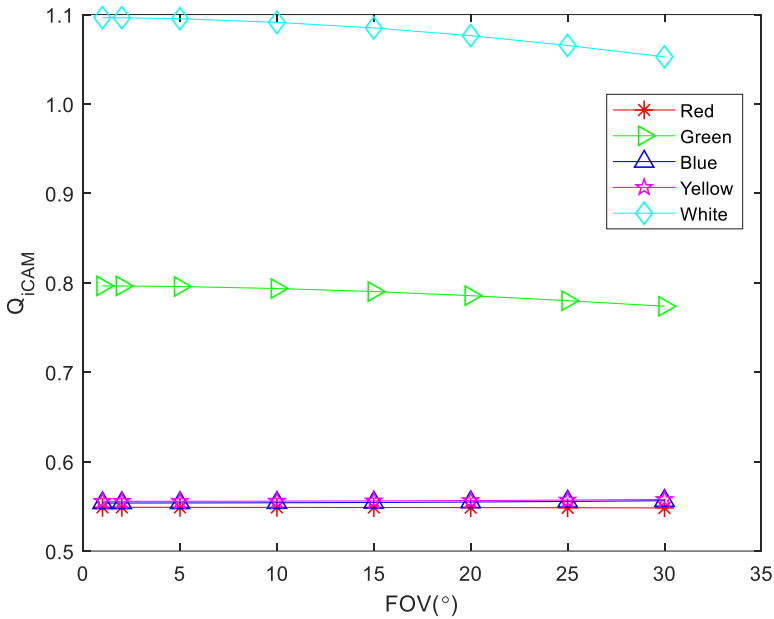


Figure 2.9: iCAM brightness as a function of stimulus size

The results are shown in Figure 2.9. According to previous studies on the stimulus size effect, it is commonly agreed that for the same stimulus luminance, the perceived brightness increases when the size of the stimulus increases [13,14,34–36]. In the model developed by Wei et al. [36], a neutral sample can become 123% brighter when the sample size increases from 2° to 50°. Figure 2.9 depicts that iCAM does not predict any change in brightness when the stimulus size changes from 1° to 30°. However, most non-imaging CAMs such as CIECAM02, CAM97u and CAM18sl do not include the stimulus size effect either. Nevertheless, for image-based color appearance models, it could be very appropriate to include this effect in a very elegant way.

IV. Conclusion

Various sets of XYZ images mimicking real self-luminous scenes consisting of a uniform stimulus surrounded by a uniform background and surround have been constructed to investigate iCAM's performance in predicting the influence of stimulus and background luminance, stimulus and background size, and Helmholtz-Kohlrausch effect on stimulus brightness. The results directly obtained with dedicated non-imaging CAMs or obtained from literature were used as a benchmark. Two filter kernel sizes have also been implemented in

the iCAM model to examine the impact of changing filter size in iCAM processing. The filter size suggested for iCAM06 implementation [10] shows a better brightness prediction. The criteria for choosing the filter kernel size are still not quite clear, whether it should be based on the receptive field size or the size of neural networks in the visual cortex, or others. Further studies are needed to verify the connection between the processing in the visual system and the choice of filter size.

The results show that iCAM adopting a large kernel can well predict the effect of background and stimulus luminance on the perceived brightness when the background is not completely dark. The model is also capable of estimating the background size effect in case of a combination of dark surround and bright background. However, there are limitations in predicting such effects when the stimuli are shown on a completely dark background due to the local adaptation determined by the low pass filtered image. Furthermore, iCAM also does not include the H-K effect and the stimulus size effect in its brightness prediction. These observations call for a new, more comprehensive image color appearance model dedicated to self-luminous scenes. The authors strongly believe that such an image-based color appearance model could be very powerful in describing the visual perception attributes of various and complex scenes. The development of such model can include the use of another color appearance model such as CAM18sl (which includes explicitly the H-K effect), the use of the DKL color space [37] and the use of different spatial filters to improve the stimulus size effect in the model. It can also be interesting to investigate the changes in perceived hue and colorfulness with the change of stimulus sizes and background sizes.

Acknowledgement

The authors would like to thank the Research Council of the KU Leuven for supporting this research project (C24/17/051).

References

1. Y. Nayatani, K. Takahama, and H. Sobagaki, "Prediction of color appearance under various adapting conditions," *Color Res. Appl.* (1986).
2. R. W. G. Hunt, *The Reproduction of Colour* (John Wiley & Sons, Ltd, 2005).
3. M. R. Luo and R. W. G. Hunt, "The structure of the CIE 1997 colour appearance model (CIECAM97s)," *Color Res. Appl.* **23**, 138–146 (1998).
4. C. Li, Z. Li, Z. Wang, Y. Xu, M. R. Luo, G. Cui, M. Melgosa, M. H. Brill, and M. Pointer, "Comprehensive color solutions: CAM16, CAT16, and CAM16-UCS," *Color Res. Appl.* **42**, 703–718 (2017).
5. N. Moroney, M. D. Fairchild, R. W. Hunt, C. Li, M. Ronnier Luo, and T. Newman, "The CIECAM02 color appearance model," in *10th Color and Imaging Conference Final Program and Proceedings* (2002), pp. 23–27.
6. S. Hermans, K. A. G. Smet, and P. Hanselaer, "Color appearance model for self-luminous stimuli," *J. Opt. Soc. Am. A* **35**, 2000–2009 (2018).
7. M. Withouck, K. A. G. Smet, W. R. Ryckaert, and P. Hanselaer, "Experimental driven modelling of the color appearance of unrelated self-luminous stimuli: CAM15u," *Opt. Express* **23**, 12045 (2015).
8. M. D. Fairchild and G. M. Johnson, "Meet iCAM: A next-generation color appearance model," in *10th Color and Imaging Conference Final Program and Proceedings* (2002), pp. 33–38.
9. G. M. Johnson and M. D. Fairchild, "A Top Down Description of S-CIELAB and CIEDE2000," *Col Res Appl* **28**, 425–435 (2003).
10. J. Kuang, G. M. Johnson, and M. D. Fairchild, "iCAM06: A refined image appearance model for HDR image rendering," *J. Vis. Commun. Image Represent.* **18**, 406–414 (2007).

11. E. Reinhard, T. Pouli, T. Kunkel, B. Long, A. Ballestad, and G. Damberg, "Calibrated image appearance reproduction," *ACM Trans. Graph.* **31**, 1–11 (2012).
12. M. Kim, J.-H. Jo, Y. Park, and S.-W. Lee, "Amendment of CIECAM02 with a technical extension to compensate Helmholtz-Kohlrausch effect for chromatic characterization of display devices," *Displays* (2018).
13. K. Xiao, M. R. Luo, and C. Li, "Colour size effect modelling," *Color Res. Appl.* **37**, 4–12 (2012).
14. K. Xiao, M. R. Luo, C. Li, G. Cui, and D. Park, "Investigation of colour size effect for colour appearance assessment," *Color Res. Appl.* **36**, 201–209 (2011).
15. G. Scheir, M. Donners, L. Geerdinck, M. Vissenberg, P. Hanselaer, and W. Ryckaert, "A psychophysical model for visual discomfort based on receptive fields," *Light. Res. Technol.* **50**, 205–217 (2018).
16. M. Safdar, M. R. Luo, M. F. Mughal, S. Kuai, Y. Yang, L. Fu, and X. Zhu, "A neural response-based model to predict discomfort glare from luminance image," *Light. Res. Technol.* **50**, 416–428 (2018).
17. M. D. Fairchild, *Color Appearance Models*, 2nd ed. (John Wiley & Sons, Ltd, 2013).
18. F. Ebner and M. D. Fairchild, "Development and Testing of a Color Space (IPT) with Improved Hue Uniformity," *Color Imaging Conf.* (1998).
19. K. A. G. Smet, W. R. Ryckaert, M. R. Pointer, G. Deconinck, and P. Hanselaer, "A memory colour quality metric for white light sources," *Energy Build.* **49**, 216–225 (2012).
20. H.-W. Bodmann and M. La Toison, "Predicted brightness-luminance phenomena," *Light. Res. Technol.* **26**, 135–143 (1994).
21. L. E. Arend and B. Spehar, "Lightness, brightness, and brightness contrast: 2. Reflectance variation," *Percept. Psychophys.* **54**, 457–468 (1993).
22. S. Hermans, K. A. G. Smet, and P. Hanselaer, "Brightness

- Model for Neutral Self-Luminous Stimuli and Backgrounds," *LEUKOS - J. Illum. Eng. Soc. North Am.* **14**, 231–244 (2018).
23. N. M. Bentley and E. Salinas, "Neural Coding of Spatial Representations," in *Encyclopedia of Neuroscience* (Elsevier, 2009), pp. 117–122.
 24. M. Fahle, "Perceptual Learning and Sensory Plasticity," in *Encyclopedia of Neuroscience*, L. Squire, ed. (Elsevier, 2009), pp. 523–533.
 25. S. Hermans, K. A. G. Smet, C. Sandoval, E. M. Colombo, J. Sandoval, and P. Hanselaer, "Towards a New Colour Appearance Model for Self-luminous Stimuli," *J. Sci. Technol. Light.* **41**, (2017).
 26. M. D. Fairchild and G. M. Johnson, "iCAM framework for image appearance, differences, and quality," *J. Electron. Imaging* **13**, 126–138 (2004).
 27. A. H. Gloriani, B. M. Matesanz, P. A. Barrionuevo, I. Arranz, L. Issolio, S. Mar, and J. A. Aparicio, "Influence of background size, luminance and eccentricity on different adaptation mechanisms," *Vision Res.* **125**, 12–22 (2016).
 28. P. Lennie and D. I. A. MacLeod, "Background configuration and rod threshold," *J. Physiol.* **233**, 143–156 (1973).
 29. K. T. Blackwell and G. Buchsbaum, "The effect of spatial and chromatic parameters on chromatic induction," *Color Res. Appl.* **13**, 166–173 (1988).
 30. J. A. S. Kinney, "Factors affecting induced color," *Vision Res.* **2**, 503–525 (1962).
 31. E. Miyahara, V. C. Smith, and J. Pokorny, "The consequences of opponent rectification: The effect of surround size and luminance on color appearance," *Vision Res.* **41**, 859–871 (2001).
 32. T. Hansen, S. Walter, and K. R. Gegenfurtner, "Effects of spatial and temporal context on color categories and color constancy," *J. Vis.* **7**, 2–2 (2007).
 33. P. L. Sun, H. C. Li, and M. Ronnier Luo, "Background luminance and subtense affects color appearance," *Color Res.*

- Appl. **42**, 440–449 (2017).
34. C. Fu, C. Li, G. Cui, M. R. Luo, R. W. G. Hunt, and M. R. Pointer, "An investigation of colour appearance for unrelated colours under photopic and mesopic vision," *Color Res. Appl.* **37**, 238–254 (2012).
 35. M. Withouck, K. A. G. Smet, and P. Hanselaer, "Brightness prediction of different sized unrelated self-luminous stimuli," *Opt. Express* **23**, 13455–13466 (2015).
 36. S. T. Wei, M. R. Luo, K. Xiao, and M. Pointer, "A comprehensive model of colour appearance for related and unrelated colours of varying size viewed under mesopic to photopic conditions," *Color Res. Appl.* **42**, 293–304 (2017).
 37. A. M. Derrington, J. Krauskopf, P. Lenniet, J. Kra, and P. Lennie, *Chromatic Mechanism in Lateral Geniculate Nucleus of Macaque* (1984), Vol. 357.

Chapter 3

Brightness appearance of self-luminous stimuli with a non-uniform background

3. Brightness appearance of self-luminous stimuli with a non-uniform background

3.1. Introduction

In Chapter 2, it has been shown that the application of iCAM to basic self-luminous scenes still has some limitations. This calls for a new comprehensive CAM for complex scenes including self-luminous stimuli, which can be referred to as a Lighting Appearance Model (LAM).

A crucial element in any CAM is the luminance adaptation step modeled by a Michaelis-Menten formula in which the semi-saturation constant represents the adaptive shift induced by the background [1,2]. For a stimulus seen against a uniform environment (hereinafter “background”), this adaptive shift depends only on the background luminance, but when non-uniform backgrounds are considered, modeling the semi-saturation constant according to the characteristics of that background becomes much more difficult.

As brightness plays an essential role in lighting applications such as defining glare levels and contrast threshold levels [3–6], the first step to move towards a LAM is to investigate how different parts of a uniform background influence the brightness perception of a central stimulus. To achieve that goal, a series of experiments were conducted to collect the visual data using the method of brightness matching.

In this chapter, firstly, the pilot experiment, together with some preliminary results and the drawbacks of the experiment, are discussed. Then, the finalized psychophysical brightness matching experiments are presented with the aim to investigate how the distance, the thickness and the luminance of a neutral luminous ring-shaped background influences the brightness perception of a neutral stimulus with respect to the reference condition where the same stimulus is surrounded by a complete dark background.

3.2. Pilot experiment

Starting with the motivation to study the impact of distance of different parts from the background to the perceived brightness of the central stimulus, several possible options to build the experimental set-up were

tested. Inspired by the experiment to determine ocular straylight by Franssen et al. [7], the experimental idea was to show the stimulus on a screen and use a separate light source positioned at different distances from the screen as a background element. The observers were asked to perform a brightness matching such that the reference stimulus on the screen shown with the background light source switched off would appear to have the same brightness as the test source shown on the screen but with the background light source switched on. After several trials with different background luminance levels and various modulation frequencies and patterns, the pilot experiment was conducted, as presented in the following sections.

3.2.1. Experiment

Experiment set-up: a Samsung Color Display Unit ED46C was used to show the reference and the test stimuli, which are generated with PsychToolbox in MATLAB. An OLED Panel Brite 3 FL300 from OLEDWorks with a dimension of 10.4 cm×10.4 cm was used as the additional stimulus in the background, which is positioned on different locations on a circle with a radius of 60 cm. The field of view of the reference, the test and the additional stimuli were 10°. The angular distances from the edge of the OLED to the corresponding edge of the stimulus were 10°, 30° and 60°. The OLED was surrounded with a black box and positioned such that the illumination of the OLED would not change the optical property of the stimulus on the TV screen. The observer uses a keyboard to adjust the brightness of the test stimuli, which consisted of a red square. A representation of the experiment set-up is shown in Figure 3.1.

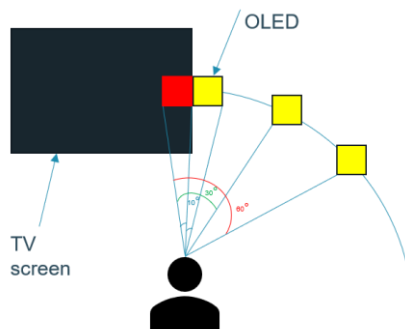


Figure 3.1: Experiment set-up

The CIE1976 u'v' chromaticity of the reference and the test stimulus was (0.440, 0.519) and that of the OLED was (0.233,0.499). To avoid starting point matching bias, two starting luminance levels (one lower starting point and one higher starting point) were chosen for the test stimulus as 6.5 cd/m² and 9 cd/m². The luminance levels of the stimuli are shown in Table 3.1.

Distance \ Stimulus	10°	30°	60°
Reference	7.7 cd/m ²	7.7 cd/m ²	7.7 cd/m ²
Test	6.5, 9 cd/m ²	6.5, 9 cd/m ²	6.5, 9 cd/m ²
OLED	51, 68, 97 cd/m ²	51, 68, 97, 130 cd/m ²	51, 68, 97, 130, 186 cd/m ²

Table 3.1: Luminance of the stimuli

For each distance, 2 scenes were randomly repeated for computing the intra-observer variability. In total, 30 test scenes were created.

Procedure: the visual data was collected using the method of brightness matching. The observer started with 5 minutes of dark adaptation. The experiment was divided into 4 sessions: 1 trial session, and 1 session for each distance. For each test scene, first, the reference stimulus with the OLED turned off was shown for 5 seconds, the observer needed to evaluate and remember the brightness of the reference stimulus. After that, the test stimulus was shown for 5 seconds with the white OLED turned on and the keyboard was activated to adjust the brightness of the test stimulus. The observer was asked to adjust the brightness of the test stimulus such that it is perceived to have the same brightness as the brightness of the reference stimulus. Then, the white OLED was turned off and the reference was shown again for 5 seconds. This sequence continued till the brightness match was made. To avoid order bias, the presented order of the test stimuli was randomized for each observer.

The observers were given the instruction as follows:

“At the start, you will see a red square for 5 seconds; try to evaluate and remember the brightness of this square.

After 5 seconds, an additional white light source pops up at the right. You will see that the brightness of the red square also will have changed.

After 5 seconds, the white light will disappear again, and you will see the original red square. This sequence will keep repeating automatically.

When the white light is on, your task is to adjust the brightness of the red square such that it has the same brightness as when the white light source is off. Please fixate on the red square and the following keys can be used:

- Home: increase the brightness with a small step
- End: decrease the brightness with a small step
- PageUp: increase the brightness with a big step
- PageDown: decrease the brightness with a big step

If you have reached the limit of the increase or decrease step, you will hear a ping sound.

If you do not succeed to adjust the brightness in the first 5 seconds, you just need to wait until the next time the white light source pops up.

Your task is finished when you think the brightness of the red square does not change whether the white light source is on or off. If this is the case, please tell me and I will start a new scene. Around 30 scenes have to be evaluated.”

Observers: the pilot study was performed with 5 observers (1 female, 4 males) with normal color vision, all observers had an “average” or “superior” color discrimination. The age of the observers ranged from 25 to 35 years old with an average age of 28.6 years.

3.2.2. Preliminary results

The results from the pilot experiment are illustrated in Figure 3.2. It shows that generally, at the same distance, the higher the luminance of the OLED, the higher the luminance the observer would select for the stimulus to make the brightness of the stimulus match with that of the reference. Meanwhile, for the same OLED’s luminance, the further the distance, the lower the impact of the OLED on the brightness of the stimulus.

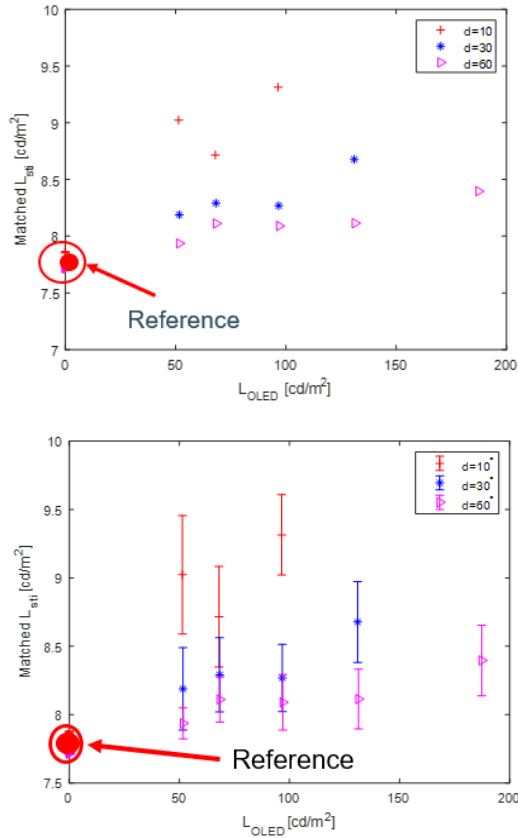


Figure 3.2: The matched luminance of the test stimuli as a function of distance and the additional stimulus luminance: (Top) Results without error bars. (Bottom) Results with error bars. The error bars represent the standard errors.

However, it is also noticeable that there are some inconsistencies in the matched results: for the closest distance, the average matched luminance for the OLED luminance of 68 cd/m^2 was lower than that with the OLED luminance of 51 cd/m^2 . The differences among the matched stimulus luminance levels when the OLED luminance reached 68 and 97 cd/m^2 in the two further distances also do not appear to be significant.

Furthermore, the observers also reported that at the closest distance between the OLED and the screen, the influence of straylight was highly noticeable and the higher ends of the OLED luminance range

could be disturbing. From this feedback, the extended pilot experiment setup was adjusted as presented in the next section.

3.3. Extended pilot experiment

3.3.1. Experiment

Based on the feedback from the observers in the previous pilot experiment, the experimental setup was modified with the parameters summarized in Table 3.2. Instead of using the closest distance as 10° , the distance of 20° was chosen, and the distance of 40° was also added to the setup. As the closest distance was chosen to be further than in the previous pilot experiment, the lower range of the OLED luminance was also changed into relatively higher values to ensure a noticeable impact from the OLED on the brightness perception of the stimulus. The stimulus was kept identical to that of the previous pilot experiment.

Distance Stimulus	20°	30°	40°	60°
Reference	7.7 cd/m ²	7.7 cd/m ²	7.7 cd/m ²	7.7 cd/m ²
Test	6.5, 9 cd/m ²	6.5, 9 cd/m ²	6.5, 9 cd/m ²	6.5, 9 cd/m ²
OLED	58, 72, 91 cd/m ²	58, 72, 91 cd/m ²	58, 72, 91, 116 cd/m ²	58, 72, 91, 116, 150 cd/m ²

Table 3.2: Summary of experimental parameters

For each distance, 2 scenes were randomly repeated for computing the intra-observer variability. In total, 38 test scenes were created.

The experimental procedure remained identical to the first pilot experiment.

Observers: The study was performed with 17 observers (5 females, 12 males) with normal color vision, all observers had an “average” or “superior” color discrimination. The age of the observers ranged from 20 to 39 years old with an average age of 25.3 years.

3.3.2. Results

The visual brightness matching data collected from the extended pilot experiment is illustrated in Figure 3.3.

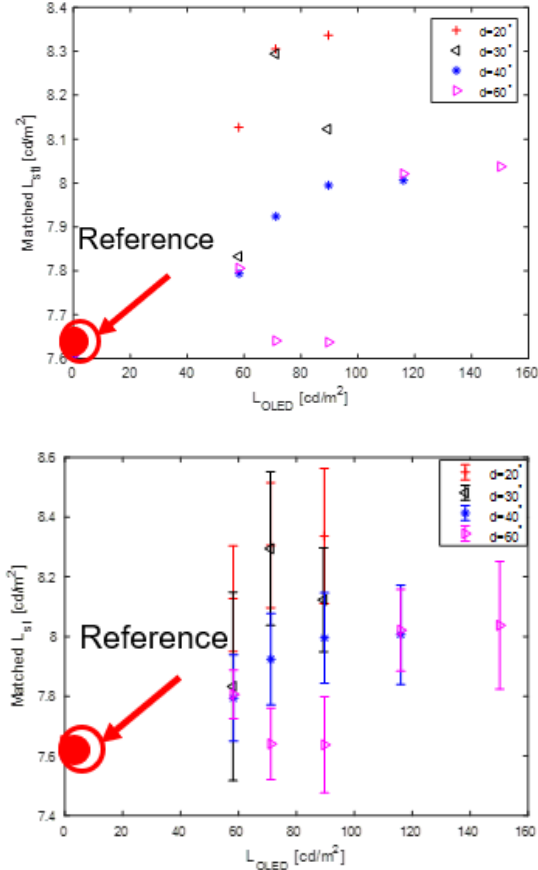


Figure 3.3: The matched luminance of the test stimuli as a function of distance and the additional stimulus luminance: (Top) Results without error bars. (Bottom) Results with error bars. The error bars represent the standard errors.

It is noticeable that the consistency of the phenomenon observed in the first pilot experiment was no longer preserved in this experiment. For the distances of 20° and 40° , the data still showed the tendency that when the OLED luminance was higher, the impact on brightness inhibition for the central stimulus was also stronger. Yet, for the distances of 30° and 60° , the same tendency was not detected: when the

OLED was positioned at 30° , the OLED luminance level of 72 cd/m^2 had a stronger influence on inhibiting the brightness of the stimulus than the OLED luminance of 91 cd/m^2 ; meanwhile, at the distance of 60° , the OLED luminance level of 58 cd/m^2 also produced a stronger effect than the OLED luminance levels of 72 cd/m^2 and 91 cd/m^2 .

Additionally, it is reported by the observers that dealing with the modulating light sources during an extended period of time induced fatigue and some difficulties in evaluating the matches. After consulting with Professor Tom van den Berg from Netherlands Institute for Neuroscience and reevaluating the setup, it was decided that the official experiment should be performed with a static reference and a static test scene simultaneously presented. An EIZO ColorEdge PROMINENCE CG3145 display was chosen for the setup. The description of the official experiment is given in full detail in the accepted manuscript presented in this chapter.

3.4. Main results and discussion

In the final and main experiment, both the test and reference scene are shown statically on one display. The reference stimulus is a circular stimulus surrounded by a complete dark background; the similar test stimulus is surrounded by a neutral luminous ring. The aim is to investigate how the distance, the thickness and the luminance of the luminous ring-shaped background influences the brightness perception of a neutral stimulus with respect to the reference condition. The ring-shaped background setting allows the observation of an equal impact of the distance of the background element on the central stimulus from all directions.

The experimental data are used to compute the relative adaptive shift of the semi-saturation constant in terms of distance, luminance and thickness of the ring. It is observed that the presence of a luminous ring induces a clear decrease in brightness perception of the central stimulus; even for the smallest thickness (0.33 cm) and the largest stimulus-to-ring distance (16.1°), the impact of the ring is still quite substantial. The effect strongly decreases with distance (except for the lowest luminance, for which it remains nearly constant) and increases with increasing luminance of the ring. The experimental results also confirm previous studies reporting the effect of the ring area: the larger the luminous area, the darker the target stimulus appears to be [8].

To model the impact of the luminous ring, the adaptive shift of the semi-saturation constant is modeled in terms of solid angle, luminance and gap distance (Gaussian weighting function). The model is extended to be applicable to a more generic situation where any shape, position and luminance level of different parts of the background can be taken into consideration. The results are overall promising, yet the model shows some shortcomings, suggesting that more complex weighting functions, consideration of different spatial scales of the stimulus and possible mutual dependencies between parameters might be needed. Considering a more detailed approach to handle the issue and impact of straylight is also a potential option to enhance the model.

The full description of the experiment, as well as the data analysis and modeling of the observed phenomena are presented in the following paper:

Phung, TH, Kong, X, Leloup, FB, Smet, KAG, Hanselaer, P. **“Brightness appearance of self-luminous stimuli on a non-uniform background.”** *Color Res Appl.* 2022; 1- 15. doi:[10.1002/col.22811](https://doi.org/10.1002/col.22811)

The complete and unedited content of this paper is included in the following section.

3.5. Publication 2

Brightness appearance of self-luminous stimuli on a non-uniform background

Thanh Hang Phung (Msc.)¹: Thanhhang.Phung@kuleuven.be

Xiangzhen Kong (PhD)¹: Kong.Kong@kuleuven.be

Frédéric B. Leloup (PhD)¹: Frederic.Leloup@kuleuven.be

Kevin A.G. Smet (Assoc. Prof.)¹: Kevin.Smet@kuleuven.be

Peter Hanselaer (Prof.)¹: Peter.Hanselaer@kuleuven.be

¹ESAT/Light&Lighting Laboratory, KU Leuven

Correspondence: Thanh Hang Phung
Email: Thanhhang.Phung@kuleuven.be

Abstract: Color Appearance Models (CAM) generate a set of visual correlates attributed to a stimulus such as hue, brightness and saturation. However, most of their applicability is limited to stimuli perceived on a uniform background. Additionally, when focusing on brightness, multiple studies have been performed to model the mechanisms of brightness perception of a stimulus on a non-uniform background. In this paper, experimental data are gathered and the insights of both approaches are combined. The influence of adding a neutral ring-shaped luminous area in the background of a neutral circular stimulus has been investigated via a series of psychophysics experiments. The ring is presented at 3 luminance levels (90 cd/m², 335 cd/m², 1200 cd/m²) with 3 thicknesses (0.33 cm, 0.67 cm and 1.00 cm) at 4 angular distances to the edge of the stimulus (1.2°, 6.4°, 11.3° and 16.1°). It is observed that when the ring is closer to the stimulus, the brightness inhibition becomes larger; obviously, the impact is also related to the ring's area and luminance. Inspired by the classical CAM, the cone excitations corresponding to the stimulus and the background are inserted in a compression-adaptation formula to obtain a cone response proportional to the perceived brightness. The semi-saturation constant occurring in this formula is modeled as a function of the cone excitation, the distance and the width of the ring. The results are overall

promising, yet the model shows some shortcomings and more complex weighting functions might be needed. In the future, image-based approaches should get more attention.

Keywords: Spatial brightness, brightness appearance, brightness modeling

I. Introduction

For decades, color appearance modeling has been one of the major research directions in color science. Various color appearance models (CAM) have been developed and applied in the fields of printing, media reproduction and lighting such as the Nayatani et al. model [9], the Hunt model [10], CIECAM97s [11], CIECAM02 [12], which are recommended by the Commission Internationale de l'Éclairage (CIE), and CAM16 [13]. Based on the optical characterization of the stimulus and the background in terms of spectral radiance or tristimulus values as input, a number of processing steps mimicking the human visual system are defined such that the output consists of a set of absolute (brightness, colorfulness, saturation and hue) and relative (lightness, chroma) visual correlates of the stimulus. When the stimulus is self-luminous, such as a light source, a number of dedicated CAMs have been developed to deal with the ambiguity in defining the reference white point or the underestimation of the Helmholtz-Kohlrausch effect [1,2].

The applicability of the vast majority of existing CAMs -including the brightness prediction- is however limited as they were developed for a uniform stimulus (typically with a defined angular extent between 2° and 10°) seen on a uniform background (typically extending for 10° from the edge of the stimulus) [14], while in reality, stimuli are often perceived in much more complex situations. Some proposals have been made to extend the application of these traditional CAMs by considering different spatial effects, such as the stimulus size effect [15–17] or the background size effect [8,18]. However, these improvements still only cover a limited category of situations.

Among all the perceptual attributes, brightness has been extensively investigated as such due to its important role in lighting and display applications, more particularly in defining glare levels or contrast threshold levels [3–6]. Multiple attempts have been reported in literature to model the mechanisms of brightness perception of a stimulus surrounded by a non-uniform background. Gilchrist et al. [19] gave an extended discussion on the perception of lightness in

complex images and proposed a lightness anchoring framework emphasizing that segments which belong to the same group (or Gestalt) of the target would influence the appearance of the target. Using Mondrian patterns, Land [20] proposed the Retinex theory which allows the calculation of lightness appearance of different regions in a scene. Nevertheless, these studies focus on the computation of lightness, and this can be challenging in the context of self-luminous stimuli due to the ambiguity of the definition of the white point, as mentioned earlier.

On the topic of brightness in complex backgrounds, Arend and Spehar [21] investigated the brightness and brightness contrast of Mondrian patterns, and Schirillo and Shevell [22] used a checkerboard pattern to study the brightness contrast on inhomogeneous surrounds. In the former study, it was found that the brightness contrast is highly correlated to the luminance ratio between the stimulus and the background regardless of the arrangements [21], while in the latter study, a difference between brightness contrast between homogenous and inhomogeneous conditions was detected [22]. However, these studies were performed with rather small-scale scenes, where the test and the reference scenes typically subtended a field of view of around 10°, and the luminance range was also rather limited, which might not be representative for some typically self-luminous scenarios.

For more extended viewing conditions, research has proven that the size and the spatial compositions of the background have a strong influence in multiple stages of visual perception, including luminance adaptation [23,24], chromatic adaptation [18], and chromatic induction – a phenomenon in which the introduction of a nearby stimulus induces a change in perceived colors of a stimulus [25]. For dark and mesopic adaptation, the adaptation process is largely affected by the local luminance of the luminous areas which are close to the target rather than by the luminous areas at a larger distance [23,24], and the adaptation field size could change the dark adaptation speed [26]. According to Stevens [27], the level of the brightness decrease is highly dependent on the area of the inhibiting field. The study by Sun et. al [8] showed that with different background sizes, the brightness (and colorfulness) of the stimuli would be perceived differently, where the larger the luminous background, the darker the stimulus appeared to be. Nevertheless, it appears that the effect induced by an additional stimulus on the brightness of the stimulus is not simply described by a weighted sum of the additional stimulus area or by local edge contrast [28].

Besides, it is found that when the separation between the additional stimulus (contrast induction field) and the target stimulus is smaller, the simultaneous contrast effect (where the brightness perception of the stimulus changes to the opposite direction of the change in the contrast induction field) is enhanced [29]. Whittle [4] also pointed out that by adding a thin outline or a hue variation between the stimulus and the background could reduce the sharp change in stimulus brightness when its luminance approaches to that of the background. A study conducted by Carter et. al [30] shows that besides being influenced by the luminance of the background immediately surrounding the target stimulus/image, the apparent brightness of the target is also affected by the luminance change in the extended area which frames the background. In addition, Miyahara et. al [25] found that the amount of chromatic induction decreases with decreasing size of the additional stimulus that induces the change (the “induction field”), and Blackwell et. al [31] showed that the amount of induction decreases exponentially with the increasing separation between the stimulus and the induction field. The latter study also suggested that when the induction field which was more than 2° away from the fovea, it can be ignored [31]. Cohen et. al [32] also presented that a desaturation of the visual fields beyond 37.5° would be mostly unnoticed.

Additionally, an extensive number of studies have been conducted to model brightness perception in complex scenes such as the MIDAAS model proposed by Kingdom and Moulden [33], which is later extended by McArthur and others [34]. Reid and Shapley also developed a model predicting how the stimulus brightness changes in the same direction (brightness assimilation) or in the opposite direction (brightness contrast) with the background luminance changes [35]. In addition, Shevell et. al developed a two-stage model mimicking the neural mechanisms of brightness induction [36]. Their model used a retinal simulation from the target area and its adjacent area, combining with the neural response from the remote area in the field of view to calculate the amount of brightness induction. Though these models are capable of modeling several well-known brightness phenomena in complex environments, they either were only performed on a small field of view (up to a few degrees) [35,36] or they were not verified with human visual experiments [33,34]. Some other highly physiological-based lightness models have also been proposed by McCann [37] and Rudd [38], yet, a link between these models and a more general color appearance model is still missing.

A crucial element in any CAM is the luminance adaptation step modeled by a Michaelis-Menten formula in which the semi-saturation constant represents the adaptive shift induced by the background [1,2]. For a stimulus seen against a uniform environment (hereinafter “background”), this adaptive shift depends only on the background luminance, but when non-uniform backgrounds are considered modeling the semi-saturation constant according to the characteristics of that background becomes much more difficult. As an exploratory step to move towards an appearance model for complex scenes, it is essential to investigate how different parts of a uniform background contribute to the change in brightness perception of a central self-luminous stimulus. To achieve that goal, in this study, psychophysical brightness matching experiments are reported with the aim to investigate how the distance, the thickness and the luminance of a neutral luminous ring-shaped background influences the brightness perception of a neutral stimulus with respect to the reference condition where the same stimulus is surrounded by a complete dark background. The experimental data are used to compute the relative adaptive shift of the semi-saturation constant in terms of the distance, the luminance and the thickness of the ring-shaped background.

II. Experiment

1. Stimuli

An EIZO ColorEdge PROMINENCE CG3145 screen was used to display the reference and the test stimuli, which were generated with PsychToolbox in MATLAB. The field of view of the reference stimulus was 10° and the screen covered a field of view of $82^\circ \times 49^\circ$ when the observer was positioned at a distance of approximately 40 cm to the screen. A black shield was placed between the reference and the test stimuli to ensure that the light from one side does not visually impact the other. An illustration of the experiment set-up is given in Figure 3.4.



Figure 3.4: Pictures of the experiment set-up. (Left) A view of the experiment set-up showing the shield and the screen; the reference stimulus is displayed at the left half and the test stimulus at the right half. (Right) An observer during the adaptation period.

The reference stimulus was a neutral grey circle of 10° with a luminance $L_{10,ref} = 65 \text{ cd/m}^2$ and CIE 1964 10° chromaticity values of ($x_{10} = 0.31$, $y_{10} = 0.32$), which is close to the chromaticity of CIE illuminant D65.

The test scene consisted of a central test stimulus of the same size but surrounded by a luminous ring. By choosing a centered luminous ring, a well-defined distance between the luminous segment of the background and the central stimulus is obtained from all directions. The test stimulus had the same CIE 1964 chromaticity as the reference stimulus but had either a low starting luminance level of 35 cd/m^2 or a high starting luminance of 335 cd/m^2 to ensure that the starting points of the test stimuli appear perceptually different from the reference stimulus. The white ring had the same chromaticity as the test and reference stimuli. It was positioned at different angular distances with respect to the outer edge of the test stimulus: 1.2° , 6.4° , 11.3° and 16.1° . These distances provided a coverage of various parts of the visual field, from paracentral to near peripheral vision. The ring thicknesses and luminance values were varied in 3 similar but separate experiments.

Experiment 1:

One fixed ring luminance of $L_{10,ring} = 1200 \text{ cd/m}^2$ and two ring thicknesses of 0.33 cm and 1.00 cm were used in this experiment. The corresponding angular widths of the ring, as seen from the observer position, range from 0.26° (at the closest ring-to-stimulus distance) to 0.23° for the thin ring and from 0.78° to 0.68° for the thicker ring.

Experiment 2:

In this experiment, only one ring thickness of 1.00 cm (0.78° to 0.68°) was used with two ring luminance levels of $L_{10,ring} = 90 \text{ cd/m}^2$ and $L_{10,ring} = 335 \text{ cd/m}^2$.

Experiment 3:

The experiment was performed with one ring thickness of 0.67 cm corresponding to an angular width ranging from 0.51° (at the closest distance) to 0.45° (at the furthest distance). Three ring luminance levels of $L_{10,ring} = 90 \text{ cd/m}^2$, $L_{10,ring} = 335 \text{ cd/m}^2$ and $L_{10,ring} = 1200 \text{ cd/m}^2$ were used in this experiment.

With the chosen ring luminance levels, the low, medium and high luminance ranges of the screen were considered.

For each experimental sequence, test stimuli at both starting luminance levels, but presented without any surrounding ring, were included to check for the matching errors of each observer. Two repeated scenes were also included in each test set to study the intra-observer variability.

To avoid the bias caused by the position of the stimuli, the test stimuli were positioned both to the left and to the right of the reference stimulus and the order of the scenes were randomized for all observers.

A summary of the stimuli used in the experiment is presented in Table 3.3.

Parameter	Value	
Reference 10° luminance (cd/m^2)	65	
Starting target 10° luminance (cd/m^2)	35 or 335	
Reference position	Left, Right	
Angular distance (in $^\circ$)	1.2° , 6.4° , 11.3° and 16.1°	
Ring 10° luminance (cd/m^2)	Experiment 1	1200
	Experiment 2	90 and 335
	Experiment 3	90, 335 and 1200
Angular ring thickness (in cm and in $^\circ$)	Experiment 1	0.33 cm ; 0.23° to 0.26°

		1.0 cm; 0.68° to 0.78°
	Experiment 2	1.0 cm; 0.68° to 0.78°
	Experiment 3	0.67 cm; 0.45° to 0.51°

Table 3.3: Experiment parameters

Each experiment was split up into two phases: one trial phase to get the observer familiar with the test procedure and one or more official phases for each ring thickness at each ring luminance level. The trial session consisted of 5 random stimuli and in each official session, 20 matches were performed (4 ring distances \times 2 starting points \times 2 reference positions + 2 scenes to test matching error + 2 repeated scenes for intra-observer variability).

2. Experimental procedure

The visual data were collected using the method of brightness matching. The observer started with 5 minutes of adaptation in a dark room while looking at a random test scene, during which the procedure was explained to the observer.

The observers were requested move back and forth to change their gaze position such that they would look perpendicular to the center of the reference and to the center of the test stimulus with binocular view, at a fixed distance of 40 cm to the screen. In case the observers reported the influence of an afterimage, they were instructed to have a short period for adaptation before performing any adjustments whenever they changed their gaze positions.

The observers were asked to perform the brightness matching task by informing the experimenter how they wanted to adjust the brightness of the test stimulus and the adjustment was made by the experimenter using a keyboard.

The observers were given the instruction as follows:

“You will see 2 gray circles on the screen. When you see a white ring around one circle, it indicates that you will need to adjust the brightness of the center circle inside the ring such that when you look perpendicularly at the circle, it is perceived as equally bright as the gray circle standing alone. The ring can be either on the left or the right.

To adjust the brightness of the target, please tell me if I should increase or decrease the brightness in small or big steps.

To check your match, please change your position such that you are looking perpendicularly to the target and the reference.

If you need a break or want to quit the experiment or have any questions, you can inform me anytime.”

Each observer performed each matching session within 20 – 45 minutes.

The subject panel comprised of 20 observers (13 males and 7 females) for Experiment 1; 12 observers (8 males and 4 females) for Experiment 2 and 17 observers (9 males and 8 females) for Experiment 3. The observer ages ranged from 21 to 61 years old with an average of 30.5 years. All observers have normal color vision as tested by the Ishihara 24-plate test.

For each observer, the spectral radiance values of the matched stimuli were measured after the experiment with a JETI Specbos 1211 spectroradiometer. The field of view consisted of the central 25 % of the stimulus area. Tests of the screen indicated no pixel cross-talk and a good uniformity with less than 2% difference between the minimum and the maximum values. As the thickness of the ring was smaller than the field of view of the spectrometer, its spectral radiance was taken to be identical to the spectral radiance of an arbitrary larger area on the display having the same RGB values as the ring.

The red, green and blue cone excitations ρ, γ, β of the stimulus are computed from the measured spectral radiance using the set of cone fundamentals $\overline{l}_{10}, \overline{m}_{10}, \overline{s}_{10}$ for 10° stimuli as provided by the CIE in 2006 [39–41]. The normalization coefficients were chosen such that the cone excitations are identical and equal to the CIE 2006 10° luminance value for a D65 stimulus:

$$\begin{aligned}
\rho &= 6886.7 \int_{390}^{830} L_{e,\lambda}(\lambda) \overline{l_{10}}(\lambda) d\lambda \\
\gamma &= 768.3 \int_{390}^{830} L_{e,\lambda}(\lambda) \overline{m_{10}}(\lambda) d\lambda \\
\beta &= 1366.1 \int_{390}^{830} L_{e,\lambda}(\lambda) \overline{s_{10}}(\lambda) d\lambda
\end{aligned} \tag{3.1}$$

with $L_{e,\lambda}(\lambda)$ the spectral radiance of the stimulus.

The cone excitations of the ring were calculated in a similar way.

As the stimuli in the experiment are achromatic and with a chromaticity close to that of D65 illuminant, the three cone excitations for the stimuli are almost identical to each other with a difference less than 2%. Hence, the arithmetic mean of the three cone excitations (denoted as α) is used as to describe the stimulus excitation. With this approach, the number of inputs of the model can be reduced from three to one, as long as the neutral stimuli are being used [42]. As the colorimetric characteristics of the ring are highly similar to those of the stimulus, the calculation of the excitation of the ring is calculated similarly and is denoted as α_{ring} .

Note that the cone excitation of the stimulus and the ring should be considered as a representation of multiple microscopic cone excitations of the retinal zones corresponding to both luminous areas. Similar to the classical CAMs, both the stimulus and the luminous ring are considered as one entity, each characterized by their “macroscopic” cone excitation α and α_{ring} respectively.

III. Observer variability

The average intra- and inter-observer variability were calculated by taking the arithmetic mean over the observers of the standardized residual sum of squares (STRESS) obtained for each observer. The value can be used to analyze the agreement between two sets of data, where two sets with perfect agreement would result in a STRESS value of zero [43]:

$$STRESS = \frac{1}{n} \sum_{i=1}^n \sqrt{\frac{\sum_{j=1}^k (A_{i,j} - f \cdot B_{i,j})^2}{\sum_{j=1}^k (f \cdot B_{i,j})^2}} \times 100 \quad (3.2)$$

with
$$f = \frac{\sum_{j=1}^k (A_{i,j})^2}{\sum_{j=1}^k (A_{i,j} B_{i,j})}$$

In Eq. (3.2), $A_{i,j}$ represents the average cone excitation α for the matched stimulus j made by observer i .

For the intra-observer variability, $B_{i,j}$ represent the results of the repeated match of the same scene which was shown twice to the observer.

For the inter-observer variability, $B_{i,j} = B_j$ is the response of the average observer for the stimulus j . The ‘‘average observer’’ result is determined by taking the arithmetic mean of the results of the individual observers:

$$B_j = \frac{1}{n} \sum_{i=1}^n A_{i,j} \quad (3.3)$$

The impact of the different reference positions on the screen (left, right) is also calculated, where $A_{i,j}$ and $B_{i,j}$ are the results from the individual observer i for a stimulus j when the reference stimulus is positioned to the left and to the right side of the display, respectively.

Similarly, the variability between the matched results due to the luminance starting point (low, high) is computed with $A_{i,j}$ and $B_{i,j}$ representing the results of stimulus j matched by the individual observer i for the low and high stimulus starting point, respectively.

To account for the matching errors made by the observers, the STRESS value is also computed with $A_{i,j}$ and $B_{i,j}$ set equal to the α value of

the reference stimulus and of the matched stimulus of observer i under a no-ring condition, respectively.

The intra-observer, inter-observer, reference position, starting luminance and matching error variability in terms of STRESS is summarized in Table 3.4.

Experiment	Intra-observer variability	Inter-observer variability	Reference position variability	Starting luminance variability	Matching errors
1	19	24	27	25	14
2	15	16	17	18	14
3	21	23	16	16	8

Table 3.4: Observer variability in terms of STRESS (range: 0-100).

For the first two experiments, the mean intra- and inter-observer variability are similar [8,17,42,44] or better [45,46] than the results mentioned in literature regarding brightness experiments using matching and magnitude estimation methods. The inter-observer variability for the third experiment is slightly higher than that in previous literature. The matching error ranges from 8% to 14% on average and this depicts a baseline of the matching reliability.

The average STRESS value of around 20% for different reference positions and different starting luminance levels suggest that the reference position and the starting luminance levels might have an impact on the brightness matching results. A Shapiro-Wilk test was performed to check the normality of the data for different factors, and it shows that the data is not normally distributed (p -value < 0.05). A Kruskal-Wallis test was done to check the statistical difference between the visual data collected from different starting points and from different reference positions for each observer. The result of the statistical tests indicates an impact of the starting luminance level ($H(1)=22.69$, p -value $=1.9e-06$), and the same conclusion is drawn for the reference position test ($H(1) = 14.37$, p -value $= .0002$). Finally, for each individual observer, an average matching result for each test scene is obtained by taking the arithmetic mean of α of the matched stimuli from different test scene positions and different starting luminance levels. The final matching result is computed by taking the arithmetic

mean of the average results from all individual observers obtained for each test scene.

IV. Results and Discussion

1. Brightness matching results

In Figure 3.5, the average cone excitation of the test stimulus α_{test} and the ratio of the average cone excitation of the test stimulus α_{test} over the cone excitation of the reference stimulus α_{ref} (surrounded by a dark background) as a function of the gap or distance from the ring to the stimulus is illustrated for the thinnest and the thickest rings in Experiment 1 (ring luminance of 1200 cd/m²). The error bars represent the standard errors.

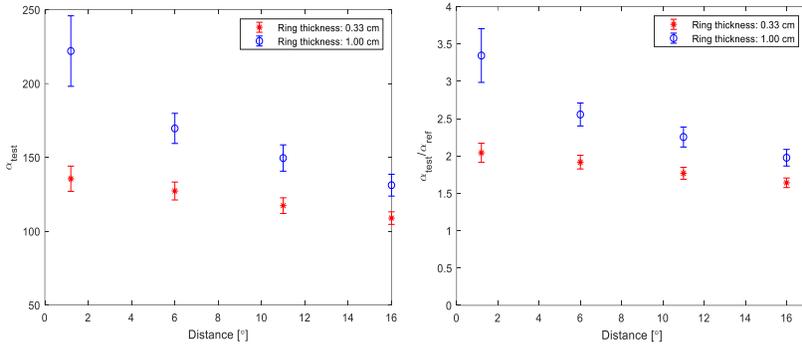


Figure 3.5: The average cone excitation (left) and the ratio of the average cone excitation (right) of the matched stimuli as a function of angular distance from the stimulus edge to the ring with different ring thicknesses. The error bars represent the standard errors.

The thickness of the ring also appears to have a large influence on the perceived brightness of the stimulus. At the closest ring distance, the thick ring (ring thickness 1.00 cm) results in an α_{test} which is around 1.7 times as high as that for the thin ring (ring thickness 0.33 cm). This ratio becomes much less for further distances, however, α_{test} always remains higher for the thick ring. This effect of the area has also been reported in a previous study by Sun et. al [8].

In Figure 3.6, the impact of the luminance of the ring is illustrated by showing the average cone excitation of the test stimulus α_{test} and the

ratios $\alpha_{test}/\alpha_{ref}$ obtained in Experiment 2 (ring thickness 1.00 cm) and Experiment 3 (ring thickness 0.67 cm) as a function of the gap or distance from the ring to the stimulus are illustrated. The error bars represent the standard errors.

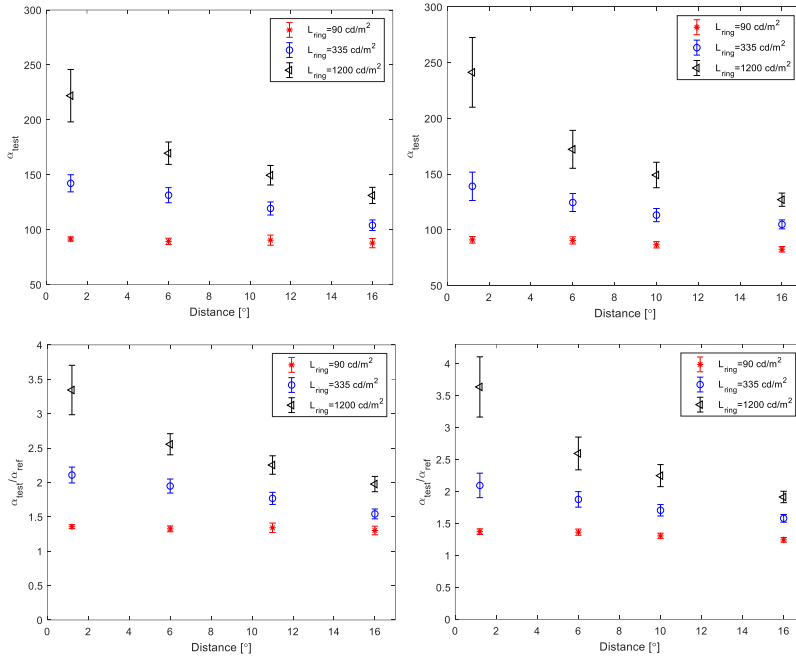


Figure 3.6: The average cone excitation (top row) and the ratio of the average cone excitation (bottom row) of the matched stimuli as a function of distance from the stimulus edge to the ring with: (left) a ring thickness of 1.00 cm with different ring luminance levels (Experiment 2); (right) a ring thickness of 0.67 cm with different ring luminance levels (Experiment 3).

It is clear that with decreasing ring luminance, the influence of the ring on the stimulus brightness decreases and the influence of the ring distance becomes less prominent, but the impact is still obvious, even at the lowest ring luminance; for the higher ring luminance levels, the influence of the ring distance is quite dominant.

The impact of a ring thickness of 1 cm compared to a ring thickness of 0.67 cm on the brightness of the stimulus seems to be very similar. A Kruskal-Wallis test to check the difference between the average

matching results collected with different ring thicknesses does not reject the null hypothesis that the pairwise difference between the two datasets has a mean equal to zero ($H(1) = 0.05$, $p\text{-value} = 0.817$). This is definitely not the case ($H(1) = 4.08$, $p\text{-value} = 0.043$) when comparing the impact of ring thickness 1.00 cm compared to ring thickness 0.33 cm as has been done in Experiment 1 (Figure 3.5).

It is noticeable that for the case of the rings with the highest luminance at the closest distance, there is a wider spread in the matching results between observers reflected through the high standard error values. This discrepancy is believed to be the result of the possible glare and afterimage caused by the high luminance level of the ring. As the ring has a rather high luminance, it is necessary to check if there is any potential influence of stray light induced by the ring on the matching results. The veiling luminance caused by the ring of highest luminance level at the central stimulus was computed using the measured vertical illuminance and the Point Spread Function recommended by the CIE [47]. The vertical illuminance at the observer's eye was measured with a Gigahertz-Optik optometer P-9710. The result shows that the veiling luminance for the 3 largest ring distances is calculated to be between 0.3 cd/m^2 and 0.8 cd/m^2 at the center, and for the worst case (a thick ring at the closest distance and highest luminance), the veiling luminance at the center of the stimulus is 2.4 cd/m^2 . This can be considered negligible when compared to the typical matched luminance of 200 cd/m^2 . Nonetheless, the matching results for the thick ring at the closest distance might be somewhat contaminated by stray light. To further investigate the impact of straylight in detail, additional measurements such as observer's pupil sizes and a proper consideration of how different scene components can generate stray light and interfere with each other will be needed. However, this does not belong to the scope of this paper.

2. Modeling

For ease of illustration, the 28 scenes and corresponding data points used for modeling are given the indices as presented in Table 3.5.

Index	L_{ring} (cd/m^2)	Ring gap	Ring thickness
1-2-3-4	90	$1.2^\circ - 6.4^\circ - 11.3^\circ - 16.1^\circ$	0.67 cm
5-6-7-8	90	$1.2^\circ - 6.4^\circ - 11.3^\circ - 16.1^\circ$	1.00 cm
9-10-11-12	335	$1.2^\circ - 6.4^\circ - 11.3^\circ - 16.1^\circ$	0.67 cm

13-14-15-16	335	1.2°- 6.4°- 11.3°- 16.1°	1.00 cm
17-18-19-20	1200	1.2°- 6.4°- 11.3°- 16.1°	0.33 cm
21-22-23-24	1200	1.2°- 6.4°- 11.3°- 16.1°	0.67 cm
25-26-27-28	1200	1.2°- 6.4°- 11.3°- 16.1°	1.00 cm

Table 3.5: Data points indexing.

The cone excitations of the matched stimulus of each scene are calculated according to Eq. (3.1). Similar to the approach used in classical color appearance models (CAM), although developed for a uniform background, the cone excitations are subject of a compression step to reduce the high-dynamic range excitation range and a luminance adaptation step to account for the background. Typically, this compression-adaptation step is modeled by a sigmoid function as proposed by Michaelis and Menten (MM) [48] and confirmed by Naka and Rushton [49]. Originally, the formula has been put forward to model the rate of an enzyme-catalyzed reaction [48], which was then more commonly used to model the adaptive shift for the photoreceptors [50]:

$$\alpha_a = \frac{\alpha^n}{\alpha^n + \sigma^n} \quad (3.4)$$

where α_a is the adapted cone response of the stimulus, n determines the slope of the response curve, and σ represents the semi-saturation constant. From this equation, the effect of compression becomes evident as the output response is always limited between 0 and 1 (although inclusion of a gain multiplication factor is possible), while the stimulus excitation α can exhibit a large dynamic range. Adaptation of the response to the adapting field surrounding the stimulus is modeled by considering the semi-saturation σ as a variable which monotonically increases with the strength of the adaptive field [51]. An increase of σ leads to a drop in the adapted cone signal, mimicking the effect of adaptation.

According to recent CAMs developed for self-luminous stimuli [1,2], the brightness of neutral stimuli is essentially proportional to the compressed cone response α_a , as saturation induced contributions to brightness, such as the Helmholtz-Kohlrausch effect, can be neglected. Consequently, in order to have the test stimulus perceived equally

bright to the reference stimulus, the following condition needs to be fulfilled:

$$\frac{\alpha_{ref}^n}{\alpha_{ref}^n + \sigma_d^n} = \frac{\alpha_{test}^n}{\alpha_{test}^n + \sigma_{test}^n} \quad (3.5)$$

Where α_{ref} and α_{test} are the α values of the reference and the test stimuli, respectively; σ_{test} is the semi-saturation value for the test situation in which a luminous ring is present; σ_d is the semi-saturation value for a dark background as occurring with the reference stimulus. Solving for σ_{test} leads to:

$$\sigma_{test} = \sigma_d \cdot \frac{\alpha_{test}}{\alpha_{ref}} \quad (3.6)$$

The Relative Adaptive Shift (*RAS*) of the semi-saturation constant with respect to the reference situation, being a complete dark background, is defined as follows:

$$RAS = \frac{\sigma_{test} - \sigma_d}{\sigma_d} \quad (3.7)$$

The experimental *RAS*-value can easily be deduced from Eqs. (3.6) and (3.7) as:

$$RAS = \frac{\alpha_{test}}{\alpha_{ref}} - 1 \quad (3.8)$$

which can be simply calculated from the experimental data shown in Figure 3.5 and Figure 3.6.

In classical CAMs where a uniform background is assumed, the semi-saturation constant or the *RAS* is modeled as a function of the background luminance, being the only variable [2,12]. For the ring-based non-uniform background, a model to predict the *RAS* is needed with the angular gap distance, the solid angle and the cone excitation α_{ring} chosen as variables. A Gaussian weighting function is used for the angular gap distance [34,52,53], while a power function is used for the solid angle. Inspired by the empirical relationship between the

adaptive shift and the background luminance proposed by Xie and Stockham [54], which has been applied later in other models [1,2,55], a power function is also applied to the cone excitation of the background ring. To display the combined dependencies of RAS on the position, the area and the intensity of the ring, a simple multiplication is proposed:

$$RAS = a \cdot \alpha_{ring}^b \cdot \Omega_{ring}^c \cdot e^{-gap^2/2\delta^2} \quad (3.9)$$

in which Ω_{ring} is the solid angle of the ring from the observer point of view, gap represents the angular gap between the ring and the stimulus in degrees, a is a proportionality factor, b and c are the power factors, and δ represents the standard deviation of the Gaussian weighting function.

By fitting the experimental data to Eq. (3.9), the optimized parameters are obtained as $a = 0.23$, $b = 0.53$, $c = 0.34$ and $\delta = 9.94^\circ$, with a root mean square error (*RMSE*) of 0.25 and a coefficient of determination R^2 of 0.81. The result of the fit is illustrated in Figure 3.7: the left figure shows the performance of the model for each scene and the right figure shows the correlation between the predicted RAS and the experimental RAS. From Figure 3.7, the predicted RAS has a good agreement with the experimental RAS, and the model performed generally well in predicting the influence of the ring, especially for the intermediate ring luminance (scenes 9-16), although in most cases, a small underestimation is detected. When the ring has the lowest luminance level (scenes 1-8), there is a slight overestimation in the effect of the ring at the closest distance, meanwhile, the influence of the furthest ring is underestimated. The same issue is observed for the case of the highest ring luminance and the thinnest ring (scenes 17-20). In the case of the thicker rings with higher luminance levels (scene 21 to 28), a strong underestimation of the impact of the distance of the ring is observed at the closest distances, suggesting that an additional inhibition effect might have occurred.

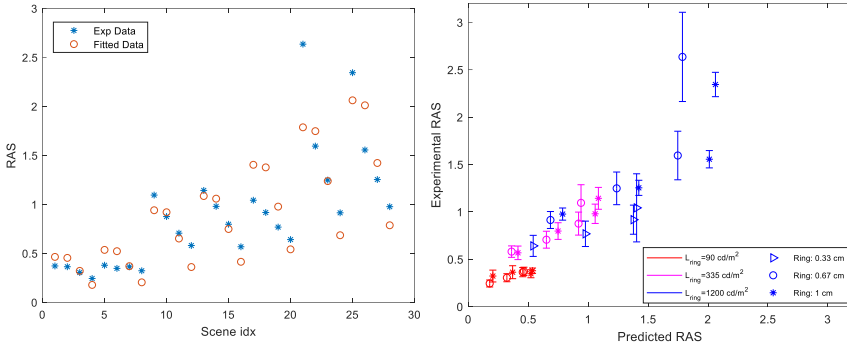


Figure 3.7: (Left) The impact of the ring to RAS: Experimental values (blue) vs. Predicted values (red). (Right) The correlation between the experimental and the predicted RAS. The error bars represent the standard error of the experimental RAS.

The fitting results imply that the RAS induced by the ring can be represented by a compressed cone excitation (with a power of $b=0.53$). In literature, the adaptive shift of the semi-saturation constant is mostly modeled as a power function of the luminance of the background. The powers reported vary from 0.33 [54], 0.57 [56], over 0.63 [57] to 0.78 [2]. In CIECAM02, the adaptive shift is somewhat hidden in the luminance adaptation factor F_L and the normalized cone responses, but a power of 0.67 is adopted [12]. Considering the reported spread of these power factors in literature, our value of 0.53 is highly acceptable.

The strong compression occurring for the solid angle of the ring (power of 0.34) implies that increasing the ring thickness would not have a large impact on the adaptive shift. The same phenomenon was observed by Sun et. al [8], where the brightness of the target stimulus did not change linearly to the extension of the luminous background in the scene and the impact of the background decreased significantly once the background reached 12.5% coverage of a 65-inch screen viewed at 40 cm (or a FOV of approximately 120°). This is also in line with the result from Miyahara et. al [25], where the amount of chromatic induction of an induction field of $3^\circ \times 3^\circ$ and $3^\circ \times 9^\circ$ appeared to be similar. In the study by Stevens [58], it is also shown that when the annulus changes from a thin one (7°) to a wider one (0.5°), the effect of the annulus on the brightness inhibition increases rapidly, however, when the annulus increases in size from 0.5° to around 1° , the influence remains somewhat stable.

With the Gaussian weighting distribution having a $\delta = 9.94^\circ$, it shows that the influence of the ring is extended up to a field of view between 30° and 40° , which appears to be corresponding to the receptive field in the visual cortex [59,60]. This is coherent with what has been found by Cohen et. al [32] about the most influential field with a size of 37.5° in terms of detecting color changes. A similar conclusion has also been drawn from the study by Sun et. al [8], where the introduction of a luminous background covering 12.5% of a 120° scene drastically influences the brightness perception of the target stimulus, while the impact starts to slow down after that.

Though the model generally gives a satisfactory performance, it still has important limitations as it will only work for the case where the element on the background (in this case, a ring) is equally distanced from the stimulus with a unique luminance level. To extend the model to be applicable to a more generic situation where any shape, position and luminance level of different parts of the background can be taken into consideration, Eq. (3.9) can be generalized and the following relation is proposed:

$$RAS = a \cdot \int_{Bg} \alpha_{Bg(\vartheta, \varphi)}^b \cdot e^{-\frac{(\vartheta-5)^2}{2\delta^2}} \sin \vartheta \cdot d\vartheta \cdot d\varphi \quad (3.10)$$

with ϑ and φ as the spherical polar and azimuth angle with the origin at the observer and the Z-axis pointed towards the center of the stimulus specified in degrees; $\alpha_{Bg(\vartheta, \varphi)}$ is the cone excitation of a surface element at position (ϑ, φ) in the background subtending a solid angle of $\sin \vartheta \cdot d\vartheta \cdot d\varphi$; a is a proportionality factor, b is again the power factor and δ represents the standard deviation (in degrees) of the Gaussian weighting function.

The more general Eq. (3.10) was also fitted to the experimental data where the ring was used as the additional background element. With the parameters of $a = 0.06$, $b = 0.58$ and $\delta = 8.06^\circ$, the model is shown to have the optimal performance with an *RMSE* of 0.37 and an R^2 of 0.67, which is worse compared to the performance of the model represented by Eq. (3.9). The shortfall of this more general model is believed to be the result of the inherently assumed additivity with solid angle expressed by Eq. (3.10) yet ignoring any compressive effect. As

the solid angle of the luminous ring as perceived by the observer is a measure of the illuminated retinal area and the number of excited cones, a linear behavior with solid angle might be expected. However, the density of cones is known to drop considerably in the peripheral zone [61] as is their sensitivity [62], affecting the effective cone excitation of the ring. These effects might be the underlying reasons for the strong compression of RAS with solid angle.

3. Discussion

Based on the data collected, the proposed model shows a generally promising performance for predicting the effects of adding a luminous ring to a dark background on the brightness perception of achromatic self-luminous stimuli. It confirms some characteristic modeling parameters obtained in previous studies [2,54,56,57], the background size effect [8] and the most influential field size of color change detections [32]. Moreover, an extended range of luminance levels together with the wider field of view were considered in developing the model. Yet, the model still has certain drawbacks that require attentions. In order to improve the model performance and applicability, more complicated weighting functions as well as a more sophisticated relationship between the adaptive shift and the independent variables of the luminous ring should be investigated. In the current proposed model, the influence of the gap between the additional ring and the stimulus is presented as one fixed continuous function from having no gap (which means the ring and the stimulus are in contact) to considerably large gaps. To tackle the overestimation of the impact of the low luminance rings and the underestimation of the high luminance rings, the model performance can be improved by considering making the standard deviation of the Gaussian weighting factor δ dependent on the cone excitation of the ring.

Furthermore, it has been reported in previous studies that the introduction of a small annulus separating the stimulus and the background could have a significant effect on visual perception, compared to when the stimulus is presented on a continuous and uniform background [4,63]. Whittle found that by adding a thin outline or a hue variation between the stimulus and the background, the “crispening effect” - a phenomenon where the lightness variation of the stimulus is enhanced when its luminance approaches that of the background – could be removed [4]. Also, according to Lennie and

MacLeod [63], the introduction of a small ring of different luminance next to the stimulus to the uniform background increases the rod detection threshold significantly, which implies a strong influence of changes in the viewing condition at a small distance from the stimuli. These observations point to the fact that the particularities of the background region close to the stimulus needs additional attention. The lack of emphasizing this small gap influence in the proposed model might be an explanation to the drawback of the current model for rings having a high luminance at a close distance. The model could be improved by including an additional gap weighting function characterized by a small standard deviation size to simulate such small gap influence.

Another aspect should be considered for enhancing the model performance is to adequately model the effect of stray light as intraocular scattering might have an impact on gray-scale appearance [64]. While the CIE PSF is widely used for computing retinal stray light, it considers the age and the eye pigmentation only [65], and has not included the pupil size, which can have a derivative effect on appearance [66]. Therefore, opting for more physical-optical point spread functions which consider pupil size [67–71] to account for intraocular stray light can be a refinement for the model. It is also essential to address that the size of the stimulus and the background can have a significant impact on the appearance of the scene [8,17,72,73]. Hence, engaging the spatial scale influence by adopting the structural and general models by Carter and Silverstein [66] could also be taken into consideration.

More experimentation will be required to resolve these issues. However, one might question if this kind of approach which sticks to the stimulus-background paradigm is the way forward for developing Color Appearance Models for stimuli with non-uniform backgrounds. Even when applying more sophisticated models, the approach will face serious challenges when dealing with scenes of higher complexity where the concept of stimulus and background becomes ambiguous. Furthermore, it will always become very difficult to upgrade the model to include non-uniformities in and adaptation to the stimulus itself. In our opinion, the development of image-based CAMs which are applicable to complex lighting scenes should get more attention.

V. Conclusion

For decades, color appearance modeling -including the brightness prediction- has been one of the major research directions in color science. The applicability of the vast majority of existing CAMs is however limited as they were developed for a uniform stimulus seen on a uniform background while in reality, stimuli are often perceived in much more complex situations. A crucial element in any CAM is the luminance adaptation step in which the semi-saturation constant represents the adaptive shift induced by the background. For a uniform background, this adaptive shift depends on the background luminance; when non-uniform backgrounds are considered, the semi-saturation constant should be modeled according to the characteristics of that background.

In this paper, the impact of adding a luminous area to a dark background, in this particular research exemplified by a ring surrounding the stimulus, on the brightness perception of a central stimulus has been investigated through a series of visual brightness matching experiments. The presence of a luminous ring induces a clear decrease in brightness perception of the central stimulus. Three parameters have been examined: the distance from the central stimulus to the ring, the thickness of the ring (angular extent) and the luminance of the ring. The impact of the ring on the central stimulus brightness is clearly present, even for the smallest thickness (0.33 cm) and the largest stimulus-to-ring distance (16.1°), the impact of the ring is still quite substantial. The effect strongly decreases with the distance (except for the lowest luminance, for which it remains nearly constant) and increases with increasing luminance of the ring. The experimental results also confirm previous studies reporting the effect of area: the larger the luminous area, the darker the target stimulus appears to be [8].

To model the impact of the luminous ring, the adaptive shift of the semi-saturation constant is modeled in terms of solid angle and intensity of the ring and the gap distance (Gaussian weighting function). The model is extended to be applicable to a more generic situation where any shape, position and luminance level of different parts of the background can be taken into consideration. The results are overall promising, yet the model shows some shortcomings, suggesting that more complex weighting functions, consideration of different spatial scales of the stimulus and possible mutual dependencies between parameters might be needed. Considering a more physical-optical approach to handle the issue of straylight is also a potential

option to enhance the model. However, sticking to the traditional stimulus-background approach can face serious challenges when dealing with scenes of higher complexity, with non-uniform stimuli or when adaptation to the stimulus itself becomes an issue. Therefore, in addition to improving this stimulus-background model, the potential offered by a pixel-by-pixel image-based brightness model which allows full flexibility regarding the complexity of the scene under study should also be explored.

Acknowledgement

The authors would like to thank the Research Council of the KU Leuven for supporting this research (C24/17/051). Author KS is supported by KU Leuven internal funds.

Disclosures

The authors declare no conflicts of interest.

References

1. M. Withouck, K. A. G. Smet, W. R. Ryckaert, and P. Hanselaer, "Experimental driven modelling of the color appearance of unrelated self-luminous stimuli: CAM15u," *Opt. Express* **23**, 12045 (2015).
2. S. Hermans, K. A. G. Smet, and P. Hanselaer, "Color appearance model for self-luminous stimuli," *J. Opt. Soc. Am. A* **35**, 2000–2009 (2018).
3. Y. Lin, Y. Liu, Y. Sun, X. Zhu, J. Lai, and I. Heynderickx, "Model predicting discomfort glare caused by LED road lights.," *Opt. Express* **22**, 18056–71 (2014).
4. P. Whittle, "Brightness, discriminability and the "Crispening Effect,"" *Vision Res.* **32**, 1493–1507 (1992).
5. S. Hermans, K. A. G. Smet, and P. Hanselaer, "Exploring the applicability of the CAM18sl brightness prediction," *Opt. Express* **27**, 14423–14436 (2019).
6. P. Whittle and P. D. C. Challands, "The effect of background luminance on the brightness of flashes," *Vision Res.* **9**, 1095–1110 (1969).
7. L. Franssen, J. E. Coppens, and T. J. T. P. van den Berg,

- "Compensation Comparison Method for Assessment of Retinal Straylight," *Investig. Ophthalmology Vis. Sci.* **47**, 768 (2006).
8. P. L. Sun, H. C. Li, and M. Ronnier Luo, "Background luminance and subtense affects color appearance," *Color Res. Appl.* **42**, 440–449 (2017).
 9. Y. Nayatani, K. Takahama, and H. Sobagaki, "Prediction of color appearance under various adapting conditions," *Color Res. Appl.* (1986).
 10. R. W. G. Hunt, *The Reproduction of Colour* (John Wiley & Sons, Ltd, 2005).
 11. M. R. Luo and R. W. G. Hunt, "The structure of the CIE 1997 colour appearance model (CIECAM97s)," *Color Res. Appl.* **23**, 138–146 (1998).
 12. N. Moroney, M. D. Fairchild, R. W. Hunt, C. Li, M. Ronnier Luo, and T. Newman, "The CIECAM02 color appearance model," in *10th Color and Imaging Conference Final Program and Proceedings* (2002), pp. 23–27.
 13. C. Li, Z. Li, Z. Wang, Y. Xu, M. R. Luo, G. Cui, M. Melgosa, M. H. Brill, and M. Pointer, "Comprehensive color solutions: CAM16, CAT16, and CAM16-UCS," *Color Res. Appl.* **42**, 703–718 (2017).
 14. M. D. Fairchild, *Color Appearance Models*, 2nd ed. (John Wiley & Sons, Ltd, 2013).
 15. K. Xiao, M. R. Luo, and C. Li, "Colour size effect modelling," *Color Res. Appl.* **37**, 4–12 (2012).
 16. K. Xiao, M. R. Luo, C. Li, G. Cui, and D. Park, "Investigation of colour size effect for colour appearance assessment," *Color Res. Appl.* **36**, 201–209 (2011).
 17. M. Withouck, K. A. G. Smet, and P. Hanselaer, "Brightness prediction of different sized unrelated self-luminous stimuli," *Opt. Express* **23**, 13455–13466 (2015).
 18. S. Ma, P. Hanselaer, K. Teunissen, and K. A. G. Smet, "Effect of adapting field size on chromatic adaptation," *Opt. Express* **28**, 17266 (2020).

19. A. Gilchrist, C. Kossyfidis, T. Agostini, X. Li, F. Bonato, J. Cataliotti, B. Spehar, V. Annan, and E. Economou, "An anchoring theory of lightness perception," *Psychol. Rev.* **106**, 795–834 (1999).
20. E. H. Land, "The Retinex Theory of Color Vision," *Sci. Am.* **237**, 108–129 (1977).
21. L. E. Arend and B. Spehar, "Lightness, brightness, and brightness contrast: 1. Illuminance variation," *Percept. Psychophys.* 1993 544 **54**, 446–456 (1993).
22. J. A. Schirillo and S. K. Shevell, "Brightness contrast from inhomogeneous surrounds," *Vision Res.* **36**, 1783–1796 (1996).
23. T. Uchida and Y. Ohno, "An experimental approach to a definition of the mesopic adaptation field," in *Proceedings of CIE 2012* (2012), pp. 71–76.
24. M. G. M. Stokkermans, I. M. L. C. Vogels, and I. E. J. Heynderickx, "The effect of spatial luminance distribution on dark adaptation," *J. Vis.* **16**, 11 (2016).
25. E. Miyahara, V. C. Smith, and J. Pokorny, "The consequences of opponent rectification: The effect of surround size and luminance on color appearance," *Vision Res.* **41**, 859–871 (2001).
26. S. Hecht, "THE DARK ADAPTATION OF RETINAL FIELDS OF DIFFERENT SIZE AND LOCATION," *J. Gen. Physiol.* **19**, 321–337 (1935).
27. J. C. Stevens, "Brightness inhibition re size of surround," *Percept. Psychophys.* **2**, 189–192 (1967).
28. S. W. Hong and S. K. Shevell, "Brightness contrast and assimilation from patterned inducing backgrounds," *Vision Res.* **44**, 35–43 (2004).
29. H. Leibowitz, F. A. Mote, and W. R. Thurlow, "Simultaneous contrast as a function of separation between test and inducing fields.," *J. Exp. Psychol.* **46**, 453–456 (1953).
30. R. Carter, L. Sibert, J. Templeman, and J. Ballas, "Luminous backgrounds and frames affect gray scale lightness, threshold, and suprathreshold discriminations," *J. Exp. Psychol. Appl.* **5**,

- 190–204 (1999).
31. K. T. Blackwell and G. Buchsbaum, "The effect of spatial and chromatic parameters on chromatic induction," *Color Res. Appl.* **13**, 166–173 (1988).
 32. M. A. Cohen, T. L. Botch, and C. E. Robertson, "The limits of color awareness during active, real-world vision," *Proc. Natl. Acad. Sci. U. S. A.* **117**, 13821–13827 (2020).
 33. F. Kingdom and B. Moulden, "A multi-channel approach to brightness coding," *Vision Res.* **32**, 1565–1582 (1992).
 34. J. A. McArthur and B. Moulden, "A two-dimensional model of brightness perception based on spatial filtering consistent with retinal processing," *Vision Res.* **39**, 1199–1219 (1999).
 35. R. Clay Reid and R. Shapley, "Brightness induction by local contrast and the spatial dependence of assimilation," *Vision Res.* **28**, 115–132 (1988).
 36. S. K. Shevell, I. Holliday, and P. Whittle, "Two separate neural mechanisms of brightness induction," *Vision Res.* **32**, 2331–2340 (1992).
 37. J. J. McCann and R. Savoy, "MEASUREMENTS OF LIGHTNESS: DEPENDENCE ON THE POSITION OF A WHITE IN THE FIELD OF VIEW," in *Human Vision, Visual Processing, and Digital Display II* (1991), Vol. 1453, pp. 402–411.
 38. M. E. Rudd, "Lightness computation by the human visual system," *J. Electron. Imaging* **26**, 031209 (2017).
 39. International Commission on Illumination., *Fundamental Chromaticity Diagram with Physiological Axes. Part 1.* (Commission internationale de l'éclairage, 2006).
 40. A. Stockman, L. T. Sharpe, and C. Fach, "The spectral sensitivity of the human short-wavelength sensitive cones derived from thresholds and color matches," *Vision Res.* **39**, 2901–2927 (1999).
 41. A. Stockman and L. T. Sharpe, "The spectral sensitivities of the middle- and long-wavelength-sensitive cones derived from measurements in observers of known genotype," *Vision Res.*

- 40**, 1711–1737 (2000).
42. S. Hermans, K. A. G. Smet, and P. Hanselaer, "Brightness Model for Neutral Self-Luminous Stimuli and Backgrounds," *LEUKOS - J. Illum. Eng. Soc. North Am.* **14**, 231–244 (2018).
 43. P. A. García, R. Huertas, M. Melgosa, and G. Cui, "Measurement of the relationship between perceived and computed color differences," *J. Opt. Soc. Am. A* **24**, 1823 (2007).
 44. W. J. Huang, Y. Yang, and M. R. Luo, "Verification of the CAM15u colour appearance model and the QUGR glare model," *Light. Res. Technol.* **51**, 24–36 (2019).
 45. C. Fu, C. Li, G. Cui, M. R. Luo, R. W. G. Hunt, and M. R. Pointer, "An investigation of colour appearance for unrelated colours under photopic and mesopic vision," *Color Res. Appl.* **37**, 238–254 (2012).
 46. B. Koo and Y. Kwak, "Color appearance and color connotation models for unrelated colors," *Color Res. Appl.* **40**, 40–49 (2015).
 47. T. J. van den Berg, "Visual efficiency of scattering and fluorescence in the human eye lens," *J. Biomed. Opt.* **1**, 262 (1996).
 48. L. Michaelis and M. L. Menten, "Die Kinetik der Invertinwirkung," *Biochem. Z.* (1913).
 49. K. I. Naka and W. A. H. Rushton, "S-potentials from colour units in the retina of fish (Cyprinidae)," *J. Physiol.* (1966).
 50. J. M. Valetton, "Photoreceptor light adaptation models: An evaluation," *Vision Res.* **23**, 1549–1554 (1983).
 51. R. A. Normann, B. S. Baxter, H. Ravindra, and P. J. Anderton, "Photoreceptor Contributions to Contrast Sensitivity: Applications in Radiological Diagnosis," *IEEE Trans. Syst. Man Cybern.* **SMC-13**, 944–953 (1983).
 52. J. Kuang, G. M. Johnson, and M. D. Fairchild, "iCAM06: A refined image appearance model for HDR image rendering," *J. Vis. Commun. Image Represent.* **18**, 406–414 (2007).

53. L. Meylan, D. Alleysson, and S. Süsstrunk, "Model of retinal local adaptation for the tone mapping of color filter array images," *J. Opt. Soc. Am. A* **24**, 2807 (2007).
54. Z. Xie and T. G. Stockham, "Toward the unification of three visual laws and two visual models in brightness perception," *IEEE Trans. Syst. Man. Cybern.* **19**, 379–387 (1989).
55. P. Ledda, L. P. Santos, and A. Chalmers, "A local model of eye adaptation for high dynamic range images," in *ACM International Conference on Computer Graphics, Virtual Reality and Visualisation in Africa* (Association for Computing Machinery (ACM), 2004), pp. 151–160.
56. M. H. Kim, T. Weyrich, and J. Kautz, "Modeling human color perception under extended luminance levels," in *ACM Transactions on Graphics* (2009), Vol. 28, p. 1.
57. D. C. Hood, T. Ilves, E. Maurer, B. Wandell, and E. Buckingham, "Human cone saturation as a function of ambient intensity: A test of models of shifts in the dynamic range," *Vision Res.* **18**, 983–993 (1978).
58. J. C. Stevens, "Brightness inhibition re size of surround," *Percept. Psychophys.* **2**, 189–192 (1967).
59. K. Amano, B. A. Wandell, and S. O. Dumoulin, "Visual field maps, population receptive field sizes, and visual field coverage in the human MT+ complex," *J. Neurophysiol.* **102**, 2704–2718 (2009).
60. S. Raiguel, M. M. Van Hulle, D. K. Xiao, V. L. Marcar, L. Lagae, and G. A. Orban, "Size and shape of receptive fields in the medial superior temporal area (MST) of the macaque," *Neuroreport* **8**, 2803–2808 (1997).
61. A. Roorda, A. B. Metha, P. Lennie, and D. R. Williams, "Packing arrangement of the three cone classes in primate retina," *Vision Res.* **41**, 1291–1306 (2001).
62. K. T. Mullen and F. A. A. Kingdom, "Losses in Peripheral Colour Sensitivity Predicted from "Hit and Miss" Post-receptor Cone Connections," *Vision Res.* **36**, 1995–2000 (1996).
63. P. Lennie and D. I. A. MacLeod, "Background configuration

- and rod threshold," *J. Physiol.* **233**, 143–156 (1973).
64. R. Carter, "CIE self-luminous gray-scale calculation: inflections, parameters, and high-contrast limiting behavior," *JOSA A*, Vol. 37, Issue 1, pp. 115-122 **37**, 115–122 (2020).
 65. T. J. T. P. van den Berg, L. Franssen, B. Kruijt, and J. E. Coppens, "History of ocular straylight measurement: A review," *Z. Med. Phys.* **23**, 6–20 (2013).
 66. R. C. Carter and L. D. Silverstein, "Perceiving color across scale: great and small, discrete and continuous," *J. Opt. Soc. Am. A* **29**, 1346 (2012).
 67. A. B. Watson, "Computing human optical point spread functions," *J. Vis.* **15**, 26–26 (2015).
 68. A. B. Watson, "A formula for the mean human optical modulation transfer function as a function of pupil size," *J. Vis.* **13**, 18–18 (2013).
 69. B. Wandell, "Image systems engineering tools for biology: ISETBIO," *J. Vis.* **17**, 10–11 (2017).
 70. B. C. Freasier and D. H. Sliney, "Evaluation of Optical Radiation Hazards," *Appl. Opt.* Vol. 12, Issue 1, pp. 1-24 **12**, 1–24 (1973).
 71. L. Franssen, J. Tabernero, J. E. Coppens, and T. J. T. P. van den Berg, "Pupil Size and Retinal Straylight in the Normal Eye," *Investig. Ophthalmology Vis. Sci.* **48**, 2375 (2007).
 72. K. Xiao, M. R. Luo, and C. Li, "Colour size effect modelling," *Color Res. Appl.* **37**, 4–12 (2012).
 73. A. H. Gloriani, B. M. Matesanz, P. A. Barrionuevo, I. Arranz, L. Issolio, S. Mar, and J. A. Aparicio, "Influence of background size, luminance and eccentricity on different adaptation mechanisms," *Vision Res.* **125**, 12–22 (2016).

Chapter 4

Towards an image-based brightness model for neutral self-luminous stimuli

4. Towards an image-based brightness model for neutral self-luminous stimuli

4.1. Introduction

In Chapter 3, an attempt to extend the traditional stimulus-background approach to include spatial impacts in predicting brightness perception for neutral self-luminous stimuli is presented. The model shows a generally promising performance; however, some improvements are still needed. It also opens the question whether using the stimulus-background approach is an appropriate solution when situations with higher complexity will be considered. That approach might face numerous challenges when the stimulus itself becomes non-uniform or when more scene elements are involved which leads to the ambiguity in defining the background and the stimulus in the scene. Hence, it is worth exploring an image-based approach to model brightness perception as a pixel-by-pixel image-based brightness model which can allow full flexibility regarding the complexity of the scene under study.

In this chapter, an image-based brightness model is presented which combines the merits of classical appearance models applicable to self-luminous sources with image-based approaches. The experiment from Chapter 3 is extended to ensure that the effect of each ring thickness is investigated combined with all distances and all luminance levels. The experimental data are modeled using a pixel-by-pixel image-based approach including cone-fundamental weighted spectral radiance, stray light, cone compression, a receptive field post-receptor organization and an adaptive shift. A connection to the CAM18sl model is made by increasing the width of the luminous ring until a uniform background within a large field-of-view is reached. Although the experimental setting is still relatively simple (neutral circular stimuli, neutral and ring-shaped induction areas), the experiments allow to develop and test a next-generation image-based brightness model for self-luminous stimuli.

4.2. Main results and discussion

An image-based model to simulate the observed brightness phenomenon is proposed, which is highly inspired by the basic

physiology of the retina [1,2]. The model includes cube root compression of the cone excitations, scattering in the eye, a receptive field concept, inhibition by neighboring pixels and sigmoid compression. The model has been applied to the experimental brightness data and three parameters are optimized: the width of a Gaussian kernel mimicking the surround signal of the receptive field, the overall weighting factor representing the inhibition strength and the semi-saturation constant for a dark-adapted environment. A standard deviation of 151 pixels representing a receptive field with the coverage up to 45° and a weighting factor of 1.9, shows the best performance of the model. The large receptive field width suggests that the brightness perception and the adaptation to the ring might be the result of the processing at the later stage of the visual pathway such as in the visual cortex, where the receptive field has a large size up to 50° [3,4]. This large filter size is also in line with previous findings [5–7], which supports the idea that the adaptation is mainly linked to the global context in which the stimulus is viewed. The model provides a generally good performance in predicting the effect of the area, the distance and the intensity of the ring, though there is some underestimation of the effect with the closest ring distance, which suggests the need of having an additional but smaller receptive field mechanism in the model to simulate more local effects.

Additionally, the performance of the model is evaluated using self-luminous scenes which are created based on previous studies about brightness for self-luminous stimuli as reported by other researchers [8,9]. The results show that the model can predict the perceived brightness behavior of those studies, illustrating its robustness. As such, the proposed image-based model appears promising to deal with non-uniform stimuli and complex scenes in the future and can be considered as an important step in search of a generic Lighting Appearance Model (LAM).

Despite the model's potential to set the foundation for the development of LAM, it is important to acknowledge that still quite some improvements are needed to create a more complete brightness model. The current experiment, though already more complex than those used in traditional CAMs, is still not reflecting the real complexity of real-life situations yet. More possibilities to investigate the same effect with different stimulus luminance levels and stimulus sizes should be considered for a more robust set of data. More sophisticated weighting functions, which are more representative for the changing of receptive field sizes according to positions and processing stages in the visual

pathway should be evaluated, and further improvements can be added with a more complete point spread function to simulate retinal straylight.

The detailed description of the experiments, the proposed brightness model followed with the thorough discussion about the model are given in the following paper:

T. H. Phung, R. M. Spieringhs, K. A. G Smet, F. B. Leloup, and P. Hanselaer, "**Towards an image-based brightness model for self-luminous stimuli**". Opt. Express 30, 9035-9052 (2022). Doi: 10.1364/OE.451265

In the following section is the complete and unedited content of this paper.

4.3. Publication 3

Towards an image-based brightness model for self-luminous stimuli

PHUNG T.H.^{1*}, SPIERINGHS R.M.¹, SMET K.A.G.¹, LELOUP F. B.¹ AND HANSELAER P.¹

¹ KU Leuven, Light&Lighting Laboratory, Ghent, BELGIUM

*thanhhang.phung@kuleuven.be

Abstract: Brightness is one of the most important perceptual correlates of Color Appearance Models (CAMs) when self-luminous stimuli are targeted. However, the vast majority of existing CAMs adopt the presence of a uniform background surrounding the stimulus, which severely limits their practical application in lighting. In this paper, a study on the brightness perception of a neutral circular stimulus surrounded by a non-uniform background consisting of a neutral ring-shaped luminous area and a dark surround is presented. The ring-shaped luminous area is presented with 3 thicknesses (0.33 cm, 0.67 cm and 1.00 cm), at 4 angular distances to the edge of the central stimulus (1.2°, 6.4°, 11.3° and 16.1°) and at 3 luminance levels (90 cd/m², 335 cd/m², 1200 cd/m²). In line with the literature, the results of the visual matching experiments show that the perceived brightness decreases in presence of a ring and the effect is maximal at the highest luminance of the ring, for the largest thickness and at the closest distance. Based on the observed results, an image-based model inspired by the physiology of the retina is proposed. The model includes the calculation of cone-fundamental weighted spectral radiance, scattering in the eye, cone compression and receptive field post-receptor organization. The wide receptive field assures an adaptive shift determined by both the adaptation to the stimulus and to the background. It is shown that the model performs well in predicting the matching experiments, including the impact of the thickness, the distance and the intensity of the ring, showing its potential to become the basic framework of a Lighting Appearance Model.

© 2022 Optical Society of America under the terms of the [OSA Open Access Publishing Agreement](#)

1. Introduction

Modeling human color perception is the main mission of color science. Multiple color appearance models (CAMs) which generate perceptual attributes of colored stimuli have been developed, such as the Nayatani et al. model [10], the Hunt model [11], CIECAM97s [12], CIECAM02 [13] and CAM16 [14], some of which are recommended by the Commission Internationale de l'Éclairage (CIE). In these models, from the optical characterization of the stimulus and background in terms of spectral radiance or tristimulus values, a number of processing steps mimicking the human visual system are defined to output a set of absolute (brightness, colorfulness, saturation and hue) and relative (lightness, chroma) visual correlates of the stimulus. Though being widely applied in the fields of printing and media reproduction, the majority of existing CAMs still have certain limitations in their applications as they assume a uniform stimulus (typically with a defined angular extent between 2 and 10°) seen on a uniform background (typically extending for 10° from the edge of the stimulus) and categorized surround [8], while real life stimuli, such as street lighting or outdoor billboards, are often observed in much more complex environments.

To extend the applications of traditional CAMs to more complex scenarios, some image color appearance models have also been created. These models are capable of predicting different spatial color perception effects such as simultaneous contrast, crispening or spreading, and are applied for image quality assessment [5], High Dynamic Range (HDR) image rendering [6,16–18] and image enhancement [7,19]. While the iCAM models [5,6] and the Reinhard et al. model [16] are mainly based on fundamental CAMs such as CIECAM02, Meylan et.al [17] and Benoit et al. [18] proposed models which are more physiologically based, with tone-mapping operators inspired by retinal processing mechanisms. Though the filter kernel size influences the performance of such models [20], the physiological background behind the choice of the kernel size has not been clearly justified [7]. Moreover, Kolas et al. [19] developed a framework for spatial color algorithms based on the Retinex theory by Land [21], and Provenzi et al. [7] suggested a color correction algorithm with a series of mathematical assumptions based on the human visual system. However, these models were not developed explicitly for predicting color appearance and the visual attributes, such as brightness, are not explicitly extracted from the models.

Applying the previously mentioned non-imaging and imaging color appearance models to self-luminous stimuli, such as light sources present in general lighting scenes, is, however, not straightforward. The absolute spectral radiance of the stimulus can be independent from that of the background leading to an ambiguity in the definition of and normalization to the white point. It has also been shown that these models underestimate the Helmholtz-Kohlrausch (H-K) effect [22]. To overcome those limitations, some CAMs have been developed for self-luminous stimuli [22,23]. One of them, CAM18sl [22], has been implemented in a wide range of applications such as visual gloss, the CIE UGR for discomfort glare, the CIE gray-scale calculation for self-luminous devices, the requirements for traffic signalization [24], as well as to predict the age effect in brightness perception for saturated (red and blue) stimuli [25]. Nevertheless, CAM18sl has the same limitations as the classical CAMs mentioned before, being only applicable to situations characterized by a uniform stimulus and background. As these limitations can be resolved by using image-based color appearance models, the application of the iCAM model to self-luminous scenes has been investigated [20]. Unfortunately, it has been shown that the model has some drawbacks, such as an underestimation of H-K effect and the stimulus size effect and an overestimation of the brightness perception of self-luminous stimuli surrounded by a dark background [20]. All these observations call for a more comprehensive color appearance model applicable for complex scenes including light sources, which might be called a Lighting Appearance Model (LAM).

A first step towards a LAM is the development of an image-based model for brightness perception of self-luminous stimuli in complex situations. Having an important role in lighting and display applications, more particularly in defining glare level or contrast threshold [24,26–28], multiple studies have been performed to investigate the impact of the complex viewing environment on the brightness perception of a stimulus. It has been shown that different properties of the background, such as its size and the spatial compositions, have a significant impact [8,27,29–31]. Stevens [29] showed that the area of the inhibiting field determined the degree of brightness decrease of the object. Later, Sun et al. [8] also confirmed that by increasing the size of the luminous background, the brightness of the stimulus would decrease. The separation between the target and background stimulus which are part of the background also appears to influence how the brightness of the target stimulus is perceived: the smaller the separation, the higher the impact on the stimulus

brightness [30]. Whittle [27] also found out that the introduction of a thin outline or a hue change between the stimulus and background could reduce the crispening effect. Carter et al. [31] pointed out that the brightness of a stimulus could also be impacted by the luminance changes of an extended area in the background.

In addition, Reid and Shapley proposed a model which considers the surrounding environment's contribution through modeling brightness contrast and assimilation effects [32]. In these effects, the stimulus brightness changes in the opposite and in the same direction as the background brightness, respectively. Shevell et al. introduced a two-stage model which simulates the neural mechanisms of brightness induction using the retinal stimulation from the target stimulus area and its adjacent area, in conjunction with the neural response from the remote area in the field of view [33]. Kingdom and Moulden also developed a multi-channel model to simulate different brightness phenomena using multiple spatial scale filtering [34], which has then been extended with the two-dimensional brightness model by McArthur et al. [35]. These models are capable of predicting various well-known brightness phenomena, such as simultaneous contrast [32], in complex situations. However, the models either only investigated the phenomena for a small field of view of only a few degrees [32,33] or the models are not verified with human perception experiments [34,35]. McCann [36] and Rudd [37] also proposed strongly physiological-based lightness computation models, which work well for various spatial conditions for neutral scenes, yet, applying these models to self-luminous stimuli might face the same issues as traditional CAMs due to the ambiguity of defining the reference white point for self-luminous scenes.

In order to extend a CAM for object colors to a LAM including light sources, mastering the perception of the brightness of light sources in a complex scene is a first crucial step. This study addresses the question how different parts of the background influence the brightness perception of a neutral self-luminous stimulus. An image-based brightness model is presented which combines the merits of classical appearance models applicable to self-luminous sources with image-based approaches in which complex backgrounds are considered. As a first step, a symmetrical ring-shaped luminous background element characterized by a well-defined gap towards the stimulus is considered. Psychophysical brightness matching experiments are conducted to investigate how the distance (up to 16° from the edge of the stimulus), the area and the luminance of a neutral luminous ring-shaped

background influences the brightness perception of a neutral stimulus. The experimental data are modeled using a pixel-by-pixel image-based approach including cone-fundamental weighted spectral radiance, stray light, cone compression, a receptive field post-receptor organization and an adaptive shift. A connection to the CAM18sl model is made by extending the width of the luminous background until a uniform background is reached. Although the experimental setting is still relatively simple (neutral circular stimuli, neutral and ring-shaped induction areas), the experiments allow to develop and test a next-generation image-based brightness model for self-luminous stimuli.

2. Experiment

2.1. Experimental setup

The stimuli used in the experiments were created with PsychToolbox [38–40] in MATLAB [41] and displayed on an EIZO ColorEdge PROMINENCE CG3145 monitor. The reference stimulus has a field of view (FOV) of approximately 10° , while the display subtends a FOV of $82^\circ \times 49^\circ$ with the observer being seated at a distance of 40 cm to the screen. A black shield is placed in the middle of the screen to ensure that the reference and the test stimuli are visually separated and do not influence the perception of one another. The set-up of the experiment is illustrated as in Figure 4.1.

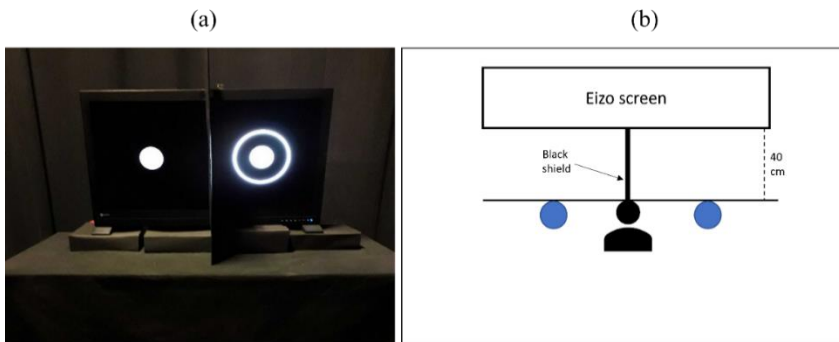


Figure 4.1: Pictures of the experiment set-up. (a) A view of the experiment set-up showing the shield and the screen; the reference stimulus is displayed at the left half and the test stimulus at the right half. (b) The top view of the setup. The blue circles indicate where the observer should position their head when viewing the experimental scenes.

The reference stimulus consists of a neutral gray circle with a 10° diameter and reference luminance $L_{10,ref}$ of 65 cd/m^2 . The CIE 2006 10° chromaticity coordinates of $(x_{10} = 0.31, y_{10} = 0.32)$, which is similar to the chromaticity of CIE illuminant D65.

The test scene was a central test stimulus having the same size as the reference stimulus surrounded by an additional luminous area. To ensure an equal impact of the distance and the luminance of the additional element to the central stimulus from all directions, the luminous area was chosen as a uniform ring. The test stimulus and ring had the same CIE 2006 10° chromaticity as the reference stimulus, but different luminance levels. The test stimulus was initially shown at either a low starting luminance of 35 cd/m^2 or a high starting luminance of 335 cd/m^2 , so that at the beginning, the test stimulus would appear clearly different in perceived brightness compared to the reference stimulus. Three ring luminance levels were used in this study: $L_{10,ring} = 90 \text{ cd/m}^2$, $L_{10,ring} = 335 \text{ cd/m}^2$ and $L_{10,ring} = 1200 \text{ cd/m}^2$, which covered the low, medium and high luminance ranges of the screen. Further, the ring was presented with three possible thicknesses of 0.33 cm, 0.67 cm and 1.00 cm (average angular widths of 0.25° , 0.49° and 0.73° , respectively) and at 4 different angular gaps with respect to the outer edge of the stimulus: 1.2° , 6.4° , 11.3° and 16.1° . Each ring thickness was used in combination with all three ring luminance levels at all four angular gaps.

To avoid positional bias and luminance starting point bias, the test stimuli were shown both to the left and to the right of the reference stimulus and were initially displayed at two different starting luminance levels. To account for the matching errors made by each observer, each experimental sequence included two test stimuli without any ring around it and shown at two starting luminance levels. Two repeated scenes were also included for checking the intra-observer variability. The test sequence for each observer at each experimental session was randomized to avoid ordinal bias.

In each experimental phase, first, each observer was asked to perform a trial session that included 5 random stimuli to get used to the procedure, and then one official session for each ring thickness at each ring luminance level. In each official experimental session, 22 test scenes were shown (4 distances of the ring \times 2 starting points \times 2 reference positions + 2 scenes to test matching error + 4 repeated scenes for intra-observer variability).

2.2. *Experimental procedure*

Visual data was collected using a brightness matching method. Starting with 5 minutes of adaptation, the observer was seated in a dark room and looking at a scene randomly chosen from the set of test scenes while receiving instructions.

The observer was asked to change their gaze position such that they would always maintain a fixed distance of 40 cm to the screen and look perpendicularly at the center of the reference and the test stimulus with binocular view, one at a time. The task given to the observer was to adjust the brightness of the test stimulus such that it could be visually perceived as equally bright as the reference stimulus. To perform the brightness matching task, the observer informed the experimenter whether they preferred to adjust the stimulus intensity with a keyboard themselves or they would rather instruct the experimenter orally. The screen is controlled with the 10-bit signal and the observer had the option to change the stimulus brightness with a coarse adjustment (5 RGB levels) and by fine-tuning (1 RGB level). These increment steps allow the observers to perform the adjustments with consistent perceptual brightness steps using the coarse adjustments while still having an option to fine-tune the match. The average time for each observer to finish one matching session was between 20 and 45 minutes.

The observer panel included 20 subjects (13 males and 7 females) aged between 21 and 61 years old with an average of 30.5 years. All observers had normal or corrected to normal color vision as tested by the Ishihara 24-plate test.

Once the matching result was obtained for each observer, the spectral radiance of the matched stimulus was measured with a JETI Specbos 1211 spectroradiometer. The measured area covered the central 25% of the stimulus area. Good uniformity of less than 2% difference between the minimum and the maximum luminance values was found; the screen did not show pixel cross-talk. To obtain the spectral radiance of the thin ring, the measurement was performed on an arbitrary larger area on the display having the same RGB values as the ring, as the thickness of the ring was smaller than the measurement spot of the spectroradiometer.

The short, medium and long cone-weighted and scaled spectral radiance values $L_\rho, L_\gamma, L_\beta$ of the matched stimulus are computed from

the measured spectral radiance $L_{e,\lambda}(\lambda)$ and the set of cone fundamentals $\overline{l_{10}}, \overline{m_{10}}, \overline{s_{10}}$ for 10° stimuli as provided by the CIE in 2006 [42–44]. The normalization coefficients were chosen such that for a D65 stimulus, the cone-weighted and scaled spectral radiance values are identical and equal to the CIE 2006 10° luminance value:

$$\begin{aligned}
 L_{\rho} &= 686.7 \int_{390}^{830} L_{e,\lambda}(\lambda) \overline{l_{10}}(\lambda) d\lambda \\
 L_{\gamma} &= 768.3 \int_{390}^{830} L_{e,\lambda}(\lambda) \overline{m_{10}}(\lambda) d\lambda \\
 L_{\beta} &= 1366.1 \int_{390}^{830} L_{e,\lambda}(\lambda) \overline{s_{10}}(\lambda) d\lambda
 \end{aligned} \tag{4.1}$$

The cone-weighted spectral radiance values of the reference stimulus and the ring are calculated similarly.

As the stimuli and the rings have a chromaticity close to that of the D65 illuminant, their three cone-weighted values are almost identical with a difference of less than 2% between the minimum and the maximum values. Therefore, the arithmetic mean, denoted as L_{α} , is used to describe the test and the reference stimulus $L_{\alpha, test}$ and $L_{\alpha, ref}$, and of the ring $L_{\alpha, ring}$, respectively. As long as neutral stimuli are targeted, this approach allows a reduction of the number of cone-weighted input values for the model [9]. As the cone-weighted spectral radiance value is a measure for the absorption rate of photons in the cones of the retina, these values can be considered as cone excitations.

3. Results

3.1. Observer variability

The average intra- and inter-observer variability were calculated by taking the arithmetic mean over the observers of the standardized residual sum of squares (STRESS) obtained for each observer. The value can be used to analyze the agreement between two sets of data, where two sets with the perfect agreement would result in a STRESS value of zero [45]. The inter-observer variability was calculated as the average of STRESS between the data collected by each individual observer to the average observer, and the intra-observer variability was calculated as the average of STRESS between the matches of the repeated scenes from each individual observer. The STRESS values

were also calculated to check the agreement between the data collected from different reference positions, starting luminance levels and the matching error variability.

The average intra- and inter-observer variability are calculated to be 18% and 21%, respectively, which are similar ([8,9,46,47]) or better ([48,49]) than the results from previous literature regarding brightness experiments using matching or magnitude estimation methods. The matching error average of roughly 12% indicates a baseline of the matching reliability.

To check if the choice of the reference position and the starting luminance level have an influence on the brightness matching results, a Kruskal-Wallis test was done, which shows that there are statistical differences between the dataset collected from different reference positions ($H(1)=13.14$, $p\text{-value}=.0007$) and from different starting luminance levels ($H(1)=34.41$, $p\text{-value}=4.47e-09$).

Finally, an average matching result for each test scene done by each individual observer is obtained by taking the arithmetic mean of L_{α} , of the matched stimuli from different test scene positions and different starting luminance levels. Then, the arithmetic mean of the average results from all individual observers is computed for each test scene to present the final average matching result.

3.2. Brightness matching results

The ratio of the average cone excitation of the test stimulus $L_{\alpha, test}$ over the cone excitation of the reference stimulus $L_{\alpha, ref}$ (surrounded by a dark background) as a function of the gap or distance from the ring to the stimulus is illustrated in Figure 4.2.

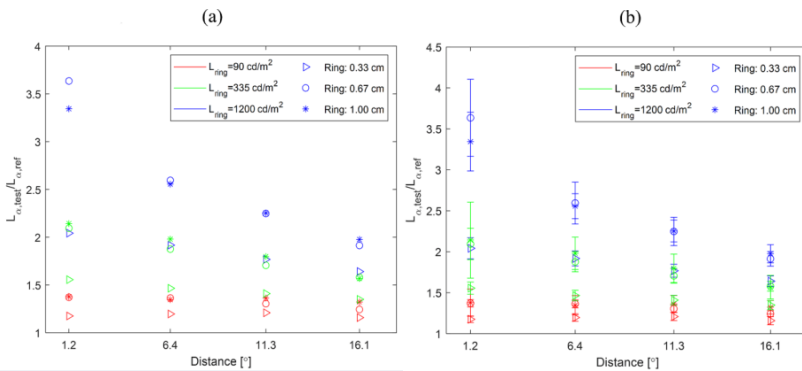


Figure 4.2: The ratio of the average cone weighted spectral radiance of

the matched stimuli as a function of angular distance from the stimulus edge to the ring with different ring thicknesses and ring luminance levels: (a) Without error bars. (b) With error bars. The error bars represent the standard error.

As $L_{\alpha, test}$ is always higher than $L_{\alpha, ref}$, the results show that the observers always select a higher radiance of the test stimulus to obtain a brightness match with the reference stimulus. This implies that by introducing a luminous ring in the visual field, whatever the luminance, gap or thickness, the perceived brightness of the center stimulus will darken. The influence of the ring luminance is occurrent as higher ring luminance levels result in a higher matching value, indicating a higher inhibiting effect. In addition, the general tendency is that when the ring is at a closer distance, the impact of the ring on the stimulus brightness is higher than when the ring is at a further distance. Even at the furthest distance of 16.1° , the ratio $L_{\alpha, test}/L_{\alpha, ref}$ is still greater than 1. However, the impact of distance seems to disappear when the ring luminance level is low, as the matching results remain almost the same for all distances.

Finally, the thickness of the ring is shown to have a certain impact on the perceived brightness of the central stimulus. The effect is highest at the closest ring distance. It becomes obvious that the rings with a thickness of 0.67 cm and 1.00 cm have quite a similar effect, while the impact of the ring with the smallest thickness (0.33 cm) is much less. This was confirmed by a Kruskal-Wallis test to check the statistical difference between the dataset obtained with the ring thickness of 0.33 cm and the ring thickness of 1.00 cm ($H(1)=3.85$, p -value=.049), and between the dataset obtained with the ring thickness of 0.67 cm and the ring thickness of 1.00 cm ($H(1)=0.05$, p -value=.82).

4. Modeling

Based on the experimental results, an image-based brightness model inspired by the physiology of the retina is proposed to predict the impact of distance, the area and the luminance of the ring on the brightness perception of the stimulus. Physiological based retinal models [1,2] adopt the following workflow: the cone excitation is compressed and the output is transmitted directly to a bipolar cell, representing the center signal. The horizontal cells connect several adjacent photoreceptors within the receptive field of the bipolar cells,

creating a surround signal. The center signal and surround signal are subtracted and transmitted. Similar processes occur in the retina's inner plexiform layer leading to a response of the ganglion cells which is sent to the brain via the optic nerve [15]. This general physiological based workflow is the main inspiration for the image-based brightness model that is described in the following section.

4.1. Proposed model framework

In this section, an image-based and retinal inspired model is proposed according to the framework illustrated in Figure 4.3. The model starts from the pixel by pixel L_α map. In the first processing step, scattering in the eye is modeled, resulting in a slightly blurred image. This step is followed by a compression, the calculation of a receptive field based feedback signal and an adaptive shift. Finally, a brightness related correlate is calculated.

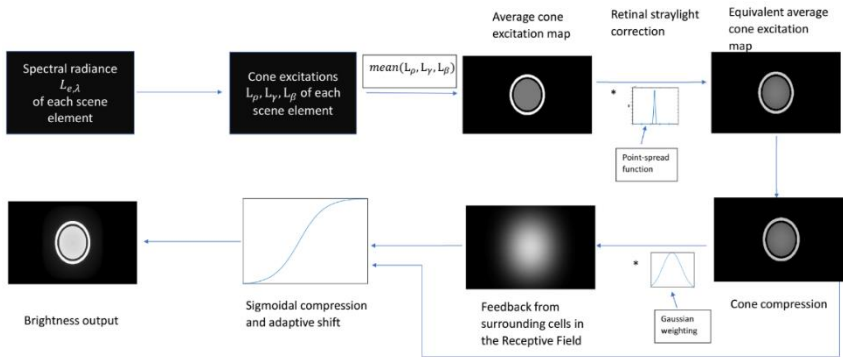


Figure 4.3: The image-based brightness prediction framework illustrated by grayscale images (with the values in each image scaled between the minimum and the maximum pixel values of the image).

The stimulus size and the ring size are adjusted for illustration purpose. The * symbol represents the convolution of the image with a filter kernel.

For the development of the model, a set of images has been created corresponding to each experimental scene. A resolution of 1280×675 pixels, corresponding to an angular resolution of around $4'$, has been chosen. The local L_α value ($L_{\alpha, test}$, $L_{\alpha, ref}$, $L_{\alpha, ring}$ and $L_{\alpha, dark}=0$) is attributed to each corresponding pixel. The central stimulus used in the

experiments corresponds to a diameter of 135 pixels in the image. This image is called the average cone excitations map $I_{\alpha}(x, y)$ (Figure 4.4).

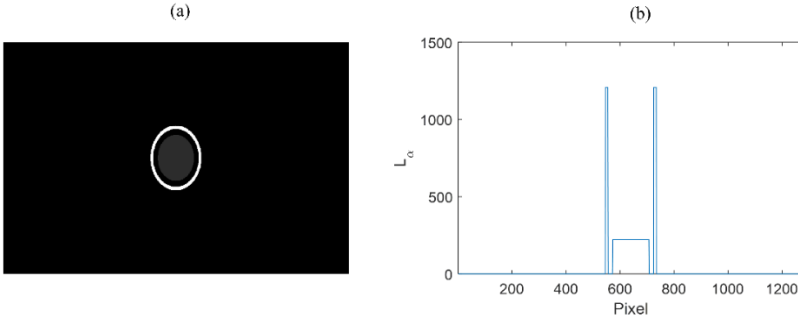


Figure 4.4: An example of the input image: (a) The full image. (b) The value of each pixel from a line cut through the image.

4.2. Impact of scattering in the eye

The presence of a luminous ring in the vicinity of a circular stimulus can also generate a veiling luminance at the stimulus, which might influence the matching results and which needs to be corrected for. In fact, in a human eye, a point source is not imaged on the retina as a single point but is spread out. This is caused by several optical effects of the eye [50]. The most common way to describe the distribution of these scattering effects is by introducing the point spread function (PSF) as defined by CIE [51]:

$$\begin{aligned}
 PSF(\vartheta) = \frac{L_{eq}(\vartheta)}{E} = & [1 - 0.08 \cdot (A/70)^4] \cdot \left[\frac{9.2 \cdot 10^6}{[1 + (\vartheta/0.0046)^2]^{1.5}} + \frac{1.5 \cdot 10^5}{[1 + (\vartheta/0.045)^2]^{1.5}} \right] + \\
 & + [1 + 1.6 \cdot (A/70)^4] \cdot \left\{ \left[\frac{400}{1 + (\vartheta/0.1)^2} + 3 \cdot 10^{-8} \right] + p \cdot \left[\frac{1300}{[1 + (\vartheta/0.1)^2]^{1.5}} + \frac{0.8}{[1 + (\vartheta/0.1)^2]^{0.5}} \right] \right\} + \\
 & + 2.5 \cdot 10^{-3} \cdot p
 \end{aligned} \tag{4.2}$$

in which E is the corneal illuminance generated by a central point source, L_{eq} the equivalent luminance, ϑ the polar angle between the direction of the point source and the location of L_{eq} , A the observer's age and p a pigmentation factor. The equivalent luminance is the luminance in the object scene that has the same visual effect on the retina in a perfect eye as the effect caused by scattering in a non-perfect

eye [52]. The PSF varies over 8 decades from 0 to 10°; light scattering beyond 1° is called stray light [50].

Note that PSF is expressed in units sr^{-1} and that the values are normalized. Indeed, the illuminance at the cornea created by the original point source should be equal to the illuminance generated by all the equivalent sources characterized by their L_{eq} . This illuminance can be calculated from basic photometry as:

$$E = \iint L_{eq}(\vartheta) \cos \vartheta d\Omega_{src} \quad (4.3)$$

with Ω_{src} the solid angle subtended by the source area.

By applying the definition of PSF in Eq. (4.2), Eq. (4.3) can be written as:

$$1 = \iint PSF(\vartheta) \cos \vartheta d\Omega_{src} \quad (4.4)$$

Eq. (4.4) expresses the normalization condition for the normalization condition for the PSF as applied by the CIE.

The model presented in this paper starts from the cone-weighted spectral radiance value L_α of each pixel while the PSF is defined in photometric quantities (Eq. (4.2)). This inconsistency can be easily solved because the PSF is in most cases only slightly wavelength dependent [53]. Under this assumption, the PSF can equivalently be defined as the ratio of the cone-weighted spectral radiance $L_{\alpha,eq}$ and irradiance values E_α .

In an image-based approach, scattering can be implemented by a convolution of the original L_α map with the PSF kernel defined per pixel. A similar concept has been adopted in the field of computer graphics to render highly realistic scenes [54–57], as well as to model how images are formed in the retina [58–60]. When applying the PSF proposed by the CIE in Eq. (4.2) as a filter kernel, discretization and truncation is required. For our implementation, the PSF is put to zero when $\vartheta > 10^\circ$ as the change in the values outside of that range is not significant. Consequently, to keep the corneal illuminance unchanged

inside the kernel, a renormalization is also required and Eqs. (4.3-4.4) can be written as:

$$E_{\alpha} = \sum_x \sum_y \frac{L_{\alpha,eq}(x, y) \cos^2 \mathcal{G}(x, y) A_{pix}}{D^2(x, y)}$$

which is equivalent to (4.5)

$$1 = \sum_x \sum_y \frac{PSF'(x, y) \cos^2 \mathcal{G}(x, y) A_{pix}}{D^2(x, y)}$$

with A_{pix} as the area of each pixel, $D(x, y)$ as the distance from pixel at position (x, y) to the observer's eye (in this experiment at 40 cm normal distance) and PSF' as the re-normalized and re-scaled PSF . When transforming Eqs. (4.3-4.4) to Eq. (4.5), the classical expression of the solid angle of one pixel has been used.

The complete procedure to correct for stray light is as follows: for each pixel under consideration, E_{α} generated from the pixel is calculated and multiplied by the PSF' to calculate an intermediate image $L_{\alpha,eq}$ which represents the equivalent cone weighted spectral radiance map generated by stray light from the pixel under consideration to the neighboring pixels. This is repeated for all pixels and all intermediate images are added to obtain the final image $L_{\alpha,eq}$.

The effect of the convolution with PSF' is illustrated in Figure 4.5 when applied on a uniform stimulus subtending 10° with $L_{\alpha,stim}=50$ and surrounded by a high luminance ring of thickness 1° and located at 6.2° off-center (a gap distance of 1.2°) and with $L_{\alpha,ring}=100$.

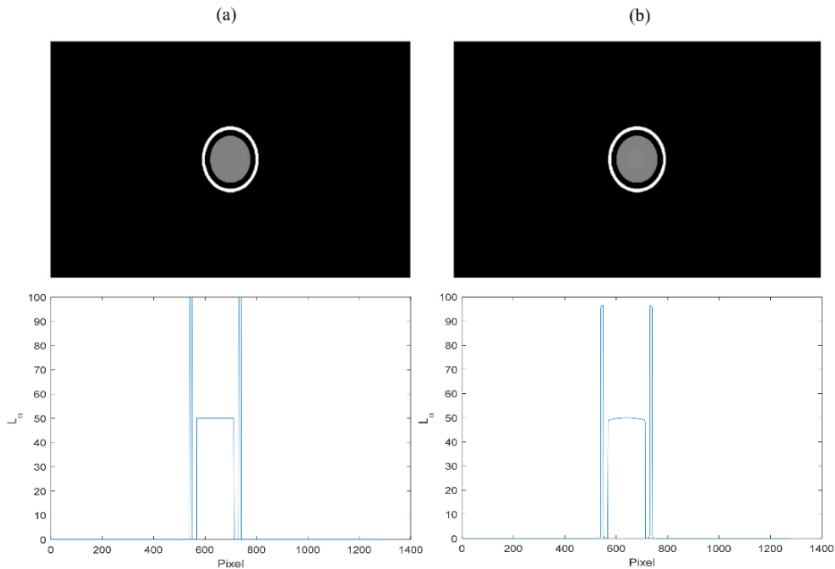


Figure 4.5: The effect of convolving the input image with a PSF kernel: The top images show the full images, and the bottom images show the changes throughout a line in the full image. (a): The original input; (b) After convolution with PSF.

The net effect of the convolution is to slightly decrease the original pixel values of the ring and the central circle (4% and 0.05%, respectively) and to generate some values within the gap (up to 0.8% of the original pixel values of the ring). Note that both circle and ring are generating stray light which partly compensate each other. A fixed kernel has been used over the whole image for simplicity, while strictly spoken the kernel and the normalization should be repeated for each pixel in the image. The impact of this simplification has been checked and is found to be only minor (around 2% difference).

In implementing our proposed brightness model, the correction for retinal straylight is applied by convolving $I_{\alpha}(x, y)$ with a PSF' kernel, defined with an observer age of 35 and a pigmentation factor of 0.5. No attempt was made to use an observer-specific kernel as the effect of the convolution is only minor for the experimental scenes under consideration. With the current image resolution, the kernel size width of 10° to each side of the center of the FOV (or 20° in total) corresponds

to 261×261 pixels. The normalization factor for the *PSF'* was found to be equal to 0.0564. The cone excitations after straylight correction is denoted as $L_{\alpha,eq}$ and the corresponding map is $I_{\alpha,eq}(x, y)$.

4.3. Compression of cone responses

A non-linear compression of the cone responses is widely believed to be one of the earliest steps in visual processing [1,17,61,62]. The cone compression signals are commonly modeled with a sigmoidal curve [16,17] or using a cubic root [23]. In this step of the model, the equivalent cone excitation values are compressed using a cubic power function. This compression has shown to perform well in CAM15u [23] and avoids the issues for a complete dark pixel ($L_{\alpha}=0$) when using a log compression:

$$L_{\alpha,c}=L_{\alpha,eq}^{1/3} \quad (4.6)$$

The image containing $L_{\alpha,c}$ values of each pixel can be considered as a compressed cone excitation map designated as $I_{\alpha,c}(x, y)$.

4.4. Receptive Field response

The signal generated by the central pixel under consideration $L_{\alpha,c}(x, y)$ is considered as the center signal of the receptive field, reflecting the fact that near the fovea, a one-to-one connection from the cone to the bipolar cell is assumed [63].

The surround feedback signal strength from the receptive field (representing the horizontal cell connection) is modeled as a weighted Gaussian response generated by the neighboring pixels, using a fixed standard deviation. To this extend, a Gaussian filtered image is computed by convolving $I_{\alpha,c}(x, y)$ with a Gaussian kernel where the Gaussian kernel $G(x, y)$ at pixel (x, y) is expressed as:

$$G(x, y)=WF \cdot \frac{e^{-\frac{x^2+y^2}{2\delta^2}}}{k} \quad (4.7)$$

with k being a normalization factor such that the sum of all elements inside the discrete Gaussian kernel is 1. The discrete Gaussian kernel is truncated at $4 \times \delta$, which corresponds to the width of the receptive

field; WF models the overall strength of the feedback from the receptive field with regard to the central contribution. Both δ and WF are parameters to be optimized. The resulting image is designated as $I_{\alpha,G}(x, y)$.

4.5. Adaptive shift and brightness output

To calculate a brightness correlate, a sigmoid function is applied as in the classical CAMs. The semi-saturation constant consists of a dark-adapted value σ_0 and the feedback signal strength is added as an adaptive shift, lowering the original central pixel output and modeling the inhibitory effect. This results in a brightness image I_Q with brightness values between 0 and 1:

$$I_Q(x, y) = \frac{I_{\alpha,c}^n(x, y)}{I_{\alpha,c}^n(x, y) + (\sigma_0 + I_{\alpha,G}(x, y))^n} \quad (4.8)$$

with n a parameter modeling the steepness of the sigmoid.

4.6. Determining the model parameters

The parameters included in the model are the width of the receptive field δ , the strength of the feedback from the receptive field WF , the semi-saturation constant in dark conditions σ_0 and the steepness of the sigmoid n . All the steps of the model have been applied for both the reference scene and the 36 test scenes. As the experimental data were collected using the method of adjustment (brightness matching), an optimization should be performed to find the optimal δ , WF and σ_0 value - such that the mean brightness values of the pixels belonging to the stimulus in the output image I_Q of the test scene would be as close as possible to those of the stimulus in the reference scene. Due to this approach, the value of n cannot be determined from the experiments. Given that the choice of n does not influence the final optimization result, the value of n is chosen as $n = 0.58$ as suggested from CAM18sl [22].

From Figure 4.2, it is observed that even for the furthest ring with the thickness of 0.33 cm, there is still an impact of the ring on the brightness of the central stimulus. For this reason, the optimization range of δ is chosen such that the width of the Gaussian kernel can cover the furthest ring; the maximum width of the kernel was taken as

wide as the smaller dimension of the image. The optimization was performed using the MATLAB built-in function and the result indicates that for a δ of 151 pixels, a WF of 1.9, and a σ_0 of 3.0, the model gives the best approximation to all the experimental data.

The mean I_Q values of the pixels inside the stimulus for the reference and for the test scenes using the optimal parameters are plotted in Figure 4.6.

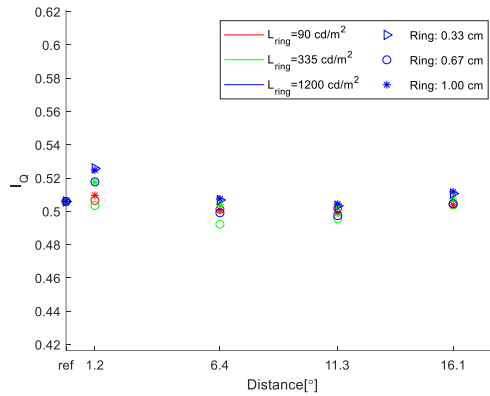


Figure 4.6: Output of I_Q as a function of distance with regard to different ring luminance levels and ring widths

Ideally, for a matching experiment, the I_Q values of the test scenes in which gap distance, luminance and width of the ring are changing should be equal to the value of the reference scene. Overall, the model works very well, with a root mean squared error (RMSE) of 0.0018 (which counts for 0.4% of the reference stimulus brightness) indicating the root mean squared error in the brightness output of the test scene when compared to the reference scene brightness. However, for the highest ring luminance level and the closest ring distance, the model's output generally underestimates the ring's influence resulting in a slightly higher I_Q value than the reference. Note that by adding the straylight correction to the model, a significant improvement in the model's performance is found when predicting the impact of the closest ring at higher luminance levels (RMSE = 0.0029 without straylight correction). The impact of stray light will become even more important when studying scenes containing high luminance areas, which also

justifies the inclusion of this step in the model. Nevertheless, this straightforward model with a limited number of free parameters is able to predict the matching experiments.

An example of the brightness output map is given in Figure 4.7.

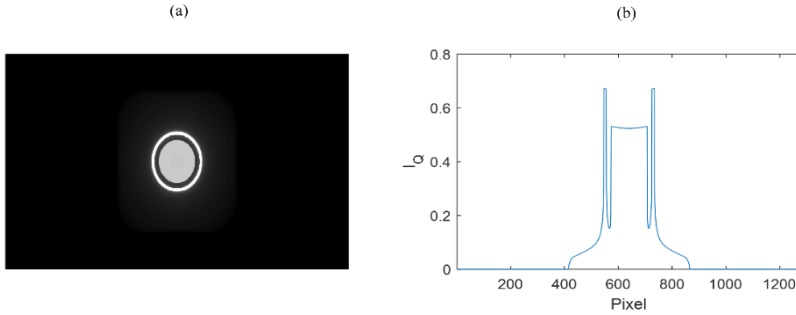


Figure 4.7: The brightness output map: (a) The full image. (b) The value of each pixel from a line cut through the image.

5. Discussion

5.1. Receptive Field size

The optimized kernel standard deviation δ of 151 pixels implies that the width of the Gaussian kernel stopped at $4 \times \delta$ is 604 pixels or approximately 45° in FOV. Typically, the receptive fields in the retina have a relatively small size, ranging from a few arc minutes (near the fovea) to a bit more than 10° in the periphery [64]. This does not fit with the large filter kernel size from the optimization, but the large filter size might correspond to the receptive field in the visual cortex, where the receptive field in the medial superior temporal area can reach to the size of 30° - 50° [3,4]. The large receptive field width is also coherent with the conclusion from previous studies [5–7], where a filter with a large size ranging from a half to the full size of the input image is implemented to account for the luminance adaptation. This suggests that the process of perceiving brightness is determined by a large-scale adaptation, which considers the context of the whole environment in which the stimulus is viewed. With such a wide receptive field, the effect of involuntarily eye movements will be masked as this contribution involves blurring on a much smaller scale of typically 1° in FOV [58]. Note that the wide receptive field is also the reason that the I_G and I_Q values do not change very much over the

stimulus area itself and no distinctive brightness jumps at the edges are observed, in line with the visual observations (Figure 4.7).

From Figure 4.6, a slight under-performance of the model when the rings are presented at the closest distance can be observed. This suggests that at such small distances, the impact might not simply be considered as an adaptation state but other effects such as simultaneous contrast should also be taken into consideration. Moreover, one should also consider that when the ring comes closer to the fovea, the receptive field size is also smaller near the fovea and the inhibition becomes stronger [64].

Additionally, it is noticeable from Figure 4.7 that the I_Q values for the pixels belonging to the dark gap between the ring and the stimulus are no longer completely dark and they receive a rather significant brightness value. However, the dark gap between the ring and the stimulus was not reported as luminous by the observers. Again, it appears that at the closer distance, a stronger contrast perception effect might be active, suggesting that an additional receptive field mechanism characterized by a smaller size should probably be considered.

5.2. *Self-adaptation*

The I_Q value of the stimulus in the reference situation (complete dark background) is very close to 0.5, which points to the fact that the $I_{\alpha,c}(x,y)$ values of the pixels of the reference are close to the sum of the dark semi-saturation value σ_0 and the feedback signal strength $I_{\alpha,G}(x,y)$ which is only due to the stimulus itself. If one would ignore this feedback (by putting WF equal to zero), I_Q values equal to around 0.55 would have been obtained. This illustrates the effect of adaptation to the stimulus itself.

5.3. *Validation of the model*

As the model is established based on rather basic and simple non-uniform backgrounds, i.e. a luminous ring in a dark area, it would be good to verify the performance of the model by applying the model to a few existing datasets from other experiments which were performed to study the perception of brightness for self-luminous stimuli. Sun et al. [8] presented a study about the influence of background luminance

and background size on the brightness perception. In their study, a brightness evaluation experiment using magnitude estimation method was performed. Within the scope of the study, the background was defined as the area immediately adjacent to the stimulus and the surround is the remaining area of the screen used in the experiment, which was adjacent to the background. The experiment was set up with 3 different stimulus luminance levels (19, 88 and 227 cd/m²), 3 background luminance levels (0.09, 88 and 478 cd/m²), 2 surround luminance levels (0.09 and 478 cd/m²), 4 background sizes (0%, 12.5%, 50% and 100% of the screen size) and 3 background orientations (horizontal rectangle, vertical rectangle and 16:9 square).

Based on their experimental details, a set of virtual images were created with the resolution of 1280×675 pixels and a central circular stimulus with a diameter of 52 pixels corresponding to a FOV of 4° when viewed from a distance of 40 cm. As the stimuli and the backgrounds described in these papers are neutral grey, the L_{α} values for the input images were chosen to be equal to the luminance levels of the stimuli and the background described in the corresponding references. Based on the nature of the experiment in our study, only the situations with luminous background and dark surround are used in this evaluation. L_{α} of the stimulus was chosen as 19, 88 and 227, and L_{α} of the background was chosen as 478. The result of the simulation is shown in Figure 4.8.

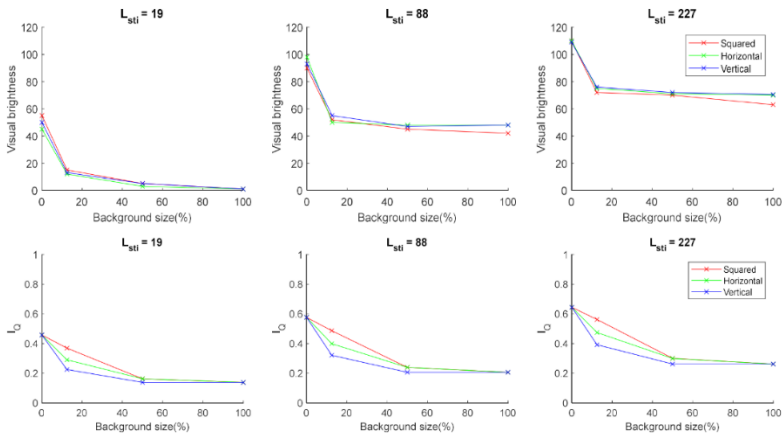


Figure 4.8: The brightness output under different stimulus luminance and background sizes with a background luminance of 478 cd/m²:

(Above) The psychophysics experimental result. (Below) The output of our proposed model.

With a Spearman's ranking correlation coefficient of 0.8281 when comparing the model's output with the visual data of Sun et al., there seems to be a reasonably good agreement between the two datasets. It is observed that the model is generally capable of predicting the decrease in perceived brightness when the luminous background increases in size. The stabilization in the perceived brightness when the background size enlarges from 50% to 100% of the screen size is also predicted, however, in the original study, the most significant brightness decrease happened when the background size went from 0% to 12.5% of the screen, an effect which is less pronounced in the model prediction. This again suggests that an additional smaller receptive field-based interaction represented as a filter with a smaller standard deviation might be needed in the model, emphasizing short distance effects. According to Sun et al. [8], there is almost no effect of background orientation for all background sizes. This is confirmed by the model as long as the background is large (50% or 100% of the image). When the background size is at 12.5% of the screen size, the model predicts a brightness difference of 0.1 when changing from vertical to horizontal, and from horizontal to squared background. This is possibly due to the changes in the number of luminous pixels contributing to the kernel with changing background orientation when convolving the image with a large filter kernel.

The concept of a neutral luminous ring in a dark background can be easily extended to a neutral and uniform luminous background by increasing the width of the ring. Under these conditions, the model CAM18sl should be applied. In establishing this model, Hermans et al. [9] performed experiments in which a uniform stimulus of 10° was seen on a uniform self-luminous background. Six stimulus luminance levels were chosen as 50, 125, 250, 500, 750 and 900 cd/m^2 and 15 background luminance levels were chosen between 0 and 960 cd/m^2 . The brightness of the stimulus is evaluated by magnitude estimation with respect to a reference stimulus; 20 observers participated in the experiment.

Based on the experimental details described in the paper, a set of virtual images were created with the resolution of 1280×675 pixels and a central circular stimulus with a diameter of 135 pixels corresponding to a FOV of 10° when viewed from a distance of 40 cm. The L_α values

chosen for the stimulus and the background were the same values as the luminance values of the stimulus and the background in the experiment by Hermans et al. [9]. In total, 90 virtual scenes were used for this evaluation. The output of the model in relation to the background luminance was compared to the experimental brightness data Q_{obs} (Figure 4.9). In Figure 4.10, the model prediction is compared to the outcome of the visual experiment results and to the prediction of CAM18sl.

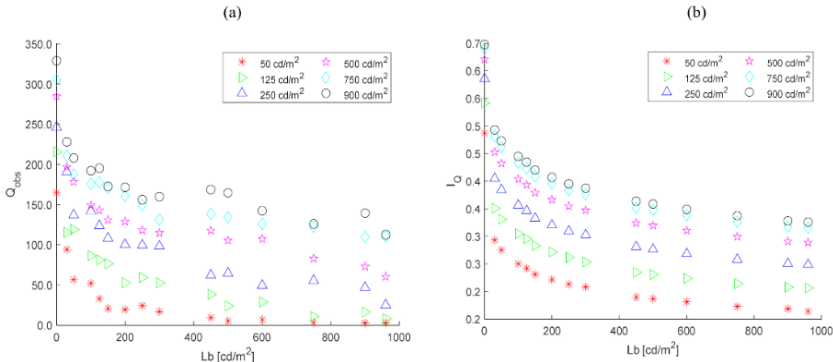


Figure 4.9: Brightness output for the tested scenes from: (a) Experimental results of Hermans et al [9]; (b) Brightness prediction of our model

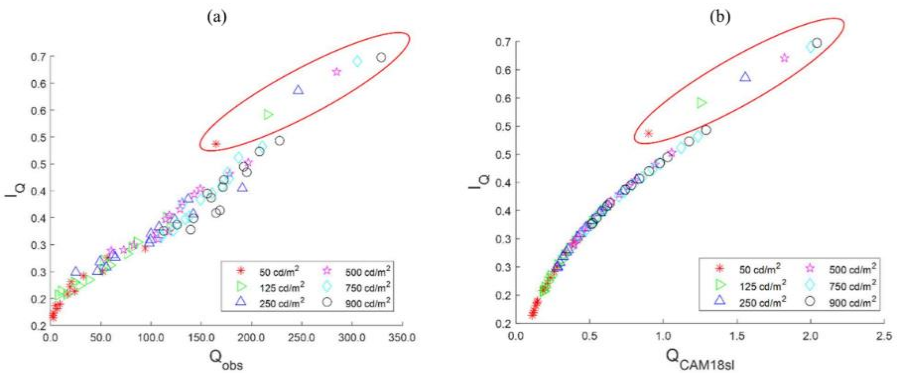


Figure 4.10: The brightness output of the model as a function of the brightness from (a) Experimental data; (b) CAM18sl prediction. The icons inside the red circles correspond to the unrelated stimuli.

From Figure 4.9, it can be seen that the image-based model is able to showcase the dependency of perceived brightness on stimulus and background luminance: when the background luminance increases, the

brightness of the stimulus decreases, and the stimulus brightness increases with increasing stimulus luminance. The model also succeeds in predicting the sharp fall in brightness when the background goes from completely dark to 50 cd/m^2 . From Figure 4.10, the proposed model also has a good agreement with the output from the observers and from CAM18sl with the Spearman's ranking correlation coefficients of 0.9870 and 0.9987, respectively. However, there is a slight overestimation in brightness for unrelated stimuli or, alternatively, a systematic underestimation of the scenes with a luminous background. It is worth noting that the model is developed based on rather small luminous background areas; applying the model to scenes with a very large background size, as is the case for the Hermans et al. data, is quite challenging.

It is also observed that there is no linear relationship between the output of our model and that of CAM18sl, which is believed to be the result of 2-step compression used in our model, while CAM18sl is only using a single compression step.

6. Conclusion

Various CAMs have been developed to predict how humans perceive colors from the optical input of the stimuli. However, with the traditional CAMs, the applications are still limited to a uniform stimulus and background [22]. To extend the applications of such CAMs to non-uniform backgrounds, image-based CAMs have been created, yet, there are still some shortcomings when they are applied to self-luminous scenes [20]. This leads to the need of a comprehensive image-based color appearance model which can overcome the limitations of current CAMs and image CAMs when working with self-luminous scenes; such a model could be called a Lighting Appearance Model (LAM). To move towards developing a LAM, we believe that the first step is to create a comprehensive brightness model for non-uniform backgrounds including self-adaptation.

In this paper, a series of visual brightness experiments have been conducted to study the impact of introducing a luminous ring-shaped area to a dark background on the brightness perception of a central stimulus. Three parameters of the luminous ring have been studied, including the distance from the central stimulus to the ring, the thickness of the ring and the luminance of the ring. In line with various studies, it is clearly shown that by adding a luminous ring to the scene, the brightness of the central stimulus decreases substantially, even for

the smallest thickness (0.33 cm) and the largest stimulus-to-ring distance (16.1°). This phenomenon appears to be stronger when the ring is closer to the stimulus and the impact also increases with the increasing luminance of the ring. The study also confirmed the area effect [8], which was already reported in the literature: as the area of the luminous ring increases, the target stimulus appears to be darker.

An image-based model to simulate the observed phenomenon is proposed, which is highly inspired by the basic physiology of the retina. The model includes cube root compression, scattering in the eye, a receptive field concept, inhibition by neighboring pixels and sigmoid compression. The model has been applied to the experimental brightness data and three parameters are optimized: the width of a Gaussian kernel mimicking the surround signal of the receptive field, the overall weighting factor representing the inhibition strength and the semi-saturation constant for a dark-adapted environment. A standard deviation of 151 pixels representing a receptive field with the coverage up to 45° and a weighting factor of 1.9, shows the best performance of the model. The large receptive field width suggests that the brightness perception and the adaptation to the ring might be the result of the processing at the later stage of the visual pathway such as in the visual cortex, where the receptive field has a large size up to 50° [3,4]. This large filter size is also in line with previous findings [5–7], which supports the idea that the adaptation is mainly linked to the global context where the stimulus is viewed. The model provides a generally good performance in predicting the effect of the area, the distance and the intensity of the ring, though there is some underestimation of the effects with the closest ring distance, which suggests the need of having an additional but smaller receptive field mechanism in the model to simulate more local effects.

Additionally, the performance of the model is evaluated using self-luminous scenes created based on previous studies about brightness for self-luminous stimuli [8,9]. The results show that the model can predict the perceived brightness behavior of those studies, illustrating its robustness. As such, the proposed image-based model appears promising to deal with non-uniform stimuli and complex scenes and can be considered as an important step in search of a generic LAM.

Future work will concentrate on considering adapting the size and the weighting factor of the Gaussian kernel applied to both the center and the surround signal, according to the retinal position, to consider both short- and long-range receptive field sizes, to include a larger range of

luminance levels and to include colored stimuli and backgrounds.

Funding

The authors would like to thank the Research Council of the KU Leuven for supporting this research (C24/17/051). Author KS is supported by KU Leuven internal funds.

Disclosures

The authors declare no conflicts of interest.

Data Availability

Data underlying the results presented in this paper are not publicly available at this time but may be obtained from the authors upon reasonable request.

References

1. A. Wohrer and P. Kornprobst, "Virtual Retina: A biological retina model and simulator, with contrast gain control," *J. Comput. Neurosci.* **25**, 219–249 (2009).
2. P. Martínez-Cañada, C. Morillas, J. L. Nieves, B. Pino, and F. Pelayo, "First stage of a human visual system simulator: The retina," in *Computational Color Imaging* (Springer Verlag, 2015), pp. 118–127.
3. K. Amano, B. A. Wandell, and S. O. Dumoulin, "Visual field maps, population receptive field sizes, and visual field coverage in the human MT+ complex," *J. Neurophysiol.* **102**, 2704–2718 (2009).
4. S. Raiguel, M. M. Van Hulle, D. K. Xiao, V. L. Marcar, L. Lagae, and G. A. Orban, "Size and shape of receptive fields in the medial superior temporal area (MST) of the macaque," *Neuroreport* **8**, 2803–2808 (1997).
5. M. D. Fairchild and G. M. Johnson, "Meet iCAM: A next-generation color appearance model," in *10th Color and Imaging Conference Final Program and Proceedings* (2002), pp. 33–38.
6. J. Kuang, G. M. Johnson, and M. D. Fairchild, "iCAM06: A refined image appearance model for HDR image rendering," *J. Vis. Commun. Image Represent.* **18**, 406–414 (2007).

7. E. Provenzi, "Perceptual color correction: A variational perspective," in *Computational Color Imaging* (Springer Berlin Heidelberg, 2009), pp. 109–119.
8. P. L. Sun, H. C. Li, and M. Ronnier Luo, "Background luminance and subtense affects color appearance," *Color Res. Appl.* **42**, 440–449 (2017).
9. S. Hermans, K. A. G. Smet, and P. Hanselaer, "Brightness Model for Neutral Self-Luminous Stimuli and Backgrounds," *LEUKOS - J. Illum. Eng. Soc. North Am.* **14**, 231–244 (2018).
10. Y. Nayatani, K. Takahama, and H. Sobagaki, "Prediction of color appearance under various adapting conditions," *Color Res. Appl.* (1986).
11. R. W. G. Hunt, *The Reproduction of Colour* (John Wiley & Sons, Ltd, 2005).
12. M. R. Luo and R. W. G. Hunt, "The structure of the CIE 1997 colour appearance model (CIECAM97s)," *Color Res. Appl.* **23**, 138–146 (1998).
13. N. Moroney, M. D. Fairchild, R. W. Hunt, C. Li, M. Ronnier Luo, and T. Newman, "The CIECAM02 color appearance model," in *10th Color and Imaging Conference Final Program and Proceedings* (2002), pp. 23–27.
14. C. Li, Z. Li, Z. Wang, Y. Xu, M. R. Luo, G. Cui, M. Melgosa, M. H. Brill, and M. Pointer, "Comprehensive color solutions: CAM16, CAT16, and CAM16-UCS," *Color Res. Appl.* **42**, 703–718 (2017).
15. M. D. Fairchild, *Color Appearance Models*, 2nd ed. (John Wiley & Sons, Ltd, 2013).
16. E. Reinhard, T. Pouli, T. Kunkel, B. Long, A. Ballestad, and G. Damberg, "Calibrated image appearance reproduction," *ACM Trans. Graph.* **31**, 1–11 (2012).
17. L. Meylan, D. Alleysson, and S. Süssstrunk, "Model of retinal local adaptation for the tone mapping of color filter array images," *J. Opt. Soc. Am. A* **24**, 2807 (2007).
18. A. Benoit, D. Alleysson, J. Herault, and P. Le Callet, "Spatio-temporal tone mapping operator based on a retina model," in

Computational Color Imaging (2009), pp. 12–22.

19. Ø. Kolås, I. Farup, and A. Rizzi, "Spatio-Temporal Retinex-inspired Envelope with Stochastic Sampling: A framework for spatial color algorithms," in *Journal of Imaging Science and Technology* (2011), Vol. 55, pp. 405031–4050310.
20. T. H. Phung, F. B. Leloup, K. A. G. Smet, and P. Hanselaer, "Assessing the application of an image color appearance model to basic self-luminous scenes," *Color Res. Appl.* **44**, 848–858 (2019).
21. E. H. Land, "The Retinex Theory of Color Vision," *Sci. Am.* **237**, 108–129 (1977).
22. S. Hermans, K. A. G. Smet, and P. Hanselaer, "Color appearance model for self-luminous stimuli," *J. Opt. Soc. Am. A* **35**, 2000–2009 (2018).
23. M. Withouck, K. A. G. Smet, W. R. Ryckaert, and P. Hanselaer, "Experimental driven modelling of the color appearance of unrelated self-luminous stimuli: CAM15u," *Opt. Express* **23**, 12045 (2015).
24. S. Hermans, K. A. G. Smet, and P. Hanselaer, "Exploring the applicability of the CAM18sl brightness prediction," *Opt. Express* **27**, 14423–14436 (2019).
25. O. U. Preciado, A. Martin, E. Manzano, K. A. G. Smet, and P. Hanselaer, "CAM18sl brightness prediction for unrelated saturated stimuli including age effects," *Opt. Express* **29**, 29257–29274 (2021).
26. Y. Lin, Y. Liu, Y. Sun, X. Zhu, J. Lai, and I. Heynderickx, "Model predicting discomfort glare caused by LED road lights.," *Opt. Express* **22**, 18056–71 (2014).
27. P. Whittle, "Brightness, discriminability and the "Crispening Effect,"" *Vision Res.* **32**, 1493–1507 (1992).
28. P. Whittle and P. D. C. Challands, "The effect of background luminance on the brightness of flashes," *Vision Res.* **9**, 1095–1110 (1969).
29. J. C. Stevens, "Brightness inhibition re size of surround," *Percept. Psychophys.* **2**, 189–192 (1967).

30. H. Leibowitz, F. A. Mote, and W. R. Thurlow, "Simultaneous contrast as a function of separation between test and inducing fields.," *J. Exp. Psychol.* **46**, 453–456 (1953).
31. R. Carter, L. Sibert, J. Templeman, and J. Ballas, "Luminous backgrounds and frames affect gray scale lightness, threshold, and suprathreshold discriminations," *J. Exp. Psychol. Appl.* **5**, 190–204 (1999).
32. R. Clay Reid and R. Shapley, "Brightness induction by local contrast and the spatial dependence of assimilation," *Vision Res.* **28**, 115–132 (1988).
33. S. K. Shevell, I. Holliday, and P. Whittle, "Two separate neural mechanisms of brightness induction," *Vision Res.* **32**, 2331–2340 (1992).
34. F. Kingdom and B. Moulden, "A multi-channel approach to brightness coding," *Vision Res.* **32**, 1565–1582 (1992).
35. J. A. McArthur and B. Moulden, "A two-dimensional model of brightness perception based on spatial filtering consistent with retinal processing," *Vision Res.* **39**, 1199–1219 (1999).
36. J. J. McCann and R. Savoy, "Measurements of lightness: dependence on the position of a white in the field of view," in *Human Vision, Visual Processing, and Digital Display II* (SPIE, 1991), Vol. 1453, pp. 402–411.
37. M. E. Rudd, "Lightness computation by the human visual system," *J. Electron. Imaging* **26**, 031209 (2017).
38. D. H. Brainard, "The Psychophysics Toolbox," *Spat. Vis.* **10**, 433–436 (1997).
39. D. G. Pelli, "The VideoToolbox software for visual psychophysics: Transforming numbers into movies," *Spat. Vis.* **10**, 437–442 (1997).
40. K. M, D. H. Brainard, and D. G. Pelli, "What's new in Psychtoolbox-3?," *Perception* **36**, ECV Abstract Supplement (2007).
41. MATLAB, "MATLAB," (2019).
42. International Commission on Illumination., *Fundamental*

Chromaticity Diagram with Physiological Axes. Part 1.
(Commission internationale de l'éclairage, 2006).

43. A. Stockman, L. T. Sharpe, and C. Fach, "The spectral sensitivity of the human short-wavelength sensitive cones derived from thresholds and color matches," *Vision Res.* **39**, 2901–2927 (1999).
44. A. Stockman and L. T. Sharpe, "The spectral sensitivities of the middle- and long-wavelength-sensitive cones derived from measurements in observers of known genotype," *Vision Res.* **40**, 1711–1737 (2000).
45. P. A. García, R. Huertas, M. Melgosa, and G. Cui, "Measurement of the relationship between perceived and computed color differences," *J. Opt. Soc. Am. A* **24**, 1823 (2007).
46. M. Withouck, K. A. Smet, and P. Hanselaer, "Brightness prediction of different sized unrelated self-luminous stimuli," *Opt. Express* **23**, 13455–13466 (2015).
47. W. J. Huang, Y. Yang, and M. R. Luo, "Verification of the CAM15u colour appearance model and the QUGR glare model," *Light. Res. Technol.* **51**, 24–36 (2019).
48. C. Fu, C. Li, G. Cui, M. R. Luo, R. W. G. Hunt, and M. R. Pointer, "An investigation of colour appearance for unrelated colours under photopic and mesopic vision," *Color Res. Appl.* **37**, 238–254 (2012).
49. B. Koo and Y. Kwak, "Color appearance and color connotation models for unrelated colors," *Color Res. Appl.* **40**, 40–49 (2015).
50. T. J. T. P. van den Berg, L. Franssen, and J. E. Coppens, "Ocular Media Clarity and Straylight," in *Encyclopedia of the Eye* (Elsevier, 2010), pp. 173–183.
51. J. J. Vos and T. J. T. P. van den Berg, "Report on disability glare," in *CIE Collection 135* (1999), pp. 1–9.
52. VOS and J. J., "Disability Glare-A state of the art report," *CIE J.* **3**, 39–53 (1984).
53. J. E. Coppens, L. Franssen, and T. J. T. P. van den Berg,

- "Wavelength dependence of intraocular straylight," *Exp. Eye Res.* **82**, 688–692 (2006).
54. G. Spencer, P. Shirley, K. Zimmerman, and D. P. Greenberg, "Physically-based glare effects for digital images," in *Proceedings of the ACM SIGGRAPH Conference on Computer Graphics* (1995), pp. 325–334.
55. R. Raskar, A. Agrawal, C. A. Wilson, and A. Veeraraghavan, "Glare aware photography," in *ACM SIGGRAPH 2008 Papers on - SIGGRAPH '08* (ACM Press, 2008), pp. 1–10.
56. H. Ando, N. Torigoe, K. Toriyama, and K. Ichimiya, "Real-time rendering of high quality glare images using vertex texture fetch on GPU," in *GRAPP 2006 - Proceedings of the 1st International Conference on Computer Graphics Theory and Applications* (2006), pp. 19–25.
57. A. Yoshida, M. Ihrke, R. Mantiuk, and H. P. Seidel, "Brightness of the glare illusion," in *APGV 2008 - Proceedings of the Symposium on Applied Perception in Graphics and Visualization* (ACM Press, 2008), pp. 83–89.
58. R. A. Normann, B. S. Baxter, H. Ravindra, and P. J. Anderton, "Photoreceptor Contributions to Contrast Sensitivity: Applications in Radiological Diagnosis," *IEEE Trans. Syst. Man Cybern.* **SMC-13**, 944–953 (1983).
59. D. C. Hood, T. Ilves, E. Maurer, B. Wandell, and E. Buckingham, "Human cone saturation as a function of ambient intensity: A test of models of shifts in the dynamic range," *Vision Res.* **18**, 983–993 (1978).
60. J. J. McCann and V. Vonikakis, "Calculating retinal contrast from scene content: A program," *Front. Psychol.* **8**, 2079 (2018).
61. T. Kunkel and E. Reinhard, "A neurophysiology-inspired steady-state color appearance model," *J. Opt. Soc. Am. A* **26**, 776 (2009).
62. M. Kamermans, D. A. Kraaij, and H. Spekreijse, "The cone/horizontal cell network: a possible site for color constancy," *Vis. Neurosci.* **15**, 787–797 (1998).
63. J. V. Forrester, A. D. Dick, P. G. McMenamin, F. Roberts, and

- E. Pearlman, "Anatomy of the eye and orbit," in *The Eye* (Elsevier, 2016), pp. 1-102.e2.
64. L. J. Croner and E. Kaplan, "Receptive fields of P and M ganglion cells across the primate retina," *Vision Res.* **35**, 7–24 (1995).

Chapter 5

Impact of colored background elements on brightness perception of neutral self-luminous stimuli

5. Impact of colored background elements on brightness perception of neutral self-luminous stimuli

5.1. Introduction

In previous chapters, the influence of distance, thickness and luminance of a neutral self-luminous ring in the background on the brightness perception of a neutral self-luminous stimulus has been investigated. Based on the collected data, two brightness models have been proposed. In these models, the L, M and S cones corresponding to the neutral background respond more or less equally (the same is true for the neutral stimulus). This has the advantage that only one input parameter has to be considered instead of three. However, to move towards a full CAM/LAM, it is essential to study how the changes in the response of each individual cone type can affect the perceived brightness of a central stimulus.

A wide range of studies regarding the influence of color on perceived brightness has been performed. One category deals with the impact of color and saturation of the stimulus itself on its brightness (the H-K effect) [1–4]; another category dealing with the impact of a colored background on chromatic induction [5–9] has also been extensively investigated. However, the number of studies available examining the effect of chromatic backgrounds on stimulus brightness is still rather limited.

In this chapter, a preliminary experiment to study the influence of chromatic rings on the brightness perception of the neutral self-luminous stimulus and the first observations from the experimental results are presented.

5.2. Experiment

Stimuli

The reference and the test stimuli were generated with PsychToolbox in MATLAB and were shown to the observers on an EIZO ColorEdge PROMINENCE CG3145 screen. The reference stimulus had the size of 10° in the field of view and the screen covered a field of view of

82°×49° when the observer was positioned at a distance of approximately 40 cm to the screen. To block the possible visual impact of the light from one side of the experimental scene to the other, a black shield was placed between the reference and the test stimuli.

The reference stimulus was a neutral grey circle of 10° with a luminance $L_{10,ref} = 60 \text{ cd/m}^2$. The CIE 2006 10° chromaticity values of the reference stimulus were ($x_{F10} = 0.310$, $y_{F10} = 0.323$), which is close to the chromaticity of CIE illuminant D65.

The test scene is composed of a central neutral grey circle of 10° and a colored ring surrounding the central circle. This choice of scene composition ensures an equal impact of the distance and the luminance of the self-luminous segment of the background on the central stimulus in all directions. The test stimulus has a starting luminance of either 53 cd/m^2 or 100 cd/m^2 . The CIE 2006 10° chromaticity of the test stimulus was identical to that of the reference stimulus. Seven colored rings were chosen based on the primary colors of the screen (red, green, blue, cyan, magenta, yellow, and neutral) such that the ρ -cone excitation would remain relatively similar for all chosen colored rings. The detailed calculation of the cone excitations is provided in Eq.(5.1) in the next section. By fixing the value of the ρ -cone type response of the additional ring, the problem is somewhat reduced to finding the influence of γ and β cones on the brightness perception of the central stimulus with the ρ -cone type response considered as constant. The ring with a thickness of 1 cm (or 0.72° in angular width) was shown at a distance of 11.3° from the outer edge of the stimulus. Two ρ -cone excitation values of approximately 42.37 and 55.56 were selected such that they could induce a perceptible impact without creating visual discomfort to observers. For each ρ -cone excitation value, a separate experiment was conducted. The CIE 2006 10° chromaticity values, γ and β cones excitations and luminance levels of the chosen rings for each experiment are summarized in Table 5.1 and Table 5.2.

Parameters Ring colors	γ	β	x_{F10}	y_{F10}	Luminance (cd/m^2)
Red	10.59	1.40	0.670	0.315	32
Green	53.84	3.01	0.270	0.682	46

Blue	74.26	456.45	0.146	0.083	53
Cyan	56.65	62.54	0.197	0.331	47
Magenta	23.60	105.12	0.335	0.161	36
Yellow	38.23	2.41	0.451	0.516	41
Neutral	42.56	44.65	0.310	0.324	43

Table 5.1: Summary of experimental parameters with ρ -cone excitation of 42.37 (Experiment 1)

Parameters Ring colors	γ	β	x_{F10}	y_{F10}	Luminance (cd/m ²)
Red	13.80	1.56	0.670	0.315	42
Green	70.77	3.68	0.270	0.682	60
Blue	94.65	601.36	0.146	0.083	67
Cyan	75.01	83.77	0.197	0.331	62
Magenta	31.57	143.73	0.335	0.161	49
Yellow	49.93	2.79	0.451	0.516	53
Neutral	55.72	60.02	0.310	0.324	56

Table 5.2: Summary of experimental parameters with ρ -cone excitation of 55.56 (Experiment 2)

The chromaticity coordinates of the chosen ring colors are illustrated in Figure 5.1.

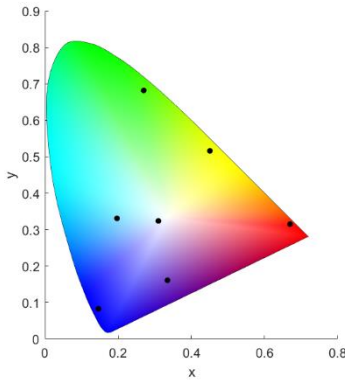


Figure 5.1: Chromaticity coordinates of the chosen rings.

In Figure 5.2, a picture from the reference scene and the test scene with a magenta ring is shown.



Figure 5.2: Experimental setup with an example of the reference scene and the test scene with a magenta ring.

In each experiment, to account for positional bias and luminance starting point bias, the test stimuli were displayed both on the left and right of the setup, at two different starting luminance levels. The matching errors made by each observer were considered with two experimental scenes in which the test stimulus was not surrounded by any ring, and the test stimulus was shown with both a high and low starting luminance level. Five repeated scenes were included for the calculation of intra-observer variability. To avoid ordinal bias, the test sequence for each observer was also randomized.

At the start of the experiment, the observer performed a trial session which included 10 test scenes to get accustomed to the experimental procedure. The 10 trial test scenes were randomly chosen from the full set of test scenes for each observer. In the official experimental session, 35 test scenes were shown (7 ring colors \times 2 starting points \times 2 reference positions + 2 test scenes for matching errors + 5 repeated scenes for intra-observer variability).

Procedure

The method of brightness matching was chosen to perform the visual data collection. Before starting the official experiment, the observers were asked to look at a test scene randomized for each observer while being seated in the dark room for 5 minutes to get adapted to the

experimental conditions. During the adaptation period, the observer also received the instructions to perform the experiment.

Similar to the experiments mentioned in Chapters 3 and 4, the observers were requested to move back and forth to change their gaze such that they always looked with binocular view perpendicularly to the central circle in the reference and the test scenes, one at a time. It was also emphasized that the distance of 40 cm between the observer and the screen should be always maintained. The observer was asked to adjust the brightness of the test stimulus such that it could visually appear to be equally bright as the reference stimulus. The matching task was performed by using the keyboard, which was connected to the computer that controlled the screen with 10-bit signal. The observer could choose to adjust the brightness of the test stimulus with three adjustment levels: 10 RGB levels, 5 RGB levels and 1 RGB level. The 10-RGB-level adjustments allowed the observer to reach quick changes, while the 5-RGB-level adjustments enabled adjustments with consistent perceptual brightness steps and the 1-RGB-level helped fine-tuning the match. The average duration of the experiment was between 45 and 90 minutes.

The observer panel of Experiment 1 consisted of 11 subjects (4 females and 7 males), aged between 23 and 37 years old with an average of 25.6 years. The observer panel of Experiment 2 consisted of 8 subjects (4 females and 4 males) between 23 and 37 years old with an average of 26.5 years. All observers had normal color vision with normal to superior discrimination as tested by the Munsell 100 hues test.

From the matching results of each observer, the spectral radiance of the matched stimuli was collected using a JETI Specbos 1211 spectroradiometer. The measured area covered 75% of the central area of the stimulus. Several tests were performed to check the uniformity of the screen, and good uniformity of less than 2% difference between the maximum and the minimum values was detected. The screen also showed no pixel cross-talk issue. With a thickness smaller than the spectrometer field of view, the spectral radiance of the colored rings was measured by taking the spectral radiance of an arbitrary larger area at the center of the display, which had the same RGB values as the ring.

From the spectral radiance, the long, medium and short cone excitations ρ, γ, β of the stimulus are computed with the set of cone

fundamentals $\bar{l}_{10}, \bar{m}_{10}, \bar{s}_{10}$ for 10° stimuli as provided by the CIE in 2006 [10–12]. The normalization coefficients were chosen such that for a D65 stimulus, the cone responses are identical and equal to the stimulus CIE 2006 10° luminance value:

$$\begin{aligned} \rho &= 686.7 \int_{390}^{830} L_{e,\lambda}(\lambda) \bar{l}_{10}(\lambda) d\lambda \\ \gamma &= 768.3 \int_{390}^{830} L_{e,\lambda}(\lambda) \bar{m}_{10}(\lambda) d\lambda \\ \beta &= 1366.1 \int_{390}^{830} L_{e,\lambda}(\lambda) \bar{s}_{10}(\lambda) d\lambda \end{aligned} \quad (5.1)$$

with $L_{e,\lambda}(\lambda)$ the spectral radiance of the stimulus.

The cone excitations for the rings were computed similarly.

With a chromaticity close to that of the D65 illuminant, the stimuli have almost identical responses for all three cone types with a difference of less than 2% between the minimum and the maximum values. Hence, the arithmetic mean of the three cone excitations of the stimulus (denoted as α) can be used to describe the stimulus.

5.3. Results and Discussion

5.3.1. Observer variability

The observer variabilities were computed using the standardized residual sum of squares STRESS obtained for each observer. The values indicate the agreement between two sets of data, where two sets with perfect agreement would have a STRESS value of zero [13]. The average intra-observer variability was calculated in the same manner as mentioned in previous chapters and presented in Table 5.3.

Experiment	Intra-observer variability	Inter-observer variability
Experiment 1	9.9	10.8
Experiment 2	12.3	10.8

Table 5.3: Observer variability in terms of STRESS (scale: 0-100)

The results indicates a better agreement in the observer variability than in previous literature, which performed brightness experiments using matching or magnitude estimation methods [14–19]. The matching error of approximately 4.3% for Experiment 1 and 8.2% for Experiment 2 give an indication of how reliable the matching results are. It is also noticeable that the STRESS values for this set of experiments are lower than those of the experiments in previous chapters. From previous experiments in Chapter 3, it is observed that the observer variabilities were lower with lower ring luminance. The lower STRESS values reported in this chapter are believed to be the result of the lower luminance range that was used.

Finally, to obtain the average matching result for each test scene from each observer, the arithmetic mean of α of the matched stimuli from different starting luminance levels and different reference positions is computed. The overall average matching result of the experiment is determined as the arithmetic mean of the average results from each individual observer.

5.3.2. Experimental results

The average cone excitation of the test stimulus α_{test} , and the ratio between the average cone excitation of the test stimulus α_{test} and the cone excitation of the reference stimulus α_{ref} are illustrated in Figure 5.3. Consistent with the findings in previous chapters, it is observed that adding a self-luminous ring to the dark background, the observer would need to give the test stimulus a higher matched cone excitation in comparison to the reference stimulus.

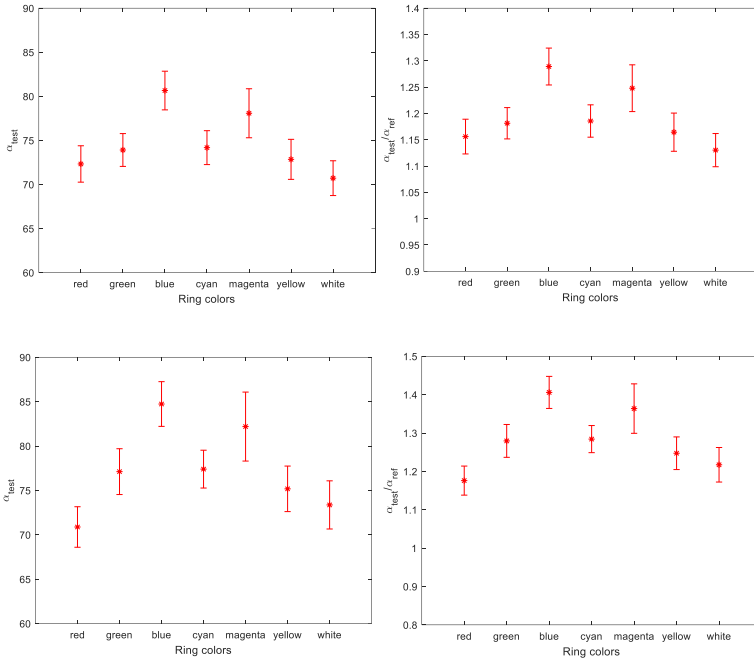


Figure 5.3: The average cone excitation (left) and the ratio of the matched stimuli as a function of the ring colors with: (top) a fixed ρ -cone excitation of 42.37 (Experiment 1), (bottom) a fixed ρ -cone excitation of 55.56 (Experiment 2). The error bars represent the standard errors.

From Figure 5.3, it is also shown that blue rings appeared to have significantly higher impact than most other colored rings (except magenta), and magenta rings also had relatively stronger influence than the rings in other colors rather than blue. For the other five ring colors (red, green, cyan, yellow and neutral), green and cyan rings seem to have a slightly higher effect on the brightness of the central stimulus, however, the difference is not too distinctive. This observation is confirmed with the pairwise Kruskal-Wallis test for each pair of ring colors in each experiment with the p-values as shown in Table 5.4 and Table 5.5.

	Red	Green	Blue	Cyan	Magenta	Yellow	Neutral
Red	1.000	0.491	0.009	0.533	0.158	0.974	0.412
Green	0.491	1.000	0.094	0.718	0.491	0.412	0.224
Blue	0.009	0.094	1.000	0.020	0.279	0.008	0.002

Cyan	0.533	0.718	0.020	1.000	0.279	0.491	0.200
Magenta	0.158	0.491	0.279	0.279	1.000	0.094	0.028
Yellow	0.974	0.412	0.008	0.491	0.094	1.000	0.577
Neutral	0.412	0.224	0.002	0.200	0.028	0.577	1.000

Table 5.4: p-values from Kruskal-Wallis test for Experiment 1

	Red	Green	Blue	Cyan	Magenta	Yellow	Neutral
Red	1.000	0.141	0.003	0.074	0.027	0.172	0.462
Green	0.141	1.000	0.027	0.753	0.248	0.674	0.141
Blue	0.003	0.027	1.000	0.074	0.345	0.021	0.005
Cyan	0.074	0.753	0.074	1.000	0.529	0.529	0.115
Magenta	0.027	0.248	0.345	0.529	1.000	0.141	0.036
Yellow	0.172	0.674	0.021	0.529	0.141	1.000	0.529
Neutral	0.462	0.141	0.005	0.115	0.036	0.529	1.000

Table 5.5: p-values from Kruskal-Wallis test for Experiment 2

The results of the statistical tests depict a significant difference between the effect of the blue rings compared to the rest, and magenta rings also have a significantly higher influence than a few colored rings such as red and neutral rings. There is no distinctive difference between the effect of the other five ring colors, though generally, the average matching results showed that red and neutral rings have lower impacts than the rest.

In Chapter 3, the impact of adding a neutral luminous ring was represented by modeling the Relative Adaptive Shift (RAS), which can be deduced from the experimental data as:

$$RAS = \frac{\alpha_{test}}{\alpha_{ref}} - 1 \quad (5.2)$$

To better understand the driving factor of the observed phenomenon, the relationships between the RAS and various parameters are illustrated.

It appears that the influence of the additional ring is not dominated by the luminance level of the ring (Figure 5.4): with relatively small changes in luminance levels, the influence of different colored rings is expected to have little to no significant differences with each other; however, the results state otherwise, with a significantly larger effect produced by the blue and magenta rings.

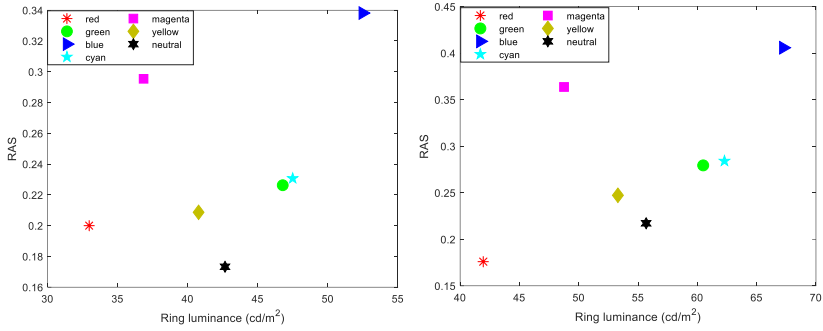


Figure 5.4: RAS as a function of ring luminance for: (left) Experiment 1, (right) Experiment 2.

It has been widely acknowledged that the apparent brightness of a light source is determined not only by its luminance but also by its saturation [3]. Therefore, it might be interesting to check the correlation between the brightness of the chromatic ring with its corresponding influence on the brightness of the central stimulus. As all the rings were shown in identical conditions and had the same size, the relative changes in brightness are compared by using the brightness of the ring computed with CAM18sl [16] using the ρ, γ, β cone responses of the rings as the input for the stimulus, and assuming that the background is completely dark. As illustrated in Figure 5.5, it seems that the apparent brightness of the ring also does not correlate well with the RAS. Although the neutral ring -which appears as the darkest- and the blue ring -appearing as the brightest- show the lowest and highest RAS-value respectively, for the case of the other rings, the orders do not appear coherently to the measured effect, e.g., the red ring has the second highest brightness (only after blue), yet the RAS was the second lowest, after the neutral ring.

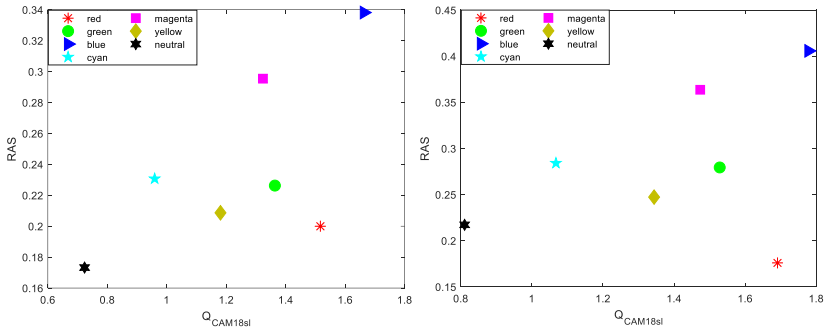


Figure 5.5: RAS as a function of ring brightness for: (left) Experiment 1, (right) Experiment 2.

When comparing the experimental results with the γ - and β -cone excitations (Figure 5.6), it shows that except for the case of the neutral ring, the increase in β -cone excitation seems to increase the influence of the chromatic ring. Few studies have pointed out that the increase in β -cone could induce a higher glare sensation [20] and it also has an important role in chromatic induction [9]. This suggests that further investigations into the influence of β -cone excitation in brightness inhibition could be a promising direction. Though Figure 5.6 shows no correlation between the γ -cone response and RAS, the reduced effect in the case of the neutral ring (which has equal cone responses) when compared to the yellow and magenta rings (which have lower β -cone excitation than the neutral ring) could imply that the inhibition from one cone type to another could be an additional factor controlling the effect.

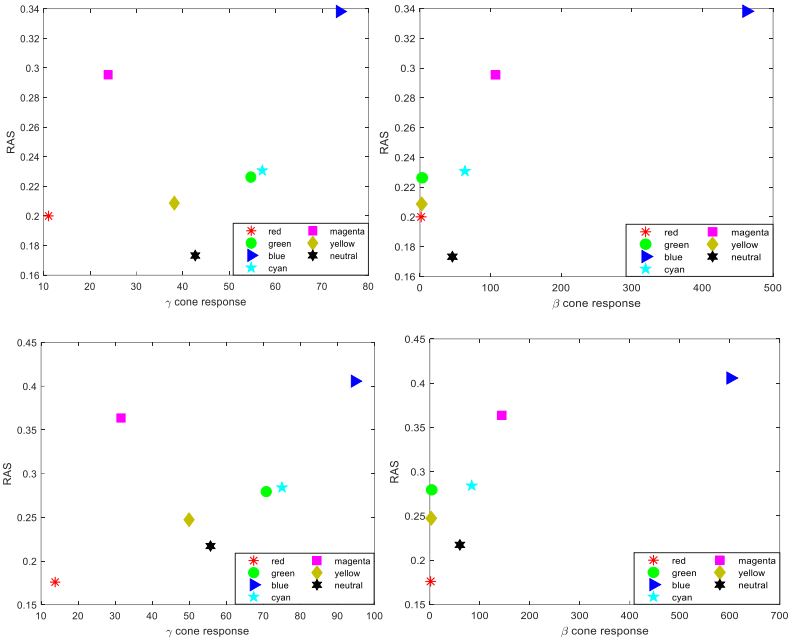


Figure 5.6: RAS as a function of γ cone response (left) and β - cone response (right) for: (top) Experiment 1, (bottom) Experiment 2.

In chromatic-related research, input parameters are commonly expressed as $\rho/(\rho+\gamma)$ and $\beta/(\rho+\gamma)$ signals and the chromatic-related effects are expressed as a function of those two signals [21,22]. As a first attempt to model the effect, a fitting function created with the Curve Fitting Toolbox of MATLAB is created to express the RAS in terms of $\rho/(\rho+\gamma)$ and $\beta/(\rho+\gamma)$ signals. The following equation appears to have the best fit to the experimental data (Figure 5.7):

$$\begin{aligned}
 RAS = & -0.0798 \left(\frac{\rho}{\rho+\gamma} \right)^2 - 0.0006 \left(\frac{\beta}{\rho+\gamma} \right)^2 + \\
 & + 0.1072 \left(\frac{\rho}{\rho+\gamma} \right) \left(\frac{\beta}{\rho+\gamma} \right) + 0.2387
 \end{aligned}
 \tag{5.3}$$

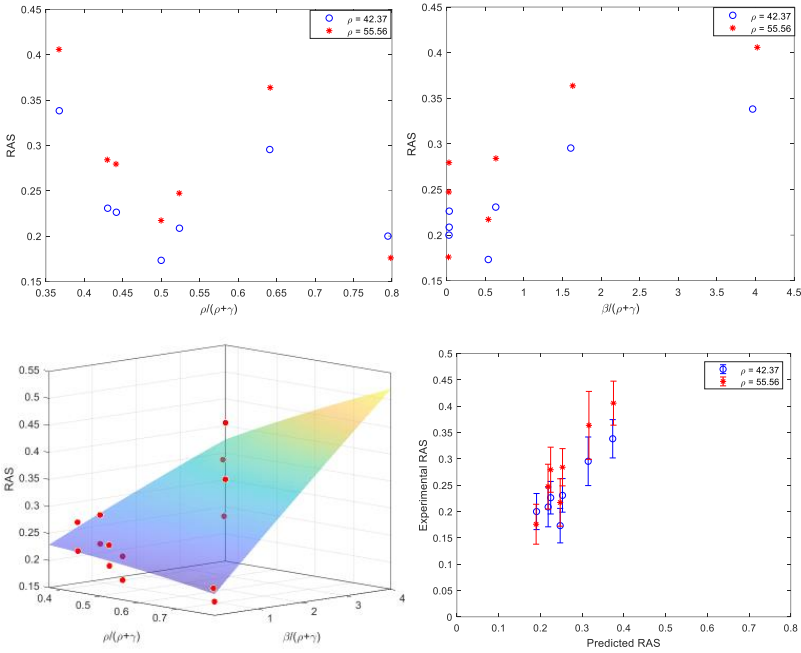


Figure 5.7: Correlation between RAS and $\rho/(\rho+\gamma)$ and $\beta/(\rho+\gamma)$ signals: (Top Left) RAS vs. $\rho/(\rho+\gamma)$. (Top Right) RAS vs. $\beta/(\rho+\gamma)$. (Bottom Left) The red dots represent the experimental data, and the surface represents the fitted model. (Bottom Right) The correlation between the predicted RAS and experimental RAS. The error bars represent the standard error of the experimental RAS.

Though the fitting function shows a relatively acceptable correlation to the experimental data with a R^2 value of 0.74, the physiological mechanism behind the model is still unclear.

Besides the cone contributions in brightness, it has been recently discovered that the change of pupil size [23] and the contribution of ipRGCs [24] also have major impacts on brightness perception. The study of Sulutvedt et al. shows that the dilation of the pupil could lead to an enhanced sense of brightness: an increase of 1 mm in pupil diameter can result in an average increase of 2.09 cd/m^2 to obtain a brightness match for a stimulus with the luminance range between 61.46 cd/m^2 and 117.61 cd/m^2 viewed with a smaller pupil diameter [23]. Additionally, Zele et al. proposed that brightness

perception depends not only on cone responses but also on the contribution of melanopsin in ipRGCs: brightness estimations should be the result of a combined interaction between cone and melanopsin contributions [24]. In a recent study by Sandoval et al. [25], it is suggested that among different parameters such as luminance, brightness and photoreceptors responses, ipRGC responses appear to be the main driving mechanism for pupil size changes. This conclusion was also suggested in an earlier study by Watson et al. [26], in which the dependency of pupil size on age, luminance, field size and binocularity was discussed. Considering the important role of pupil size and ipRGCs contribution in visual adaptation, a correlation between RAS and ipRGC responses is also checked. The ipRGC responses are computed such that for a D65 stimulus, the ipRGC response is equal to the stimulus CIE 2006 10° luminance value:

$$ipRGC = 847.3 \int_{390}^{830} L_{e,\lambda}(\lambda) N_z(\lambda) d\lambda \quad (5.4)$$

With N_z is the melanopic sensitivity function.

The correlations between RAS and ipRGC responses for each experiment are plotted in Figure 5.8.

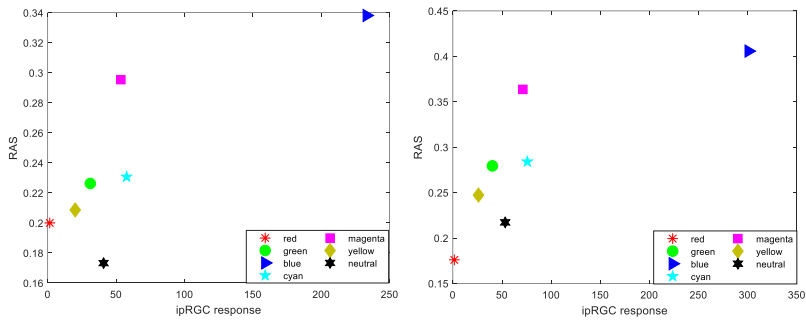


Figure 5.8: RAS as a function of ipRGC response for: (left) Experiment 1, (right) Experiment 2.

From Figure 5.8, it appears that the ipRGC response has quite good correspondence to the variation tendency observed with RAS, excluding the case of a neutral ring, where the ipRGC response of the

neutral ring is higher than for that of red, yellow and green rings, yet the RAS of the neutral ring is lower than others.

In Chapter 3, a model representing RAS as a function of the ring thickness, ring distance and the average of cone excitations (α) of the ring was proposed in Eq (3.9) as repeated below:

$$RAS = a \cdot \alpha_{ring}^b \cdot \Omega_{ring}^c \cdot e^{-gap^2/2\delta^2} \quad (5.5)$$

As the α was the average of three cone responses which were computed to be nominally equal to the luminance of the D65 stimulus, and so is the ipRGC response, it might be relevant to apply the proposed model using the ipRGC response instead of the α value for the ring.

For ease of illustration, the data points are given the indices as summarized in Table 5.6.

Index	ρ -cone excitation	Ring colors order
1-7	42.37	Red – Green – Blue – Cyan – Magenta – Yellow - Neutral
8-14	55.56	Red – Green – Blue – Cyan – Magenta – Yellow - Neutral

Table 5.6: Data points index

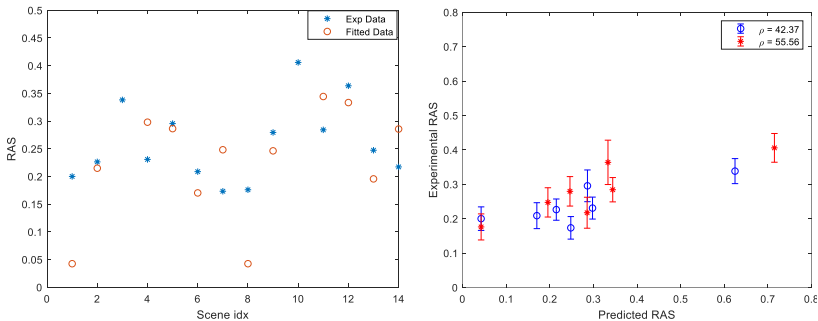


Figure 5.9: Modeled vs. Experimental RAS: (Left) The results per experimental scene. (Right) The correlation between the predicted RAS and experimental RAS. The error bars represent the standard error of the experimental RAS.

The correlation between the modeled data and the experimental data is rather low ($R^2 = 0.68$, $RMSE = 0.13$). It shows a systematic strong overestimation of the blue rings effect, while underestimating the influence of the red and the yellow rings.

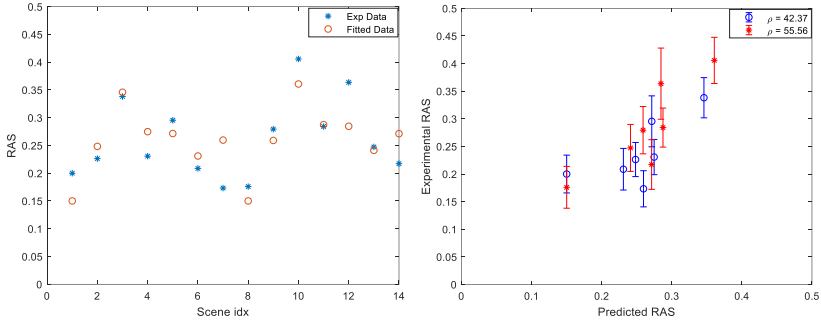


Figure 5.10: Modeled vs. Experimental RAS: (Left) The results per experimental scene. (Right) The correlation between the predicted RAS and experimental RAS. The error bars represent the standard error of the experimental RAS.

Another attempt to optimize the model’s parameters for ipRGCs response was also performed, which results in the set of parameters as $a = 0.36$, $b = 0.16$, $c = 0.18$ and $\delta = 15.3^\circ$ for Eq (3.9). The results of the optimization based on the data collected from Chapter 3 and this chapter are summarized in Table 5.7.

	a	b	c	δ
Data from Chapter 3	0.23	0.53	0.34	9.94°
Data from Chapter 5	0.36	0.16	0.18	15.3°

Table 5.7: Summary of optimized parameters.

Generally, it has a smaller predicting error than the previous set of parameters, as shown in Figure 5.10 with a $RMSE = 0.04$. However, the correlation between the predicted and the experimental RAS is not as good (R^2 value of 0.61) as the order of the effect strength was poorly followed.

This shows that ipRGCs is not the only factor that determines the strength of the effect. This opens the question of how to correctly identify the interaction between various factors that drive the perception of brightness.

5.4. Conclusion

A preliminary experiment studying the effect of adding a chromatic ring in the background to the brightness perception of the neutral self-luminous stimulus is performed with 6 chromatic rings and 1 neutral ring.

The result shows that the influence of the ring does not depend only on the luminance when they have different chromaticity. The apparent brightness of the ring also does not appear to be the main driving factor of the brightness inhibition effect, while the changes in β -cones and ipRGCs could play an important role in the observed phenomenon. A few preliminary attempts to find the relationship between the RAS and the cone and ipRGC excitations have been performed, yet it is still inconclusive what the physiological mechanism behind the effect could be.

However, due to time constraints, the study could not be concluded with a better performing model of the effect and future research is required to complete this study.

5.5. References for Chapter 5

1. M. Withouck, K. A. G. Smet, W. R. Ryckaert, G. Deconinck, and P. Hanselaer, "Predicting the brightness of unrelated self-luminous stimuli," *Opt. Express* **22**, 16298 (2014).
2. Y. Nayatani and M. Nakajima, "Prediction of the Helmholtz-Kohlrausch Effect Using the CIELUV Formula," (n.d.).
3. G. High and P. Green, "The impact of the Helmholtz-Kohlrausch effect on the appearance of near-white paper colours," (n.d.).
4. M. Kim, J.-H. Jo, Y. Park, and S.-W. Lee, "Amendment of CIECAM02 with a technical extension to compensate Helmholtz-Kohlrausch effect for chromatic characterization of display devices," *Displays* (2018).
5. E. Miyahara, V. C. Smith, and J. Pokorny, "The consequences of opponent rectification: The effect of surround size and luminance on color appearance," *Vision Res.* **41**, 859–871 (2001).
6. A. D. D'ANTONA and S. K. SHEVELL, "Induced steady color shifts from temporally varying surrounds," *Vis. Neurosci.* **23**, 483–487 (2006).
7. K. T. Blackwell and G. Buchsbaum, "The effect of spatial and chromatic parameters on chromatic induction," *Color Res. Appl.* **13**, 166–173 (1988).
8. S. K. Shevell and J. Wei, "Chromatic induction: border contrast or adaptation to surrounding light?," *Vision Res.* **38**, 1561–1566 (1998).
9. P. Monnier and S. K. Shevell, "Chromatic induction from S-cone patterns," *Vision Res.* **44**, 849–856 (2004).
10. International Commission on Illumination., *Fundamental Chromaticity Diagram with Physiological Axes. Part 1.* (Commission internationale de l'éclairage, 2006).

11. A. Stockman, L. T. Sharpe, and C. Fach, "The spectral sensitivity of the human short-wavelength sensitive cones derived from thresholds and color matches," *Vision Res.* **39**, 2901–2927 (1999).
12. A. Stockman and L. T. Sharpe, "The spectral sensitivities of the middle- and long-wavelength-sensitive cones derived from measurements in observers of known genotype," *Vision Res.* **40**, 1711–1737 (2000).
13. P. A. García, R. Huertas, M. Melgosa, and G. Cui, "Measurement of the relationship between perceived and computed color differences," *J. Opt. Soc. Am. A* **24**, 1823 (2007).
14. M. Withouck, K. A. Smet, and P. Hanselaer, "Brightness prediction of different sized unrelated self-luminous stimuli," *Opt. Express* **23**, 13455–13466 (2015).
15. P. L. Sun, H. C. Li, and M. Ronnier Luo, "Background luminance and subtense affects color appearance," *Color Res. Appl.* **42**, 440–449 (2017).
16. S. Hermans, K. A. G. Smet, and P. Hanselaer, "Color appearance model for self-luminous stimuli," *J. Opt. Soc. Am. A* **35**, 2000–2009 (2018).
17. W. J. Huang, Y. Yang, and M. R. Luo, "Verification of the CAM15u colour appearance model and the QUGR glare model," *Light. Res. Technol.* **51**, 24–36 (2019).
18. C. Fu, C. Li, G. Cui, M. R. Luo, R. W. G. Hunt, and M. R. Pointer, "An investigation of colour appearance for unrelated colours under photopic and mesopic vision," *Color Res. Appl.* **37**, 238–254 (2012).
19. B. Koo and Y. Kwak, "Color appearance and color connotation models for unrelated colors," *Color Res. Appl.* **40**, 40–49 (2015).
20. P. I. Bodrogi, N. A. Wolf, and T. Q. Khanh, "Spectral sensitivity and additivity of discomfort glare under street and

- automotive lighting conditions," *Light Eng.* **20**, 66–71 (2012).
21. P. Monnier and S. K. Shevell, "Large shifts in color appearance from patterned chromatic backgrounds," *Nat. Neurosci.* **6**, 801–802 (2003).
 22. T. DeLawyer, M. Tayon, C. Yu, and S. L. Buck, "Contrast-dependent red-green balance shifts depend on S-cone activity," *J. Opt. Soc. Am. A* **35**, B114 (2018).
 23. U. Sulutvedt, D. Zavagno, J. Lubell, S. Leknes, S. A. de Rodez Benavent, and B. Laeng, "Brightness perception changes related to pupil size," *Vision Res.* **178**, 41–47 (2021).
 24. A. J. Zele, P. Adhikari, B. Feigl, and D. Cao, "Cone and melanopsin contributions to human brightness estimation," *J. Opt. Soc. Am. A* **35**, B19 (2018).
 25. C. Sandoval Salinas, S. Hermans, J. Sandoval, K. A. G. Smet, P. Hanselaer, and E. Colombo, "Relationship between pupillary size, brightness, and photoreceptor responses for unrelated self-luminous stimuli at low photopic light levels," *Color Res. Appl.* **45**, 977–991 (2020).
 26. A. B. Watson and J. I. Yellott, "A unified formula for light-adapted pupil size," *J. Vis.* **12**, 12–12 (2012).

Chapter 6

Valorization Plan: A tool for assessing lighting design quality based on glare

6. Valorization Plan: A tool for assessing lighting design quality based on glare

Color and Lighting Appearance Models (CAMs, LAMs)) not only give an understanding of how humans perceive colors in terms of perceptual attributes derived from physical/optical properties but also provide a tool to evaluate a wide range of issues occurring in industrial applications. The usage of CAMs can be found in cross-media color reproduction, such as the printing color management pipeline, image quality control and color management for movie production as a plugin for software, such as Microsoft Windows Color System [1], etc... Hermans et al. [2] has also discussed the possible applications of a non-image CAM for self-luminous stimuli in various applications such as predicting glare level, the brightness of variable message signs, estimating visual gloss based on brightness and calculating a grey scale for self-luminous displays.

In this chapter, the valorization plan for connecting this doctoral research to industrial applications in collaboration with the industrial partner - Schréder - is presented. Firstly, the motivation for the cooperative project is briefly discussed, followed by the freedom-to-operate study, which includes the list of relevant literature and patents. Then, the potential product and service that can be derived from this doctoral research are presented. Afterwards, an overview of the market entry timeline for the proposed product, together with the ownership of legal rights in the development process, is provided. Finally, the potential societal and economic impact of the proposed project is discussed.

6.1. Background and key problems

Along with fire and wheels, the light bulb/luminaire is one of the greatest inventions of human beings. Starting from a small light bulb for household lighting, the presence of luminaires is now almost ubiquitous: from our homes to our offices, from the streets to the supermarkets, from the bus to the hospitals. By providing illumination when the natural light is absent, this invention has changed our daily life significantly: it prolongs the active time of the day, improves the safety level for night activities and enhances the sense of security. Besides the basic illumination functions, the evolution of the lighting industry has also contributed greatly to the advancement of marketing

schemes and tourism with various lighting projects such as the iconic billboards arrangement in Times Square (New York City), the lighting of the Eiffel tower (Paris) or many famous lighting festivals (Fête des Lumières – Lyon, Brussels Bright – Brussels, Glow Festival Eindhoven – Eindhoven, Lichtfestival-Gent etc.).

Thanks to the evolving technologies, it is now possible to produce luminaires with high performance and high aesthetic values. In addition to improving the energy efficiency of luminaires, the focus of the lighting industry is shifted towards enhancing the user experience with human centric lighting. However, when it comes to a good lighting design, there are still some problems that need to be taken into consideration besides having high-performance luminaires: the color fidelity, the mood created by the lighting design and especially the level of comfort for the users. Among these criteria, the problem of glare - a sensation caused by light sources, which can give rise to an annoying or painful sensation (discomfort glare) or can impair the vision of objects (disability glare) [3]- has been extensively investigated, as it is linked directly to the level of comfort and safety that a lighting system can provide to the users. Though many measures have been taken to improve the lighting design, there are still increasing numbers of complaints regarding glare caused by billboards, streetlights or city decoration lights.

The Light&Lighting Laboratory from KU Leuven has been receiving multiple requests from different authorities, organizations, and companies to deal with discomfort glare in outdoor lighting and some partnerships have been established based on these collaborations. Among these partners, Schréder is the chosen partner for this exploitation plan based on the existing collaboration to develop a new tool for assessing glare in outdoor lighting (AMODEB project). According to the non-disclosure agreement signed between KU Leuven and Schréder, the details of the products and the bibliography study should be kept confidential, hence, some details from sections 6.2 and 6.3. are omitted or altered in this public version of the manuscript to ensure the level of confidentiality.

6.2. Freedom to operate

To ensure the novelty of the proposed exploitation plan, a freedom-to-operate survey has been conducted. Within the framework of the AMODEB project, two freedom-to-operate reports were delivered with the summary of existing scientific research on glare evaluation and the

summary of relevant patents regarding glare reduction in lighting design. Due to the confidentiality of the project, the unpublished details of the reports are omitted in this public version of the manuscript.

6.2.1. Scientific Literature

Discomfort and disability glare have been a major research topic for lighting quality. Multiple attempts have been done to predict discomfort glare in outdoor lighting, among which, the Cumulative Brightness Evaluation system (CBE) introduced by the American IES Roadway lighting subcommittee [4], Threshold Increment (TI) defined in the European/British/Belgian standard EN13201 [5] for outdoor lighting and the British standard BS 5489-1 2013 [6], Glare Control Mask (GCM) recommended by CIE [7], Glare Rating (GR) proposed in [8] and Unified Glare Rating are the most commonly used models for visual discomfort estimation for outdoor lighting. For indoor lighting, the CIE Glare Index (CGI) proposed by Einhorn et al. [9], Daylight Glare Probability (DGP) suggested by Wienold and Christoffersen [10] and Unified Glare Rating (UGR) recommended by CIE [11] are the most commonly known glare metrics.

Brémond et al. [4] have evaluated different models for predicting the discomfort glare experienced by pedestrians, including UGR and CBE models. According to this study, the UGR model has overestimated the discomfort glare that might be introduced to pedestrians, which is understandable as UGR is a model used to predict visual discomfort experience in indoor lighting. Another study focusing on glare sensation by pedestrians from Liu et al. [12] suggests that under filtered and shielded light conditions, the sensation of glare will be lower than that in a normal light condition. The study also shows that the degree of discomfort is directly related to the luminance of the luminaire and the size of the luminous area.

Bullough et al. [13] proposed a model to predict discomfort glare sensation as a function of vertical illuminance, which takes into consideration light source illuminance, surrounding illuminance and ambient illuminance. Lin et al. [14] developed a model which predicts the visual discomfort caused by LED road lights, and in the same study, different glare rating scales were evaluated. It is found that de Boer rating, a nine-point scale used for rating glare, was significantly different when comparing several levels of glare source luminance, solid angle and background luminance. The discomfort level is believed to increase when the eye illuminance increases, the background luminance decreases and the angle with the line-of-sight

decreases. The study also shows the discomfort level increases when the correlated color temperature increases. Another model predicting discomfort glare in outdoor environment was proposed by Schmidt-Clausen & Bindels [15] for motor vehicle lighting. In this model, the effect of various factors on the discomfort glare rating, including the glare illuminance, the adaptation luminance, the angle of the glare and several glare sources, were investigated.

Kohko et al. [16] introduced another model for discomfort glare prediction in pedestrian zones which considers the luminance of the light source, the solid angle of the light source, the background luminance and the Guth position index of the light source. According to this article, the discomfort glare is also reduced as the distance between the observer and the light source increases. Spectral power distribution of the light source is also taken into consideration when evaluating the discomfort glare as proposed by Sweater-Hickcox et al. [17]. The discomfort level appears to be lessened when there is a colored luminous region (yellow, blue) surrounding the light source. In [18], it is also shown that the degree of discomfort glare changes as the spectral power distribution changes. The discomfort level is reported to be high at 577nm, while at 480nm, the level of discomfort is relatively low. Wienold & Christoffersen [10] proposed the usage of Daylight Glare Probability model, which takes into account the individual glare sources of each situation. In this model, instead of using the luminance of the background to measure the adaptation level, the author suggested using vertical eye illuminance for the adaptation level.

The previous models usually assume the luminaires as point sources or uniform light sources, and the physiological elements are still not properly considered. This motivated the development of the glare models by Scheir et al. [19] and Safdar et al. [20], which consider the neural responses from the retinal receptive fields in calculating glare level for non-uniform light sources. In 2019, the CIE also proposed a modified UGR (or UGR') to adapt the UGR to non-uniform light sources [21].

6.2.2. Patents

Besides a scientific research survey, a patent survey has also been performed. The search has been done using the Espacenet patent database, which provides access to European and Worldwide patents. A summary of the first statistics given by the patent search is provided in Table 6.1.

Query words: "Glare", "Glare + luminaire" and "Glare + reduction".

	Keywords	Databases	Raw number of patents
1	Glare	Espacenet	5366
2	Glare + luminaire	Espacenet	344
3	Glare + reduction	Espacenet	497

Table 6.1: Summary of the query results

As the raw number of hits with the keyword "Glare" is really high with a large number of irrelevant results in the first 200 results, the search is narrowed down to the keyword combinations such as "Glare + luminaire", "Glare + reduction" and so on.

Many of the possible relevant patents were not delivered with English/French/Dutch translation. Hence, these results are excluded from the report for Schröder.

It is noticed that the relevant patents we found mainly provide a solution for reducing glare based on changing the hardware design of the luminaires and the number of patented works about a glare evaluation tool is really limited: only one among the relevant patents proposed a method to evaluate glare. In the software market, the implementation of a glare index calculation can be found in Dialux [22] as a UGR table and Relux [23] with the calculation of TI.

6.3. Products and services

In this section, the development of products and services based on the results of this doctoral research will be presented. This includes software prototypes to calculate the glare level based on the modified UGR suggested by the CIE -called UGR'- [21], a modified version of the glare model proposed by Scheir et al. [19] (hereinafter, called "Receptive Field-based model"), and a new tool to assess the glare level for complex scenes based on the results of this doctoral study. Due to the confidentiality of the AMODEB project, the details of the developed softwares are removed in this public version of the manuscript.

6.3.1. A tool for glare assessment

In collaboration with Schröder, a few software prototypes for calculating discomfort glare level based on published glare models have been developed. First, the calculations of UGR' and the classical UGR based on a luminance image with some modifications are

presented. Note that the implementation of the UGR and the UGR' calculation according to the standard and based on a single luminance image is not that simple, especially when the method should be very quick, practical and user-friendly.

After that, the modified Receptive-field based model is briefly explained.

a. UGR and UGR'

The input used for the calculation of UGR and UGR' is captured with a luminance camera (TechnoTeam LMK5). The luminance camera is equipped with an array detector or CCD with a pixel size d_{pix}^{cam} (assumed to be a square) and a lens with focal length f . The aperture of the camera is located at a distance D from the center of the luminaire. According to CIE 232:2019, this distance must be chosen such that the luminous area of the luminaire is within $\pm 5^\circ$.

From these parameters, the solid angle subtended by the central pixel can be calculated:

$$\omega_{pix} = \frac{(d_{pix}^{cam})^2}{f^2} \tag{6.1}$$

Since the whole luminous area is within 5° of the center, this equation can be applied to all the relevant pixels.

The size of a pixel *at the luminaire on a plane perpendicular to the viewing direction* is given by d_{pix}^{lum} and can be calculated in first approximation as

$$d_{pix}^{lum} = (d_{pix}^{cam} \cdot \frac{D}{f}) \tag{6.2}$$

This value can also be determined experimentally by positioning a ruler at the luminaire and recording an image. According to CIE 232:2019, this value should be preferentially lower than 12 mm and the initial image should be blurred afterward using a Gaussian filter with a full width at half maximum (FWHM) of 12 mm. The resolution of 12 mm/pixel is recommended in CIE 232:2019 based on the assumption of a typical viewing condition of indoor lighting, where the luminaire is normally installed at a height difference of 1.2 m from the height of

the observer's eyes and the minimum observable feature diameter is estimated to be 0.01 times that height difference [21].

As for implementation, the Gaussian filter is commonly defined with a standard deviation δ given in number of pixels, a conversion from FWHM in mm to standard deviation in pixels will be needed before the implementation of the glare metric.

$$\delta = \frac{FWHM}{2.3548d_{pix}^{lum}} \quad (6.3)$$

General UGR formula

Generally, the UGR for a luminaire is computed as:

$$UGR = 8 \log \left[\frac{0.25 L_s^2 \omega}{L_b p^2} \right] \quad (6.4)$$

in which L_s is the luminance of the luminaire, ω is the solid angle subtended by the luminous area of the luminaire, L_b is the background luminance and p is the Guth's position index (or Guth index).

UGR'

The number of "effective" pixels (pixels having a luminance higher than 500 cd/m²) is called n_{eff} . This value is determined by considering all the pixels from the *blurred image* (yet including pixels which do not cover the source area; no image cropping has been applied).

The corresponding effective solid angle ω_{eff} can be determined:

$$\omega_{eff} = n_{eff} \cdot \omega_{pix} \quad (6.5)$$

The effective luminance L_{eff} is calculated as the average luminance value over the pixels considered for n_{eff} .

The new UGR value for non-uniform luminaires UGR' is calculated as

$$UGR' = 8 \log \left[\frac{0.25 L_{eff}^2 \omega_{eff}}{L_b p^2} \right] \quad (6.6)$$

The Guth index p can be determined from the standard tables and is given as 5.4477 for $\gamma = 50^\circ$ and 2.664 for $\gamma = 65^\circ$. UGR' is calculated for the four orientations stipulated in the standard: $C / \gamma = 0/50; 0/65; 90/50; 90/65$.

UGR_{image}

Next to UGR', the classical UGR in the same four directions can be calculated too. Two approaches are possible: in a first approach, the basic UGR formula in terms of luminance is used and the input is fully captured from the image:

$$UGR_{image} = 8 \log \left[\frac{0.25 L_s^2 \omega}{L_b p^2} \right] \quad (6.7)$$

in which L_s is the average luminance over the luminous area and ω is the solid angle subtended by the luminous area. The luminous area of the luminaire A_{src} is characterized by the horizontal dimensions (width W and length L) and eventually by a vertical height H . The area is defined by the operator and is considered as input in the .ldt file. This value is to some extent arbitrary because it is not always clear which area of the luminaire must be considered as "luminous". To calculate the projected source area A_p when viewed under a particular direction, some geometrical relations have been defined by CIE. If the source area only has a horizontal area, A_p is given by:

$$A_p = A_{src} \cdot \cos \gamma \quad (6.8)$$

As the image normally contains more pixels than those corresponding to the luminous area (no cropping applied), we need to find an optimized way to determine the relevant pixels corresponding to the luminous area for which the average luminance L_s must be calculated. The number of pixels in the image corresponding to the luminous area, called n , can be found as follows:

$$n = \frac{A_p}{(d_{pix}^{lum})^2} \quad (6.9)$$

This number is rounded up to an integer value. The corresponding solid angle ω is given by

$$\omega = n \cdot \omega_{pix} (= \frac{A_p}{D^2}) \quad (6.10)$$

L_s is now calculated as follows: all the pixels in the *unblurred image* are ranked according to their luminance value. The n highest luminance values are assumed to belong to the luminous area and considered to calculate the average value. The use of the unblurred image to calculate the average luminance L_s is motivated by the fact that blurring an image can increase the number of luminous pixels which causes an inconsistency with respect to the predefined A_{src} .

UGR_{image} is calculated for the four relevant directions as defined in the standard.

The correction factor to be applied when converting from UGR_{image} to UGR' , called k_{image}^2 , is defined according to CIE 232:2019 as:

$$k_{image}^2 = \frac{L_{eff}^2 \cdot \omega_{eff}}{L_s^2 \cdot \omega} \quad (6.11)$$

In view of what follows, it would also be interesting to calculate the luminous intensity corresponding to this average luminance value. This can be done as follows:

$$I_{image} = L_s \cdot A_p \quad (6.12)$$

UGR_{LID}

Until now, classical indoor UGR values are not based on luminance measurements. The UGR value is calculated from the intensity values of the LID, called I_{LID} , using a conversion from average luminance to the experimental intensity in the corresponding direction. The UGR value calculated in this way is called UGR_{LID} and is obtained as

$$UGR_{LID} = 8 \log \left[\frac{0.25}{L_b} \frac{I_{LID}^2}{A_p \cdot D^2 \cdot p^2} \right] \quad (6.13)$$

The correction factor to be applied when converting from UGR_{LID} to UGR' , called k_{LID}^2 , is defined according to CIE 232:2019:

$$k_{LID}^2 = \frac{L_{eff}^2 \cdot \omega_{eff} \cdot A_p \cdot D^2}{I_{LID}^2} \quad (6.14)$$

The abovementioned calculations and modifications were integrated into one standalone software prototyped developed in MATLAB for Schröder.

b. Modified Receptive Field-based Model

Initiated by Donners and Vissenbergs and further developed by Scheir et al. [19], Receptive Field values (RFV) provide a physiologically based approach to computing discomfort glare. The model makes use of the pupillary light reflex in combination with the center-surround mechanism of the receptive fields in the retina to evaluate the level of discomfort glare for non-uniform light sources. The RFV is computed based on the retinal illuminance map weighted with the position index, and the center-surround mechanism of the retinal receptive field using the Difference-of-Gaussian (DoG) filter. The details of the calculations can be found in the corresponding publication.

In the original model, the standard deviation of the center and surround signals of the receptive fields were computed for the case where the observer is looking directly at the luminaire. However, as the density of retinal cells varies with the eccentricity, the receptive field size can be considered to be different for various positions in the retina [24]. To consider the changes in receptive field size with viewing angle, the model is modified such that the receptive field size increases with increasing distance from the fovea. This model is called the "modified RFV".

The modified version of the model was implemented in MATLAB and provided as a standalone prototype under the AMODEB project with Schröder.

6.3.2. Future product: A new tool for assessing glare based on an image color appearance model

Another approach would be to consider the brightness correlate as a glare indicator. Indeed, as pointed out by Hermans et al. [2], a CAM can be applied to evaluate the level of discomfort glare introduced by a light source. This opens the possibility for an image-based CAM to be utilized in assessing the glare level for complex scenes, which will be a highly relevant application in lighting design. Currently, as the models developed from this doctoral research only output a brightness

value, additional experiments will be needed to create a scale that can correspond the brightness value to the level of discomfort glare perceived by the users. Following the suggested future works in previous chapters and as presented in the modified Receptive Field-based glare model, extensions could be made to enhance the performance of the proposed brightness model, including consideration of changes in receptive field sizes with eccentricity and a spectral-dependent straylight correction.

Once the new glare scale is defined, the first product that could be patented is the method for evaluating glare. Furthermore, the glare index calculation can be implemented as a plugin for a lighting design simulation software such as the Schröder plugin for Dialux. Such plugin will be able to give the prediction of the glare level produced from the simulation of a lighting design, or from a field-measured luminance map.

6.4. Exploitation trajectory

6.4.1. Partner

Established in 1907 in Liège (Belgium), Schröder is one of the market leaders in outdoor lighting, with a network in more than 40 countries around the world. It has been active not only in street lighting but also in city decoration lighting, such as the lighting setup of Grand Place (Brussels), Place du Capitole (Toulouse), Marché Saint Germain (Paris) and so on. Bearing in mind the concern about different types of discomfort that might be caused by the decorative lighting setup, Schröder has reached out to us to develop a more effective method to predict the discomfort glare in outdoor lighting. With the high demand for a more comprehensive model to assess the perception of glare in a complex lighting design, the outcome of this doctoral research is expected to provide a great assistance in evaluating and improving the quality of a lighting design and addressing the need of our partner.

6.4.2. Timeline for market entry

The study of the glare evaluation method started in September 2018 and the software prototypes based on published glare evaluation methods were delivered to Schröder in August 2020. Within the framework of AMODEB project, Schröder also invested in the facility to create an experimental setup for glare evaluation. For the development of the new glare evaluation method, additional experiments will need to be performed after the end of this doctoral

research. If a new project is established, the extended glare research and experiments can be integrated as a part of another 4-year PhD project.

The implementation of the software/software plugin could be done by the in-house software engineers of Schröder. With the algorithm already defined by the research project, the release of the software could be expected within 6 months after the model is finalized.

6.4.3. Financial plan

The AMODEB project was funded by Schröder and supported by the regional authorities. A few initiatives have been taken to discuss the potential to apply the result of this doctoral research in future projects. If an agreement is reached to establish future projects and collaborations, further research may be performed by hiring a new junior researcher funded either by the KU Leuven internal funding or with an industrial doctoral program funded by Schröder. The cost of software implementation will be covered by Schröder.

The deployment of a software which can estimate the glare level during the phase of simulation and design will give the manufacturer better control over the comfort quality of their luminaires, which can be an important added value. This also implies an improvement of the overall product quality for the luminaires produced by Schröder. As the product of the research is intended to be a software owned by Schröder, a possible additional revenue for Schröder will come from the purchase of the software license. Another source of revenue can come from sharing the technological stake of the filed patent related to the glare evaluation method: if another company wants to use the patented method, they will need to pay for the rights to use the invention.

To file a patent, several costs should be taken into account, including the application fee and a renewal fee during the life of the granted patent till it expires (usually in the course of 20 years). The patent application procedure includes an international application phase and a national/regional phase. A summary of patent application cost is given in Table 6.2.

Type of expenses		Price (EUR)
International phase	Filing + application for search report	10000 to 15000
	Supplementary search	4000

National/Regional phase	Submission cost	2000 to 6000 per country/region
	Costs to grant patent	2000 to 10000 per country/region
	Validation fee (if the patent is granted)	500 to 4000 per country
	Cumulative annual fees	3000 to 17000 per country

Table 6.2: Patent application and renewal fees

The process of filing the patent can be supported by the LRD department of KU Leuven or the legal department of Schröder. The patent can be owned either fully by one party of the collaboration or shared by both parties. The original inventor can also benefit from the patent with a royalty from the net revenue of the patent.

6.4.4. Legal rights

The research results which were obtained during the framework of AMODEB project are owned by Schröder, according to the agreement that KU Leuven signed with Schröder:

"As regards the exploitation modes of the Right, the Supplier shall transfer to Schröder all rights of ownership related to and associated with the Work or resulting directly or indirectly, partially or totally from the Mission, including any invention (patentable or not) resulting from the Mission. These rights of ownership shall cover all exclusive exploitation rights and modes, in whatsoever form and by whatsoever means, and notably:

- *All points that are already covered through the « Master development agreement »*
- *The KUL is not allowed to publish on the method used to evaluate the glare itself, and insofar it is not likely to invalidate new inventions about the Project.*
- *KUL is not allowed to publish any link between this project and Schröder or R-Tech.*
- *KUL is NOT allowed to publish the results related to the correlation between the model and the human feedback while the*

luminaire resulting from the glare study has not been launched on the market for at least 5 years after the end of the Project.

- *KUL is NOT allowed to publish the results related new Schröder's design rules.*
- *All development and the code of the algorithm must be secret and still ownership of Schröder.*
- *The conclusion on the bibliographic study can't be published.*
- *But we allow KUL to publish on the MODEL itself, and partially on the equation used while the published equation don't make the publication self-standing. The purpose is to allow KUL to show that they are able to create and work on new glare model without making the reader of the wall publication able to apply itself the model. This mean that Schröder R-Tech have to be agree on the publication in that field."*

The source codes of the glare evaluation programs based on UGR' and that of the glare model by Scheir et al. [19] are considered the property of Schröder.

Currently, the intellectual property rights of other results obtained in this doctoral research are still fully owned by KU Leuven. This implies that KU Leuven has full freedom to operate the current research results and can apply them for future research and educational activities after the conclusion of this doctoral program. However, the ownership of intellectual property might be shared or transferred to the partner if future collaboration is established.

The intellectual property of the research results will be protected according to the nature of the products. For the software, the source codes and the program should be protected under copyrights. Meanwhile, the details of the glare evaluation method could be filed as a patent. The choice of the patent office/organization – if relevant- will be determined by our partner.

6.4.5. Data distribution

The current visual experiment data obtained from this doctoral research is stored in a KU Leuven database. According to the GDPR regulations, all personal information that could be linked to the collected data must be anonymized and the data distribution must be approved by the KU Leuven Privacy and Ethics Review Board. Depending on the future

collaboration, extended experimental data might be required to be reallocated to another location/storage.

6.5. Potential impact of the valorization plan

The development of a tool to assess glare of non-uniform luminaires will provide a more human-centric way to evaluate the level of comfort induced by a lighting design thanks to the psychophysical- and physiological-based approach. By providing the glare prediction in the phase of design simulation, it can reduce the number of prototypes and of glare complaints from the users and enhance the comfort and the safety of a lighting design. A decreasing number of complaints from users also implies the reduction on the reinstallation costs for owners of the lighting installations, which are commonly the cities/states where the designs are installed.

6.6. References for Chapter 6

1. "WCS Color Appearance Model Profile Schema and Algorithm - Win32 apps | Microsoft Docs," <https://docs.microsoft.com/en-us/windows/win32/wcs/wcs-color-appearance-model-profile-schema-and-algorithm>.
2. S. Hermans, K. A. G. Smet, and P. Hanselaer, "Exploring the applicability of the CAM18sl brightness prediction," *Opt. Express* **27**, 14423–14436 (2019).
3. J. D. Bullough, K. S. Hickcox, and N. Narendran, *A Method for Estimating Discomfort Glare from Exterior Lighting Systems* (2011).
4. R. Brémond, E. Saint-Jacques, and E. Dumont, "PREDICTING THE DISCOMFORT GLARE EXPERIENCED BY PEDESTRIANS: UGR AND CBE," (2017).
5. "EN 13201 Standards for Road lighting all parts - European Standards," <https://www.en-standard.eu/csn-en-13201-1-4-road-lighting/>.
6. "BS 5489-1:2013 Code of practice for the design of road lighting. Lighting of roads and public amenity areas, British Standards Institution - Publication Index | NBS," <https://www.thenbs.com/PublicationIndex/documents/details?Pub=BSI&DocID=302587>.
7. Internationale Beleuchtungskommission., *Glare and Uniformity in Road Lighting Installations* (CIE Central Bureau, 1990).
8. International Commission on Illumination. and CIE Technical Committee TC-5.04., *Glare Evaluation System for Use within Outdoor Sports and Area Lighting* (CIE Central Bureau, 1994).
9. H. D. Einhorn, "Discomfort glare: a formula to bridge differences," *Light. Res. Technol.* **11**, 90–94 (1979).
10. J. Wienold and J. Christoffersen, "Evaluation methods and development of a new glare prediction model for daylight environments with the use of CCD cameras," *Energy Build.* **38**, 743–757 (2006).

11. CIE Technical Committee, "CIE 117-1995 Discomfort Glare in Interior Lighting," 39 (1995).
12. X. LiU, T. Fujita, Y. Akashi, and K. Yamamoto, "The Effect of High-luminous-flux Luminaires on Target Detection, Glare Sensation, and Perceived Safety and Security in Streets," *J. Sci. Technol. Light.* **41**, 186–194 (2018).
13. J. Bullough, J. Brons, R. Qi, and M. Rea, "Predicting discomfort glare from outdoor lighting installations," *Light. Res. Technol.* **40**, 225–242 (2008).
14. Y. Lin, Y. Liu, Y. Sun, X. Zhu, J. Lai, and I. Heynderickx, "Model predicting discomfort glare caused by LED road lights.," *Opt. Express* **22**, 18056–71 (2014).
15. H. J. Schmidt-Clausen and J. T. H. Bindels, "Assessment of discomfort glare in motor vehicle lighting," *Light. Res. Technol.* **6**, 79–88 (1974).
16. S. Kohko, M. Ayama, M. Iwata, N. Kyoto, and T. Toyota, "Study on Evaluation of LED Lighting Glare in Pedestrian Zones," *J. Light Vis. Environ.* **39**, 15–25 (2015).
17. K. Sweater-Hickcox, N. Narendran, J. D. Bullough, and J. P. Freyssinier, "Effect of different coloured luminous surrounds on LED discomfort glare perception," *Light. Res. Technol.* **45**, 464–475 (2013).
18. P. I. Bodrogi, N. A. Wolf, and T. Q. Khanh, "Spectral sensitivity and additivity of discomfort glare under street and automotive lighting conditions," *Light Eng.* **20**, 66–71 (2012).
19. G. Scheir, M. Donners, L. Geerdinck, M. Vissenberg, P. Hanselaer, and W. Ryckaert, "A psychophysical model for visual discomfort based on receptive fields," *Light. Res. Technol.* **50**, 205–217 (2018).
20. M. Safdar, M. R. Luo, M. F. Mughal, S. Kuai, Y. Yang, L. Fu, and X. Zhu, "A neural response-based model to predict discomfort glare from luminance image," *Light. Res. Technol.* **50**, 416–428 (2018).
21. CIE, "CIE 232:2019 Discomfort Caused by Glare from Luminaires with a Non-Uniform Source Luminance," (2019).

22. "UGR : Knowledge Base DIALux evo," <https://evo.support-en.dial.de/support/solutions/articles/9000116115-ugr>.
23. "Observer TI : Relux," <https://relux.freshdesk.com/support/solutions/articles/17000064561-beobachter-ti>.
24. P. Martínez-Cañada, C. Morillas, J. L. Nieves, B. Pino, and F. Pelayo, "First stage of a human visual system simulator: The retina," in *Computational Color Imaging* (Springer Verlag, 2015), pp. 118–127.
25. L. J. Croner and E. Kaplan, "Receptive fields of P and M ganglion cells across the primate retina," *Vision Res.* **35**, 7–24 (1995).
26. A. Ransom-Hogg and L. Spillmann, "Perceptive field size in fovea and periphery of the light- and dark-adapted retina," *Vision Res.* **20**, 221–228 (1980).

Chapter 7

Conclusions and Future Work

7. Conclusions and Future Work

7.1. Conclusions

Throughout the history of color science, numerous CAMs, including non-image CAMs for surface colors [1–5] and self-luminous colors [6,7], and image CAMs for surface colors [8–11] have been developed. Despite the number of existing CAMs, an image CAM for a complex self-luminous scene is still missing. With the rapid growth of lighting technology and the huge shift in the focus of the lighting industry to human-centric lighting, the needs for an image CAM for self-luminous stimuli are even more emphasized. This motivates the goal of developing a Lighting Appearance Model, an appearance model which uses a hyperspectral image as the input to predict the appearance of complex scenes, including light sources, based on the physiology of the human visual system.

The aim of this doctoral research, funded by KU Leuven BOF project C24/17/051, was to set the first steps to move towards such a LAM by considering a non-image and an image CAM for related self-luminous stimuli with a focus limited to the brightness perception for neutral stimuli. Within the scope of this doctoral research, the following research questions were defined:

1. Investigate the possibility of applying an existing image CAM (iCAM) for surface colors to self-luminous stimuli.
2. Investigate the impact of a non-uniform neutral and colored self-luminous background on the brightness perception of neutral self-luminous stimuli through a series of visual experiments.
3. Develop the brightness models based on the collected visual data using a non-image-based and an image-based approach.

Following are the main conclusions drawn after this 4-year doctoral research.

7.1.1. Performance of iCAM for simple self-luminous scenes

iCAM is an image CAM developed by Fairchild and Johnson [9] which can give perceptual attributes such as brightness, lightness, hue, saturation and chroma for each pixel from an input RGB or XYZ image. The model was originally designed for image reproduction and image quality evaluation [12]. During the first year of this doctoral research, the possibility of applying iCAM for self-luminous stimuli

was explored by applying the model to simple self-luminous scenes. The study was performed using different sets of XYZ images which simulated real self-luminous scenes consisting of a uniform self-luminous stimulus seen on a uniform self-luminous background and surround. The experimental scenes were based on the experimental setup presented in previous studies, which investigated the impact of stimulus and background luminance [13], stimulus size [14], background size [15] and Helmholtz-Kohlrausch effect [16] on the brightness perception of self-luminous stimuli. The effect of changing the filter kernel size (one of the main parameters in iCAM) was also briefly discussed in this study.

It is observed that by changing the size of the filter kernel, the performance of iCAM is strongly influenced, and it appears that adopting a large filter kernel size as proposed by the developers provides a better prediction. Generally, the model can well predict the effect of stimulus and background luminance, as well as the background size, on the brightness perception for neutral self-luminous stimuli. However, iCAM also shows some limitations in its performance for stimuli shown on a completely dark background which is caused by the local adaptation computed with the low pass filtered image. In addition, the Helmholtz-Kohlrausch effect and the stimulus size effect on brightness perception are not explicitly included in iCAM. These results imply the need for a new comprehensive image CAM that is dedicated to self-luminous scenes.

7.1.2. Brightness perception of neutral self-luminous stimuli on a non-uniform neutral self-luminous background

The first step to establishing a new image-based model for self-luminous stimuli color appearance is to investigate the impact of spatial arrangements of neutral self-luminous backgrounds on the brightness perception of neutral self-luminous stimuli. This starts with studying the effect of distance, luminance and area of different parts of the background on the target stimulus brightness. To achieve such a goal, the brightness matching method was chosen in this doctoral research to collect visual data from the observers. The experimental setup was designed as follows: a uniform 10° neutral circle on a dark background was used as the reference scene and a uniform 10° neutral circle surrounded by a luminous ring on a dark background served as the test scene. The luminous ring could vary in its thickness (0.33 cm, 0.67 cm and 1.00 cm), luminance levels (90 cd/m², 335 cd/m² and 1200 cd/m²) and distance to the outer edge of the stimulus (1.2°, 6.4°, 11.3° and

16.1°). The thinnest ring was shown at the highest luminance, while the two thicker rings were shown at all three ring luminance levels. By using the disk-annulus configuration, the impact of the ring luminance will be uniform from all directions. The experimental data shows that with increasing luminance and thickness, the ring makes the stimulus appear darker while increasing the ring distance reduces its impact. This result is in line with the findings in previous literature [13,15,17].

From the collected visual data, a non-imaging model which simulates the influence of the self-luminous ring on the stimulus brightness was proposed based on the Michaelis-Menten (M-M) approach for compression and adaptation. The adaptive shift of the semi-saturation constant is expressed as a function of solid angle, luminance and the distance between the edge of the stimulus and the edge of the ring. The effect of distance is modeled using a Gaussian weighting function. The model generally provides a promising result with a root mean square error (*RMSE*) of 0.25 and a coefficient of determination R^2 of 0.81 when compared to the visual data. However, the model still shows a few drawbacks in its performance: the effect of the thin ring is slightly overestimated for the closest ring, while that of the furthest ring is strongly underestimated. For the thickest ring, the influence of the closest ring is underestimated, which implies that an additional inhibition effect might occur.

The model is also extended such that it could be applied to any shape, position and luminance level of various background sections. However, the extended model shows a poorer performance compared to the former one, with an *RMSE* of 0.37 and an R^2 of 0.67. One possible reason for this shortfall is that the extended model assumed additivity with respect to the solid angle and has not taken into account any compressive effects.

7.1.3. Towards an image-based brightness model for neutral self-luminous stimuli

Despite its promising performance, the non-image-based approach shows some severe limitations in extending the model to much more complex scenarios: the model has not yet considered the case of non-uniform stimuli, the self-adaptation of the stimulus is not included, and higher scene complexity also means more ambiguity in defining whether a part of the scene belongs to the background or the stimulus. Therefore, an image-based approach is believed to give more flexibility in predicting the brightness perception in highly complex scenes.

With that motivation, additional experiments with more combinations of the ring thickness and luminance levels were performed to create a more complete dataset for modeling the effect of the self-luminous ring on the central stimulus. In this experiment, each ring thickness was shown at all luminance levels and at all distances, as described in the previous experiments. Based on the experimental data, an image brightness model was proposed, which includes cube root cone compression, retinal straylight correction, receptive-field post-processing, inhibition by neighboring pixels and sigmoid compression. The surround signal of the receptive field is expressed with a Gaussian kernel, while the strength of the inhibition is indicated with a weighting factor. A semi-saturation constant for a dark environment is also computed. The result shows that the model gives the best performance with a Gaussian kernel covering a receptive field of approximately 45° . This suggests that the adaptation to the ring and the brightness perception might be the result of later stage in visual processing in the visual cortex, where the receptive field size can be as large as 50° [18,19]. This large kernel size is also found in previous literature [9,20,21]. In general, the model gives a sufficiently good performance in predicting the ring's influence with different areas, luminance levels and distances to the central stimulus. Note that the model also includes the adaptation to the stimulus itself, which is part of the scene. Yet, an underestimation is observed in the prediction for the closest ring distance, which implies the need for an additional smaller receptive field to simulate more local effects.

7.1.4. From a neutral ring to a colored ring

To set one step closer to the development of a complete image CAM, an experiment studying the impact of a chromatic ring on the brightness perception of neutral stimuli was conducted. The method of adjustment was chosen to perform the experiment. Based on the primaries of the display used for the experiment (EIZO ColorEdge PROMINENCE CG3145), 6 chromatic rings (red, green, blue, cyan, magenta and yellow) and 1 neutral ring, all having the same ρ -cone excitation, were chosen for this study. The result shows that adding a chromatic ring would have a higher impact on the brightness perception of the stimulus than adding a neutral ring surrounding the central neutral stimulus, even though the luminance of the chromatic ring could be lower than that of the neutral ring. The effect also does not appear to follow the apparent brightness of the ring as the driving factor for the adaptive shift. It is, however, interesting to observe that, except for the

case of the neutral ring, the influence of the additional ring seems to follow the changing tendency of the β -cone responses and ipRGC responses. It is still unclear how the model describing the correlation between the observed inhibitory effect and the β -cone and ipRGC excitation should look like. A few attempts to model the effect are presented, yet no conclusion is drawn.

Due to time constraints, the study is not yet finished in the time frame of this doctoral research and further investigation is still needed in the future.

7.1.5. Imaging CAM and glare: an exploitation track of the doctoral research

During the 4 years of this doctoral research, a collaboration with Schröder to investigate a new tool for glare assessment for outdoor lighting was established. The project included a patent survey and a literature review to explore the freedom to operate, the implementation of existing glare evaluation methods as software prototypes and the extension of the recently proposed glare metrics by Scheir et al. [22]. The glare model by Scheir et al. [22], which predicts the level of discomfort glare for non-uniform light sources using the concept of the receptive field (as in the imaging CAM), was extended such that the size of the receptive fields would change according to the position of the light sources in the user's field of view. This extension is believed to provide a more realistic computation for glare index as the sensitivities of the human eye and the size of the receptive fields also change with eccentricity. Based on this collaboration and on a previous study about the applications of CAM18sl [23], a valorization plan to develop a tool for assessing glare in outdoor lighting conditions from the results of this doctoral research was also proposed. Within the scope of this project, two freedom-to-operate reports and three software prototypes in MATLAB were delivered.

7.2. Future work

Developing a Lighting Appearance Model (LAM) is an ambitious goal that requires many further steps to be done in the future. In this section, possible directions for future research will be suggested from two perspectives: how to improve the current results and how to proceed further in the long term.

7.2.1. Possible improvements to the current research

Firstly, as observed in the proposed models for brightness perception of achromatic self-luminous stimuli with non-uniform backgrounds, the size of the receptive field still requires further investigation. Though the current models seem to provide promising performance on the global adaptation level, for local contrast effects at closer distances, another smaller receptive field size that gives sharper responses is needed. It is also worth noting that the cone density and the retinal receptive field size change with eccentricity [24,25]. To develop a model which conforms to the physiology of the human visual system, it is essential to accurately take the change of the receptive field size into account, as has been done in the glare application and exploitation project.

Secondly, extensions to adequately include straylight correction in modeling brightness perception should be made. Currently, the CIE PSF is used in the proposed model with an average age and pigmentation factor from the observers. However, as pupil size, age and eye pigmentation play an important role in straylight, it is important to have a more personalized model when it comes to straylight correction. Furthermore, the wavelength dependence of the effect has been ignored.

Moreover, the current research is still limited to a 10° uniform and achromatic stimulus, which does not represent all the possible self-luminous stimuli. With multiple studies emphasizing the effect of stimulus size on its brightness perception [14,26,27], it is important to carry out the research with various stimulus sizes, preferentially in an imaging model, as it includes the size in a very "natural" way.

7.2.2. Future research

To establish a complete Lighting Appearance Model, solely improving the current work will not be sufficient, and a much more extended perspective will need to be considered.

Within the scope of this doctoral research, we are still restricted to the investigation of brightness perception for achromatic self-luminous stimuli. This implies that for future stages, colored stimuli should also be used for future experiments with different reference luminance levels. Finally, the perception of a non-uniform stimulus should also get some attention.

Another crucial step is to extend the research to chromatic backgrounds with higher complexity than a colored ring. And finally, next to brightness, the other perceptual correlates should be investigated.

Looking from a somewhat wider perspective, to reach the development of a Lighting Appearance Model, an approach using a hyperspectral image input seems to be the way forward.

Hyperspectral images contain the most complete description of a visual scene since it contains the spectral radiance in the viewing direction of each "pixel" in the scene. As the availability of spectral data for each pixel in the scene is key to developing a complete model, using hyperspectral images as the input for a LAM is the most suitable option. With most of the available hyperspectral camera models giving the output as spectral reflectance instead of spectral radiance, future adaptations are needed to get the required output from the hyperspectral camera. Furthermore, the specific data format should be considered, and the model needs to be adapted to read hyperspectral images.

Moreover, the traditional approach for developing both non-image and image CAMs is still based on processing the signals from the three types of cones. This can be a limitation as the visual perception is influenced by various factors beyond the cone excitations, such as rod intrusion [28], ipRGCs contributions [29] and so on. Therefore, accounting for the contribution of those parameters can be an essential step to creating a LAM which is highly physiological based.

In addition, more detailed processing at each stage of human visual processing should also be considered. ISETBIO [30,31], one of the most recently developed toolboxes for visual encoding, can also be used as the base to develop the next steps of LAM. This toolbox allows the calculation of the spectral image of the object scene projected on the retina based on human optics (the wavelength-dependent optical blur, transmission through the lens, etc.). This image can be sampled with the cone distribution to calculate a cone excitation map.

From the cone excitation map, a few more processing steps will need to be taken to achieve the output of LAM as a set of perceptual attribute maps. Current advanced retinal simulation models [30,32] provide some valuable insights about the detailed processing at each processing stage at the retinal level. This knowledge can be useful for extracting the response map of each retinal cell layer, which can later be used to calculate the output from the visual neural pathways in the later stages of human visual processing. For computing the neural responses,

combining the background knowledge about visual coding in the visual cortex [18,33] with neural networks [34,35] can be a promising approach to compiling the visual attribute information. Furthermore, visual perception is a highly dynamic process that depends both on time and space. Hence, including the temporal aspect of visual perception is also crucial for modeling lighting appearance in the future.

7.3. References for Chapter 7

1. Y. Nayatani, K. Takahama, and H. Sobagaki, "Prediction of color appearance under various adapting conditions," *Color Res. Appl.* (1986).
2. R. W. G. Hunt, *The Reproduction of Colour* (John Wiley & Sons, Ltd, 2005).
3. M. R. Luo and R. W. G. Hunt, "The structure of the CIE 1997 colour appearance model (CIECAM97s)," *Color Res. Appl.* **23**, 138–146 (1998).
4. C. Li, Z. Li, Z. Wang, Y. Xu, M. R. Luo, G. Cui, M. Melgosa, M. H. Brill, and M. Pointer, "Comprehensive color solutions: CAM16, CAT16, and CAM16-UCS," *Color Res. Appl.* **42**, 703–718 (2017).
5. N. Moroney, M. D. Fairchild, R. W. Hunt, C. Li, M. Ronnier Luo, and T. Newman, "The CIECAM02 color appearance model," in *10th Color and Imaging Conference Final Program and Proceedings* (2002), pp. 23–27.
6. M. Withouck, K. A. G. Smet, W. R. Ryckaert, and P. Hanselaer, "Experimental driven modelling of the color appearance of unrelated self-luminous stimuli: CAM15u," *Opt. Express* **23**, 12045 (2015).
7. S. Hermans, K. A. G. Smet, and P. Hanselaer, "Color appearance model for self-luminous stimuli," *J. Opt. Soc. Am. A* **35**, 2000–2009 (2018).
8. G. M. Johnson and M. D. Fairchild, "A Top Down Description of S-CIELAB and CIEDE2000," *Col Res Appl* **28**, 425–435 (2003).
9. M. D. Fairchild and G. M. Johnson, "Meet iCAM: A next-generation color appearance model," in *10th Color and Imaging Conference Final Program and Proceedings* (2002), pp. 33–38.
10. J. Kuang, G. M. Johnson, and M. D. Fairchild, "iCAM06: A refined image appearance model for HDR image rendering," *J. Vis. Commun. Image Represent.* **18**, 406–414 (2007).
11. E. Reinhard, T. Pouli, T. Kunkel, B. Long, A. Ballestad, and G. Damberg, "Calibrated image appearance reproduction,"

- ACM Trans. Graph. **31**, 1–11 (2012).
12. M. D. Fairchild and G. M. Johnson, "iCAM framework for image appearance, differences, and quality," J. Electron. Imaging **13**, 126–138 (2004).
 13. S. Hermans, K. A. G. Smet, and P. Hanselaer, "Brightness Model for Neutral Self-Luminous Stimuli and Backgrounds," LEUKOS - J. Illum. Eng. Soc. North Am. **14**, 231–244 (2018).
 14. M. Withouck, K. A. Smet, and P. Hanselaer, "Brightness prediction of different sized unrelated self-luminous stimuli," Opt. Express **23**, 13455–13466 (2015).
 15. P. L. Sun, H. C. Li, and M. Ronnier Luo, "Background luminance and subtense affects color appearance," Color Res. Appl. **42**, 440–449 (2017).
 16. M. Withouck, K. A. G. Smet, W. R. Ryckaert, M. R. Pointer, G. Deconinck, J. Koenderink, and P. Hanselaer, "Brightness perception of unrelated self-luminous colors," J. Opt. Soc. Am. A **30**, 1248 (2013).
 17. M. A. Cohen, T. L. Botch, and C. E. Robertson, "The limits of color awareness during active, real-world vision," Proc. Natl. Acad. Sci. U. S. A. **117**, 13821–13827 (2020).
 18. K. Amano, B. A. Wandell, and S. O. Dumoulin, "Visual field maps, population receptive field sizes, and visual field coverage in the human MT+ complex," J. Neurophysiol. **102**, 2704–2718 (2009).
 19. S. Raiguel, M. M. Van Hulle, D. K. Xiao, V. L. Marcar, L. Lagae, and G. A. Orban, "Size and shape of receptive fields in the medial superior temporal area (MST) of the macaque," Neuroreport **8**, 2803–2808 (1997).
 20. J. Kuang, G. M. Johnson, and M. D. Fairchild, "iCAM06: A refined image appearance model for HDR image rendering," J. Vis. Commun. Image Represent. **18**, 406–414 (2007).
 21. E. Provenzi, "Perceptual color correction: A variational perspective," in *Computational Color Imaging* (Springer Berlin Heidelberg, 2009), pp. 109–119.
 22. G. Scheir, M. Donners, L. Geerdinck, M. Vissenberg, P.

- Hanselaer, and W. Ryckaert, "A psychophysical model for visual discomfort based on receptive fields," *Light. Res. Technol.* **50**, 205–217 (2018).
23. S. Hermans, K. A. G. Smet, and P. Hanselaer, "Exploring the applicability of the CAM18sl brightness prediction," *Opt. Express* **27**, 14423–14436 (2019).
 24. D. H. Brainard, "Color and the Cone Mosaic," *Annu. Rev. Vis. Sci* **1**, 519–565 (2015).
 25. L. Peichl and H. Wässle, "Size, scatter and coverage of ganglion cell receptive field centres in the cat retina.," *J. Physiol.* **291**, 117–141 (1979).
 26. R. C. Carter and L. D. Silverstein, "Perceiving color across scale: great and small, discrete and continuous," *J. Opt. Soc. Am. A* **29**, 1346 (2012).
 27. S. Y. Choi, M. R. Luo, M. R. Pointer, C. Li, and P. A. Rhodes, "Changes in colour appearance of a large display in various surround ambient conditions," *Color Res. Appl.* **35**, 200–212 (2010).
 28. J. Walraven, "Discounting the background—the missing link in the explanation of chromatic induction," *Vision Res.* **16**, 289–295 (1976).
 29. A. J. Zele, P. Adhikari, B. Feigl, and D. Cao, "Cone and melanopsin contributions to human brightness estimation," *J. Opt. Soc. Am. A* **35**, B19 (2018).
 30. B. Wandell, "Image systems engineering tools for biology: ISETBIO," *J. Vis.* **17**, 10–11 (2017).
 31. L. Q. Zhang, N. P. Cottaris, and D. H. Brainard, "An image reconstruction framework for characterizing initial visual encoding," *Elife* **11**, 71132 (2022).
 32. A. Wohrer and P. Kornprobst, "Virtual Retina: A biological retina model and simulator, with contrast gain control," *J. Comput. Neurosci.* **25**, 219–249 (2009).
 33. D. Xing, A. Ouni, S. Chen, H. Sahmoud, J. Gordon, and R. Shapley, "Brightness-color interactions in human early visual cortex.," *J. Neurosci.* **35**, 2226–32 (2015).

34. B. Chai, N. Liao, and D. Zhao, "Implementing color transformation across media based on color appearance model by neural networks," <https://doi.org/10.1117/12.570757> **5637**, 297–304 (2005).
35. M. Senthilkumar, "Use of artificial neural networks (ANNs) in colour measurement," *Colour Meas. Princ. Adv. Ind. Appl.* 125–146 (2010).

Curriculum vitae

Thanh Hang Phung

Email: hangphung.usth@gmail.com Mobile: +32 488 82 48 01

Education

- 2018.05 - **KU Leuven**
Present PhD in Engineering Technology, Department of Electrical Engineering (ESAT)
- 2015.09 – **Université Jean Monnet – Norwegian University of Science and Technology**
2017.09 Master's Degree in 3D Media Technology
- 2011.09 – **University of Science and Technology of Hanoi**
2015.01 Bachelor's Degree in information and Communication Technologies
- 2013.08 – **Vilnius Gediminas Technical University**
2014.02 Exchange study in Information System Engineering

Experience

- 2017.01 – **Technicolor R&I**
2017.07 Research Intern
- 2016.06 – **Hubert Curien Laboratory**
2016.07 Research Intern
- 2014.05 – **University of New Brunswick**
2014.08 Research Intern

Journal Publications

- Spieringhs RM, Phung TH, Audenaert J, Hanselaer P. “Exploring the applicability of the Unified Glare Rating for an outdoor non-uniform residential luminaire”. *Journal of Sustainability* (Submitted)
- Phung TH, Kong X, Leloup FB, Smet KAG, Hanselaer P. “Brightness appearance of self-luminous stimuli on a non-uniform background”. *Color Res Appl.* 2022; 1- 15. doi:10.1002/col.22811
- Phung T. H., Spieringhs R. M., Smet K. A. G, Leloup F. B., and Hanselaer P., "Towards an image-based brightness model for self-luminous stimuli," *Opt. Express* 30, 9035-9052 (2022). Doi: 10.1364/OE.451265
- Phung TH, Leloup FB, Smet KAG, Hanselaer P. “Assessing the application of an image color appearance model to basic self-luminous scenes”. *Color Res Appl.* 2019;1–11. <https://doi.org/10.1002/col.22414>

International Conferences

- Spieringhs R. M., Phung T. H., Hanselaer P., “Applying the Unified Glare Rating for a non-uniform residential luminaire”. *Proceedings of the 17th EEDAL-LS-2022: International Conference on Energy Efficiency in Domestic & Light Sources*, 1 June – 3 June 2022. Toulouse, France
- Phung, T.H, Leloup, F.B, Smet, K.A.G, Hanselaer, P. “Applying an image colour appearance model for simple self-luminous scenes”, *Proceedings of the 29th Session of the CIE: Washington DC, USA, 14 June – 22 June 2019 Vol. 1.* Washington DC, USA: CIE Central Bureau
- Pouli T. and Phung T.H., 2018. VR Color Grading using Key Views. In *Proceedings of the Virtual Reality International Conference - Laval Virtual (VRIC '18)*. Association for Computing Machinery, New York, NY, USA, Article 2, 1–8. <https://doi.org/10.1145/3234253.3234287>

Posters & Meeting Abstracts

- “Predicting brightness of simple self-luminous scenes using an image color appearance model” – Poster presentation at ICA

Belgium Colour symposium 2019, 23-25 June 2019, Ghent, Belgium.

Talks

- “Towards a next-generation color appearance model for self-luminous stimuli” – Visiting scholar at Munsell Color Science Lab, Rochester Institute of Technology, 02-06 February 2020, Rochester (USA).